

EXACT EQUILIBRIUM CRYSTAL SHAPES  
IN TWO DIMENSIONS  
AND  
PERTURBATION EXPANSIONS FOR  
THE FACET SHAPE AND STEP FREE ENERGY OF  
A THREE-DIMENSIONAL EQUILIBRIUM CRYSTAL

by

Mark Holzer

B. Sc. (Honours), Simon Fraser University, 1984

A THESIS SUBMITTED IN PARTIAL FULFILLMENT OF  
THE REQUIREMENTS FOR THE DEGREE OF  
DOCTOR OF PHILOSOPHY

in the Department

of

Physics

© Mark Holzer 1990

SIMON FRASER UNIVERSITY

August, 1990

All rights reserved. This work may not be  
reproduced in whole or in part, by photocopy  
or other means, without permission of the author.

APPROVAL

Name: Markus Bernhard Holzer

Degree: Ph.D. Physics

Title of Thesis: Exact Equilibrium Crystal Shapes in Two Dimensions and Perturbation Expansions for the Facet Shape and Step Free Energy of a Three-Dimensional Equilibrium Crystal

Examining Committee:

Chairman: Prof. E. Daryl Crozier

---

Prof. Michael Wortis  
Senior Supervisor

---

Prof. Michael Plischke

---

Prof. Richard Enns

---

Prof. Robert F. Frindt

---

Prof. Martin Grant

External Examiner  
Department of Physics  
McGill University

Date Approved: 15 August, 1990

PARTIAL COPYRIGHT LICENSE

I hereby grant to Simon Fraser University the right to lend my thesis, project or extended essay (the title of which is shown below) to users of the Simon Fraser University Library, and to make partial or single copies only for such users or in response to a request from the library of any other university, or other educational institution, on its own behalf or for one of its users. I further agree that permission for multiple copying of this work for scholarly purposes may be granted by me or the Dean of Graduate Studies. It is understood that copying or publication of this work for financial gain shall not be allowed without my written permission.

Title of Thesis/~~Project/Extended Essay~~

Exact Equilibrium Crystal Shapes in Two Dimensions and

---

Perturbation Expansions For The Facet Shape and Step

---

Free Energy of a Three-Dimensional Equilibrium Crystal

---

---

Author: \_\_\_\_\_

(Signature)

Markus Bernhard HOLZER

---

(Name)

Aug. 23, 1990

---

(Date)

## Abstract

The fundamentals of the theory of equilibrium crystal shapes (ECS's) are reviewed. The concepts developed are then applied to two model calculations:

Using a conceptually novel approach which maps a two-dimensional (2D) interface exactly onto a Feynman-Vdovichenko lattice walker, we derive an exact and general solution for the ECS of free-fermion models. The ECS for these models is given by the locus of purely imaginary poles of the determinant of the "momentum-space" lattice-path propagator. The ECS may, therefore, be read off simply from the analytical expression for the bulk free energy. From these shapes one can then obtain numerically (but to arbitrary accuracy) the anisotropic interfacial free energy per unit length and, therefore, the high-temperature direction-dependent correlation length of the dual system. We give several examples of previously unknown Ising ECS's, and we examine in detail the free-fermion case of the eight-vertex model. The free-fermion eight-vertex model includes the modified potassium dihydrogen phosphate (KDP) model, which is not in the Ising universality class. The ECS of the modified KDP model is shown to be the limiting case of the ECS of an antiferromagnetic  $2\times 1$  phase on a triangular lattice in the limit of infinite interactions. The ECS of the modified KDP model is lenticular at finite temperature and has sharp corners. We explain the physics of this lens shape from an elementary calculation.

To obtain the facet shapes and anisotropic step free energies for the 3D simple-cubic nearest-neighbour Ising model, we develop systematic low-temperature perturbation expansions about the exact solution for the ECS's and interfacial free energies of the 2D square Ising model. An expansion scheme is developed which makes explicit use of the

conjugacy between the step free energy and the facet shape. We find that the facet shape is approximated to better than 1% by the equilibrium crystal shape of the corresponding 2D Ising model for temperatures less than about 72% of the roughening temperature. In that temperature range overhangs and bubbles contribute less than 0.1% to the step free energy. At higher temperatures the facet shape is nearly circular with anisotropies of less than 0.4% and a ratio of facet diameter to crystal diameter of less than 0.4. Extrapolations into the isotropic region give critical roughening amplitudes consistent with recent Monte Carlo data.

## Acknowledgements

First and foremost I thank my thesis advisor, Prof. M. Wortis, for many long discussions, for innumerable helpful suggestions, for his clear pedagogical manner of communicating physics which almost always turned my confusion into understanding, and for his generosity and kindness. I consider myself very lucky to have an advisor who always has time to discuss physics and who is unfailingly conscientious, encouraging, and tolerant.

I am very grateful to M. Plischke for helpful discussions throughout my time as a physics student, for his prompt, critical reading of my manuscripts, for his frank advice, and for his positive influence in general.

On the subject of this thesis, I have enjoyed additional helpful discussions with M. Rao and R. K. P. Zia.

Financial support from Simon Fraser University is gratefully acknowledged.

During my time as a graduate student, my understanding of physics has benefitted substantially from discussions with many individuals. I am particularly thankful to S. Breed, K. Heiderich, M. Hürlimann, C. Lusher, A. H. MacDonald, and A. Roberge. Especially inspiring and helpful were discussions with M. W. Reynolds.

I am also indebted to J. Berlinsky, P. Diamond, and M. N. Rosenbluth for advising and directing me in my early studies of theoretical physics. I am grateful to W. Hardy and R. Cline for tolerating me in their laboratory, where they generously provided me with the opportunity to learn some of the skills of low-temperature experimental physics.

Finally, I would like to thank my friends, and K. Heiderich in particular, for providing moral support along with my parents.

# Table of Contents

Approval	ii
Abstract	iii
Acknowledgements	v
Table of Contents	vi
List of Tables	viii
List of Figures	ix
<b>1. Introduction</b>	<b>1</b>
1.1 The ECS as a classical variational problem and Wulff's Theorem	3
1.2 Formulations of Statistical Mechanics: Canonical and Grand Canonical Descriptions of the ECS	17
1.3 Organization and Motivation	24
<b>2. A General, Exact Solution for Equilibrium Crystal Shapes in Two Dimensions for Free-Fermion Models</b>	<b>25</b>
2.1 Introductory Remarks	25
2.2 Derivation	27
2.3 An example of non-Ising free-fermion crystal shapes: The modified KDP model	45
2.4 Conclusion	60
<b>3. Low-Temperature Expansions For The Step Free Energy and Facet Shape of the Simple-Cubic Ising Model</b>	<b>62</b>
3.1 Background and Introductory Remarks	62
3.2 Step free energies and facet shapes from interfacial free energies and equilibrium crystal shapes	69
3.3 Low-Temperature Series for the SFE/EFS of the simple-cubic Ising model	76
3.4 Results and Discussion	92

3.5	Conclusions	103
Appendix A:	Analytic structure of the Feynman-Vdovichenko matrix - two examples	105
Appendix B:	Inversion of the ECS of the 2D rectangular Ising model	117
Appendix C:	Series expansions for the 2D square Ising model	119
Appendix D:	Series for $\gamma(\frac{\pi}{4})$ of the BCRSOS model	121
Appendix E:	Combinatorial Details	123
References		143



## List of Tables

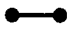
2.I	Examples of Exact Equilibrium Crystal Shapes	44
3.I	Definitions for Class 1 Diagrams	83
3.II	Diagrams and their Numerical Equivalents	87
3.III	Summary of the Low-T Expansion of the Step Free Energy $\gamma(\theta)$	93
3.IV	Summary of the Low-T Expansion of the Equilibrium Facet Shape $y(x)$	93
3.V	Summary of Critical Parameters	99
C.I	Coefficients of the low-T expansion of the 2D-Ising interfacial free energy $\Gamma_{2D}(\theta)$	107
C.II	Coefficients of the low-T expansion of the 2D-Ising equilibrium crystal shape $y_{2D}(\theta)$	108
E.I	The possible configurations of a path from (0,0) to (N,M) with two extra vertical bonds and two extra horizontal bonds without immediate backtracking	116

## List of Figures

1.1	Electron micrographs of a small crystalite of lead approximately $6\mu\text{m}$ in diameter at $\sim 300^\circ\text{C}$ as prepared by Heyraud and Métois (see Heyraud and Métois, 1983).	2
1.2	Phase diagram of a generic substance.	5
1.3	The Wulff construction.	7
1.4	Geometry used in deriving the Wulff construction.	9
1.5	The planes constructed from Eq. (1.4) for fixed $\hat{\mathbf{m}}$ given $\mathbf{R}(\hat{\mathbf{r}})$ .	10
1.6	The geometrical construct of the Brunn-Minkowski theorem for two compact "bodies" $B_1$ and $B_2$ .	13
1.7	The geometrical construct for Dinghas' proof.	14
2.1	A configuration of a ferromagnetic Ising model defined on the square lattice of thin black lines.	29
2.2	The boundary conditions considered in the derivation of the exact 2D solution, illustrated on a rectangular lattice;	30
2.3	The ECS (left) and corresponding Wulff plot (right) of the diced lattice (Fig. 2.5c) for equal, ferromagnetic couplings.	42
2.4	Same as Fig. 2.3 for the 4-8 lattice with ferromagnetic couplings $K_1=K_2=K_3=K_4$ and $K_5=K_6$ as indicated in Fig. 2.5d with $K_1/K_5=3/2$ .	42
2.5	The lattices of Table 2.I in duality pairs;	43
2.6	The eight vertex configurations of the eight-vertex model.	46
2.7	The antiferromagnetic sector of the free-fermion model, defined by the vertex weights of Eq. (2.26), in the $h$ - $v$ plane of horizontal and vertical (electric) fields.	51

2.8	An interface between two degenerate $2 \times 1$ phases of the antiferromagnetic triangular Ising model.	53
2.9	The one-to-one correspondence between vertex configurations of the eight-vertex model and composite elementary interfaces on the hexagonal lattice.	53
2.10	Equilibrium crystal shapes of the free-fermion model defined by the vertex weights of Eq. (2.25) at $h=v=0$ and for various values of $e_1/\epsilon$ .	55
2.11	The Feynman-Vdovichenko walker for the modified KDP model performs a very simple walk on the honeycomb lattice.	58
2.12	The ECS of the modified KDP model (solid lines, left) and the corresponding Wulff plot (right) for $h=v=0$ .	59
3.1	Sketch of the thermal evolution of a ("type A") ECS of cubic symmetry.	63
3.2	An <i>island</i> excitation on an otherwise flat crystalline interface (atoms have been coarse grained into bricks).	64
3.3	Top: The SOS model. The interface is represented by an array of stacks of cubes. Bottom: A lattice-gas version of the interface. Overhangs, bubbles, and handles are present.	66
3.4	The Wulff construction in the vicinity of a cusp (point A).	70
3.5	Perspective view of a fixed- $\theta$ cut through the ECS and its Wulff plot as described in the text.	72
3.6	A strip of vicinal surface projected onto the $xy$ plane.	75
3.7	Typical step configurations of the simple cubic Ising (100) interface.	78
3.8	This figure illustrates that the step cannot be chosen as a single non-self-intersecting line without ambiguity.	82
3.9	Polar plots of the low-temperature series of $\gamma(\theta)$ at the temperatures indicated.	94

- 3.10 The facet shape at different temperatures, normalized to the centre-of-crystal to centre-of-facet distance as obtained from the 11th order series for  $y(x)$  (dotted curve) and the Legendre transform of the 5th order series for  $\gamma(\theta)$  (solid curve).\_\_\_\_\_ 95
- 3.11 a.) The canonical series  $\gamma(\frac{\pi}{4}, N)$  for the step free energy and b.) the grand canonical series  $y(0, N)$  for the facet shape, summed to the orders  $N$  indicated, as a function of temperature.\_\_\_\_\_ 96
- 3.12 Plots for the 3D Ising model of  $B(T) \equiv \gamma(\theta, N) \exp[C(T)/\sqrt{T_R - T}]$ , with  $C(T) \equiv -2(T_R - T)^{3/2} \partial \ln \gamma(\theta, N) / \partial T$ , and of  $C(T)$  versus temperature  $T$  for various values of  $T_R$ .\_\_\_\_\_ 100
- 3.13 The normalized facet radius  $\rho_f$  in the symmetry directions as a function of temperature.\_\_\_\_\_ 102
- A.1 Trajectories of the two zeros of  $\text{Det}[1 - \Lambda(k_x, -i\beta\lambda X)]$  in the  $k_x$ -plane for the square lattice [cf. Eq. (A.6)] as  $X$  ranges from  $-\infty$  to  $\infty$ .\_\_\_\_\_ 107
- A.2 Trajectories of the two zeros of  $\text{Det}[1 - \Lambda(k_x, -i\beta\lambda X)]$  in the  $z$ -plane for the square lattice [cf. Eq. (A.6)] as  $X$  ranges from  $-\infty$  to  $\infty$ .\_\_\_\_\_ 108
- A.3 The real zeros of  $\text{Det}[1 - \Lambda(k_x, -i\beta\lambda X)]$  for the square lattice in the  $z$ -plane as a function of  $X$ .\_\_\_\_\_ 108
- A.4 Regions of nonconvergence (black squares) of  $\Lambda(k_x, -i\beta\lambda X)$  in the  $k_x$ -plane for the square lattice at  $T = T/2$  for the values of  $X$  indicated.\_\_\_\_\_ 109
- A.5 Regions of nonconvergence (black squares) of  $\Lambda(k_x, -i\beta\lambda X)$  in the Brillouin zone for the square lattice at  $T/2$  for the values of  $X$  indicated.\_\_\_\_\_ 110
- A.6 Trajectories of the two zeros of  $\text{Det}[1 - \Lambda(k_x, -i\beta\lambda X)]$  in the  $k_x$ -plane for the hexagonal lattice [cf. Eq. (A.6)] as  $X$  ranges from  $-\infty$  to  $\infty$ .\_\_\_\_\_ 112
- A.7 Trajectories of the two zeros of  $\text{Det}[1 - \Lambda(k_x, -i\beta\lambda X)]$  in the  $z$ -plane for the hexagonal lattice [cf. Eq. (A.6)] as  $X$  ranges from  $-\infty$  to  $\infty$ .\_\_\_\_\_ 113

- A.8 The real zeros of  $\text{Det} [1 - \Lambda(k_x, -i\beta\lambda X)]$  in the  $z$ -plane for the hexagonal lattice as a function of  $X$ . \_\_\_\_\_ 113
- A.9 Regions of nonconvergence (black squares) of  $\Lambda(k_x, -i\beta\lambda X)$  in the  $k_x$ -plane for the hexagonal lattice at  $T=T_c/2$  for the values of  $X$  indicated. \_\_\_\_\_ 115/116
- A.10 Regions of nonconvergence (black squares) of  $\Lambda(k_x, -i\beta\lambda X)$  in the Brillouin zone for the hexagonal lattice at  $T=T_c/2$  for the values of  $X$  indicated. \_\_\_\_\_ 116
- E.1 The vertical bonds of a step from  $(0,0)$  to  $(N,M)$  may be considered to be distributed over  $N+1$  bins. \_\_\_\_\_ 125
- E.2 (a) The eight orientations of the L shape of diagram #16 (10 extra plaquettets). (b) The possible straddling configurations of the L shape of orientation 1 for a fixed realization of the step. (c) The possible straddling configurations of the L shape of orientation 3 for a fixed realization of the step. (d) The vertical bonds of the realization of the step shown stacked in their bins. \_\_\_\_\_ 131
- E.3 Fixed realizations of the diagram (  ) in the 2D and 3D interpretations. \_\_\_\_\_ 135

# 1. Introduction

Crystals have undoubtedly fascinated mankind since ancient times. Perhaps the most intriguing and most easily appreciated property of crystals is that they have interesting, symmetrical shapes. This thesis will be concerned with equilibrium crystal shapes (ECS's), the shapes of crystals which are in equilibrium with their environment. ECS's may be quite different from the familiar polyhedral ones commonly observed in nature. A typical example of an ECS, as observed in the laboratory, is shown in Fig. 1.1. To observe such shapes, conditions must be carefully controlled to ensure true equilibrium. Under natural conditions (e.g., geodes in cooling magma, ice on windshields), crystals are usually formed far from equilibrium. If equilibrium conditions are established after non-equilibrium growth is completed, only the shape of very small crystals (on the order of microns for ionic insulators such as sodium chloride, and for metals like gold and lead), at relatively high temperatures (close to the triple point) can change sufficiently to reach equilibrium in practical times. The reason for this is that changes in shape require the transport of macroscopic amounts of material via surface diffusion and ad- and desorption of atoms. Generally, naturally occurring crystals have complex non-equilibrium forms which depend on their precise thermal history. For non-equilibrium situations it is, therefore, not the shape as such that is of physical interest but rather the *dynamics* of crystal growth and surface morphology. Here, we will concentrate on equilibrium only.

Equilibrium shapes are history independent, free from the complications of dynamics, and therefore reveal the nature of the crystal/environment equilibrium interface. It now makes sense to speak of the shape of a macroscopic crystal as something which may, at least in principle, be defined by a mathematical function which depends on the type of materials involved and on the thermodynamic coordinates such as pressure or temperature but not on the particular thermal history of a given sample. While the

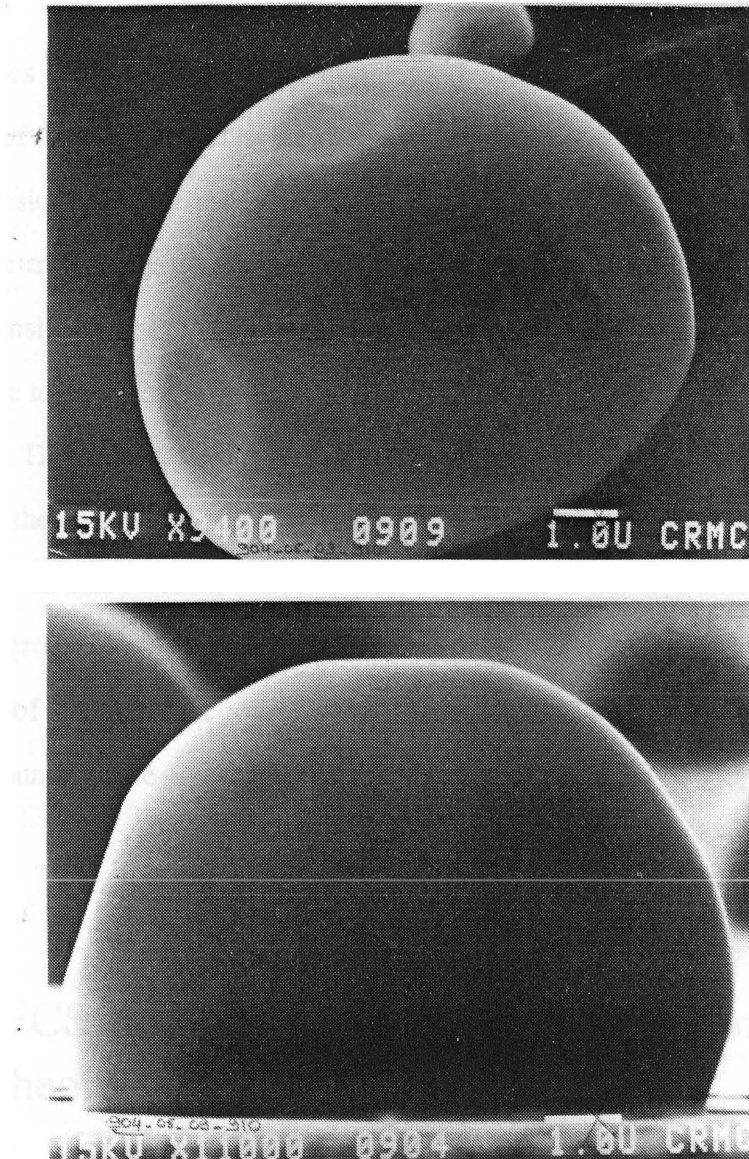


FIG. 1.1. Electron micrographs of a small crystalite of lead approximately  $6\mu\text{m}$  in diameter at  $\sim 300^\circ\text{C}$  as prepared by Heyraud and Métois (see Heyraud and Métois, 1983). The vapour pressure at this temperature is so low ( $\sim 10^{-9}$  Torr) that pressure control is not important in this case and the sample can simply be maintained in a high vacuum.

Top: Viewing the crystal along the [100] direction: The large, slightly hexagonal {111} facets are easily seen. The {100} facets are also present but smaller and difficult to see.

Bottom: Viewing the crystal along the [110] direction: The facets are flat and join the curved parts of the shape smoothly.

These photographs are reproduced here with the permission of M. Wortis, to whom J. C. Heyraud and J. J. Métois kindly made these photographs available.

thermodynamics of ECS's has been understood nearly a century ago by Wulff, the determination of these shapes from the statistical mechanics of a microscopic Hamiltonian has been of considerable interest only in recent years. This interest has been fueled on the theoretical side mainly by the discovery of surface phase transitions (most notably the roughening transition) and, on the experimental side, by technological advances which make it possible to attain true equilibrium conditions under which to observe the shapes of small crystals. The field has been very active over the last decade and several excellent reviews cover these developments: Zia, 1984; Rottman and Wortis, 1984a; Abraham, 1986; van Beijeren and Nolden, 1987; Wortis, 1988; Zia, 1988. We shall, therefore, only give such background as is needed for this thesis to be reasonably self-contained. During the remainder of the Introduction, we will develop the fundamentals of ECS theory. Further background will be provided at the beginning of each main Section.

## 1.1 The ECS as a classical variational problem and Wulff's Theorem

A crystal can only be in equilibrium with another phase when the state of the system crystal-plus-other-phase lies on a first-order coexistence curve of the system's phase diagram. We take our system to be contained in a box of volume  $V_B$ . The box is in contact with a heat bath whose temperature  $T$  is under our control. For simplicity and definiteness, consider a pure substance  $X$  at gas/solid coexistence, as shown in Fig. 1.2. The box contains a fixed amount of  $X$ , enough so that after equilibrium has been reached the pressure inside the box lies on the gas/solid coexistence curve, i.e.,  $P=P_0(T)$ . The solid and gas densities and, therefore, the volume of the crystal,  $V$ , are then determined and



fixed (see Fig 1.2). To keep the physics as simple as possible, we assume the box to be in free fall so that we need not worry about the rather subtle effects of gravity (see, for example, Avron et al., 1983; Zia and Gittis, 1987; Avron and Zia, 1988). Further, we assume the crystal to be freely floating in the interior of the box, far away from the walls of the container, so that we need not worry about substrate geometries and other complications due to the presence of the walls of the box. The important point now is that the bulk free energies of the solid and gas and the free energy coming from the wall/gas interactions are fixed. The only way in which the system can lower its free energy to attain true equilibrium is to change the shape of the crystal, so as to minimize the total free energy of the crystal/gas interface,  $F[S]$ , where  $S$  is the surface of the crystal.<sup>†</sup> Denote by  $\Gamma(\hat{\mathbf{m}})$  the interfacial free energy per unit area for a planar interface of (crystal-to-gas) normal  $\hat{\mathbf{m}}$  and for now take  $\Gamma(\hat{\mathbf{m}})$  as a given, well defined thermodynamic quantity. The starting point of the theory is the free energy functional  $F[S]$  given by

$$F[S] = \int_S dS \Gamma(\hat{\mathbf{m}}) . \quad (1.1)$$

That this is, indeed, the correct expression for  $F[S]$  is actually not obvious, since it is assumed in Eq. (1.1) that the ECS may locally be constructed from macroscopically planar pieces which do not influence each other's thermodynamics. However, for short ranged forces (1.1) is certainly a reasonable Ansatz. It has been rigourously proved to be correct for simple cases (Dobrushin et al., 1988; Kotecký, 1988).

What makes the ECS interesting is that  $\Gamma(\hat{\mathbf{m}})$  depends on the orientation,  $\hat{\mathbf{m}}$ , of the interface with respect to the crystal axes. If  $\Gamma(\hat{\mathbf{m}})$  were just a constant, as in the case of a

---

<sup>†</sup> To be precise, the surface  $S$  dividing the two phases is to be chosen with the Gibbs convention (e.g., Griffith, 1980), so that we need not consider excess volumes, densities, etc. associated with an interfacial region of finite thickness.

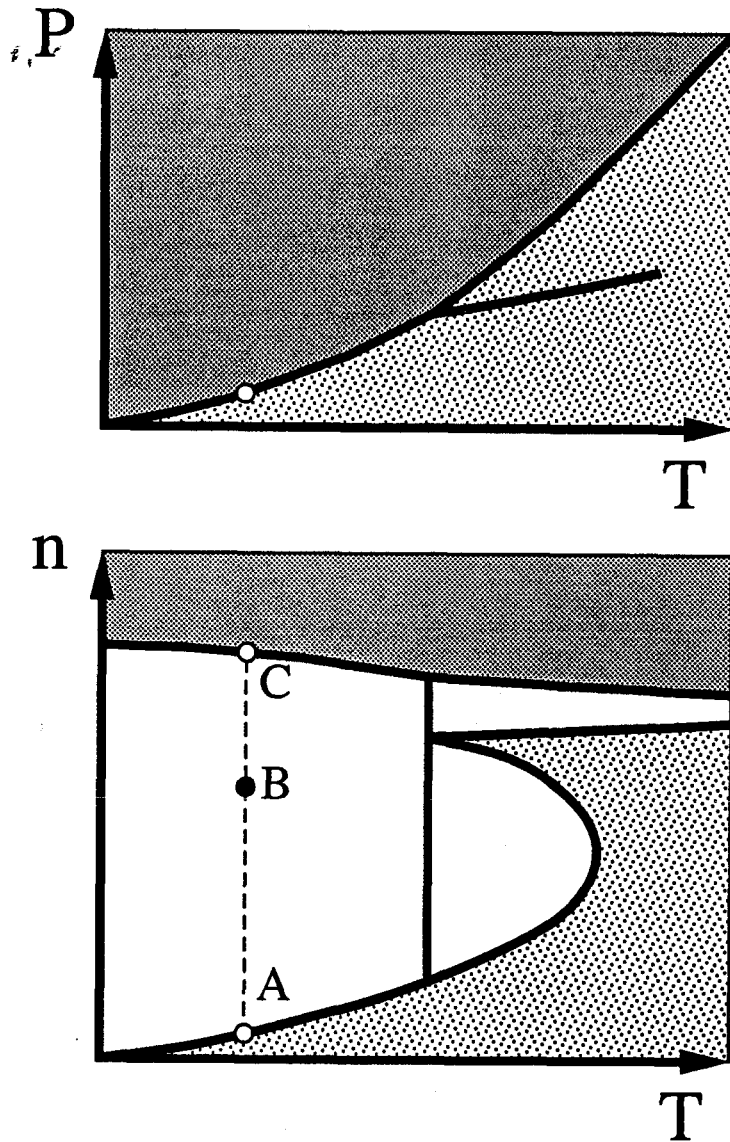


FIG. 1.2. Phase diagram of a generic substance. Top: Pressure,  $P$ , versus temperature,  $T$ . Bottom: density,  $n$ , versus  $T$ . The dark shading indicates a crystalline solid phase; the light shading, a fluid phase. An ECS is possible only if the state of the system lies on a phase coexistence curve,  $P=P_0(T)$ . If there are  $N$  particles in the box of volume  $V_B$ , the average density,  $n_0=N/V_B$ , has to lie between points A and C to be at coexistence, i.e.,  $n_0 \in [n_A, n_C]$ . If  $n_0=n_A$  or  $n_0=n_C$ , the box is filled with a pure phase. If  $n_0 \in (n_A, n_C)$ , (e.g., point B) the system phase separates into a fluid of density  $n_A$  and a crystal of density  $n_C$ . The volume of the crystal,  $V$ , is then determined by  $V=V_B(n_0-n_A)/(n_C-n_A)$ .

fluid/fluid interface, it follows from symmetry that the equilibrium shape would be a sphere. The anisotropy of  $\Gamma(\hat{\mathbf{m}})$  for a crystal/anything interface results in a non-spherical equilibrium shape which assigns as little area as possible to high-energy orientations and as much area as possible to low-energy orientations. This weighted assignment of areas takes place in such a way as to minimize  $F[S]$  subject to the constraint that the volume,  $V[S]$ , enclosed by the surface  $S$  remain fixed. This statement, with  $F[S]$  of the form (1.1), was already asserted in 1885 by P. Curie. Incorporating the constant volume constraint via a Lagrange multiplier  $(D-1)\lambda$  (defined for later convenience in terms of  $D$ , the spatial dimension of the bulk crystal), the ECS describes a surface  $S$  for which the functional

$$\Phi[S] = F[S] - (D-1)\lambda V[S] \quad , \quad (1.2)$$

is stationary. In case of multiple solutions, the ECS corresponds to the one for which  $F[S]$  is smallest. [The Euler-Lagrange equations of (1.2) are generally nonlinear.]

The solution to this variational problem was first stated by G. Wulff in 1901. His solution, after it was proven to be correct by several authors,<sup>†</sup> has become known as Wulff's theorem. For physicists, the content of the theorem is best expressed in terms of a geometrical construction (the "Wulff construction") which tells us how to obtain the ECS given  $\Gamma(\hat{\mathbf{m}})$  [see Fig. 1.3 for an illustration]:

- 1.) Make a polar plot of  $\Gamma(\hat{\mathbf{m}})$  (the "Wulff plot").
- 2.) For every point  $\hat{\mathbf{m}}\Gamma(\hat{\mathbf{m}})$  on the Wulff plot construct a plane which goes through that point and is perpendicular to  $\hat{\mathbf{m}}$ .

---

<sup>†</sup> Incomplete proofs were given by Hilton in 1903, by Liebmann in 1914, and by von Laue in 1943; the first true proof was given by Dinghas in 1944.

- 3.) Take the interior envelope of the resulting family of planes. This envelope is, to within an overall (constant) scale factor, the surface,  $S$ , of the ECS. The scale factor is chosen such that  $V[S] = V$ .

The fact that the shape depends on the volume only through an overall scale factor (except, of course, for finite-size effects) shows that the ECS, like  $\Gamma(\hat{\mathbf{m}})$ , is an intensive thermodynamic quantity.

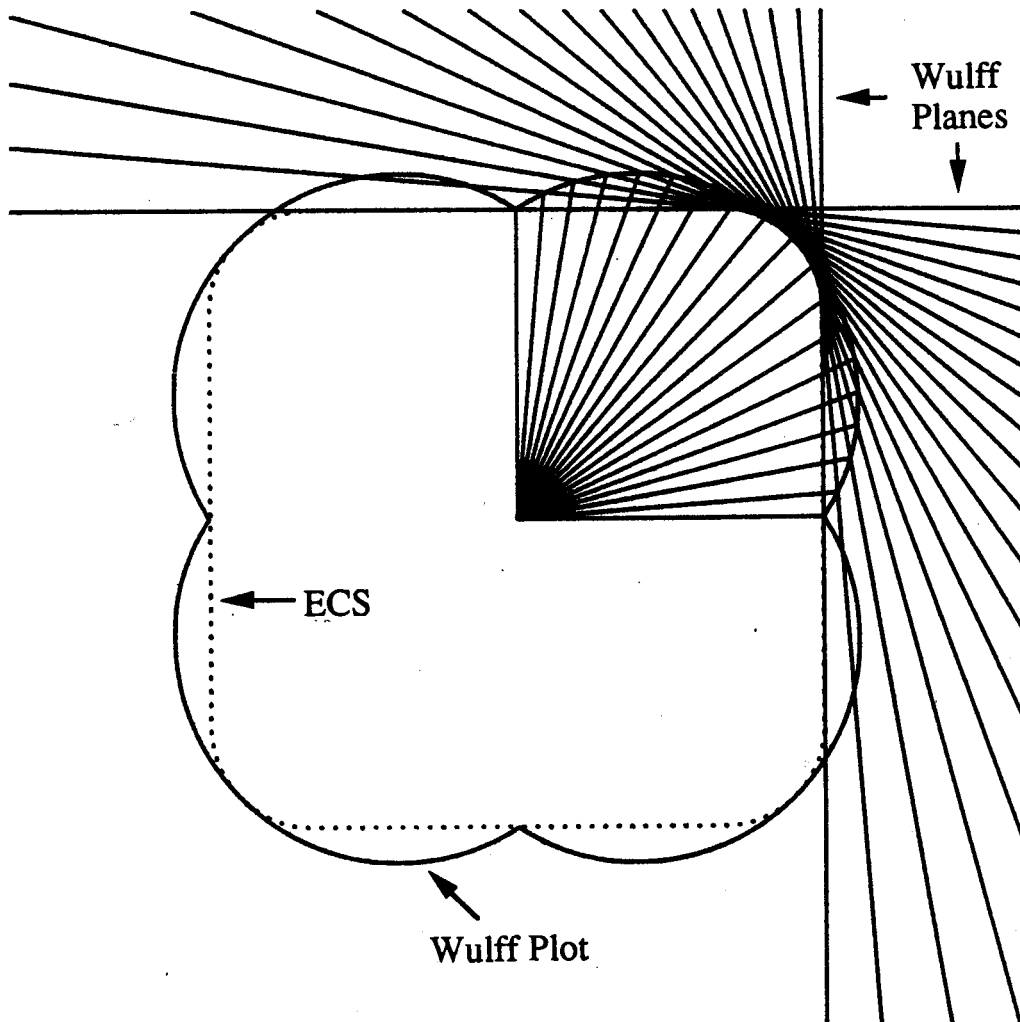


FIG. 1.3. The Wulff construction. Notice that cusps in the Wulff plot (fat solid line) generate flat regions or facets of the ECS (dotted line).

Since the Wulff theorem is the cornerstone of this thesis, we will now motivate it and then present its proof (a physicist's version) as given by Herring in 1951. Consider first the case of a fluid/fluid interface, i.e.,  $\Gamma(\hat{\mathbf{m}})=\Gamma_0=\text{constant}$ . By symmetry we may restrict ourselves to spheres<sup>†</sup> of some yet-to-be-determined radius  $R$ . A trivial calculation shows that

$$\lambda R = \Gamma_0 \quad (1.3)$$

locally stationarizes the functional  $\Phi[S]$  and that the corresponding sphere is the unique spherically symmetric minimum of  $F[S]$ . Since  $\Gamma_0$  is just the surface tension of the interface, it follows from mechanical equilibrium that  $(P_2-P_1)/2=\Gamma_0/R$ , where  $P_2$  and  $P_1$  are the hydrostatic pressures inside and outside the sphere, respectively. Thus, we may make the identification  $\lambda=(P_2-P_1)/2$ .

For the crystal/anything interface,  $\Gamma(\hat{\mathbf{m}})$  has explicit  $\hat{\mathbf{m}}$  dependence. Let the surface  $S$  be described as a function  $R(\hat{\mathbf{r}})$ . Break up  $S$  into small pieces  $dS$ , small enough so that  $\hat{\mathbf{m}}$  does not vary appreciably over  $dS$ . The piece  $dS$  subtends a small solid angle  $d\Omega$  at the origin. Energetically,  $dS$  at energy density  $\Gamma(\hat{\mathbf{m}})$  is equivalent to a small spherical cap of area  $dA$  and energy density  $\Gamma(\hat{\mathbf{m}})/\hat{\mathbf{m}}\cdot\hat{\mathbf{r}}$  (for  $\hat{\mathbf{m}}\cdot\hat{\mathbf{r}}\neq 0$ ), where  $dA$  is at the same distance  $R$  from the origin as  $dS$  and subtends the same solid angle  $d\Omega$  (Fig. 1.4). To first order in the differentials the volume contained in  $d\Omega$  between the origin and  $dS$  is the same as the volume contained in  $d\Omega$  between the origin and  $dA$ . Thus, if  $dS$  is locally in equilibrium, so is  $dA$  and, therefore, by Eq. (1.3), we have

---

<sup>†</sup> Rigorous mathematical proofs that the the equilibrium shape exists and is, indeed, spherically symmetric were given by Schwarz in 1884 and by Minkowski in 1901 (see Minkowski, 1903, 1911). Dinghas' proof is a generalization of those works.

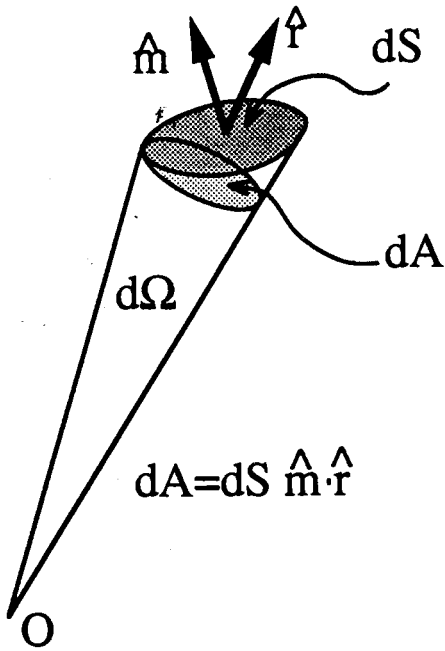


FIG. 1.4. Geometry used in deriving the Wulff construction.

$$\lambda R = \frac{\Gamma(\hat{\mathbf{m}})}{\hat{\mathbf{m}} \cdot \hat{\mathbf{r}}} \quad (1.4)$$

For each  $\hat{\mathbf{m}}$ , Eq. (1.4) describes a plane perpendicular to and through the point  $\hat{\mathbf{m}}\Gamma(\hat{\mathbf{m}})$ , which is the Wulff plane associated with  $\hat{\mathbf{m}}$ . For a given volume, the ECS is to be constructed with the planes (1.4), and we now have to find that construction which minimizes  $F[S]$ . For any shape constructed with the planes (1.4) we can evaluate  $F[S]$  explicitly as

$$F[S] = \int d\Omega \frac{\Gamma(\hat{\mathbf{m}})}{\hat{\mathbf{m}} \cdot \hat{\mathbf{r}}} R^D = \int d\Omega \lambda R^D = \lambda DV[S], \quad (1.5)$$

which is minimized at fixed  $\lambda$  when  $V[S]$  is a minimum. Since the smallest possible volume enclosed by the Wulff planes (1.4) is their interior envelope, we arrive at the Wulff theorem, which we may simply state as

$$\lambda R = \min_{\hat{\mathbf{m}}} \left( \frac{\Gamma(\hat{\mathbf{m}})}{\hat{\mathbf{m}} \cdot \hat{\mathbf{r}}} \right) \Bigg|_{\hat{\mathbf{r}}} \quad (1.6)$$

This relation has a simple inverse, which provides  $\Gamma(\hat{\mathbf{m}})$  given  $R(\hat{\mathbf{r}})$ . Since the ECS is the interior envelope of the perpendicular planes through  $\hat{\mathbf{m}}\Gamma(\hat{\mathbf{m}})$  and since these planes are tangent to the ECS, we must have (see Fig. 1.5)

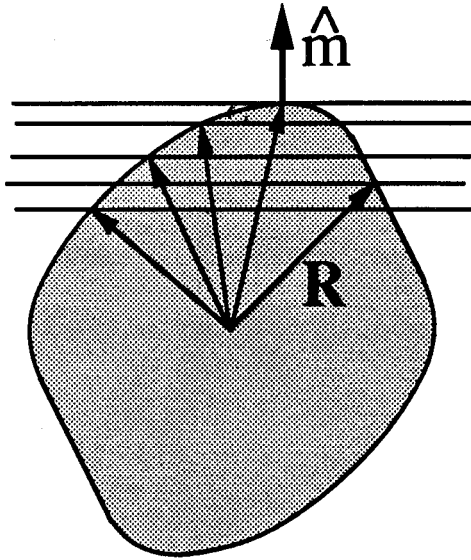


FIG. 1.5. The planes constructed from Eq. (1.4) for fixed  $\hat{\mathbf{m}}$  given  $\mathbf{R}(\hat{\mathbf{r}})$ . These planes are tangent to the ECS (shaded) when  $\mathbf{R} \cdot \hat{\mathbf{m}}$ , the perpendicular distance from the centre, is maximized.

$$\Gamma(\hat{\mathbf{m}}) = \max_{\hat{\mathbf{r}}} (\lambda \mathbf{R} \cdot \hat{\mathbf{m}}) \Big|_{\hat{\mathbf{m}}}, \quad (1.7)$$

where  $\mathbf{R} = \hat{\mathbf{r}} R(\hat{\mathbf{r}})$ . Since  $\max_x [f(x)] = \min_x [1/f(x)]$ , this may be written in the form of (1.6) as

$$\lambda \Gamma^{-1}(\hat{\mathbf{m}}) = \min_{\hat{\mathbf{r}}} \left( \frac{R^{-1}(\hat{\mathbf{r}})}{\hat{\mathbf{r}} \cdot \hat{\mathbf{m}}} \right) \Big|_{\hat{\mathbf{m}}}, \quad (1.8)$$

which states that the inverse interfacial free energy,  $1/\Gamma(\hat{\mathbf{m}})$ , is given by the Wulff construction of the inverse crystal shape,  $1/R(\hat{\mathbf{r}})$ .

We shall refer to the shape obtained with  $\lambda=1$  as the "normalized ECS". It will be useful below to express the total interfacial free energy,

$F_0$ , of the ECS in terms of the volume,  $V_w$ , of the normalized ECS. The scale invariance of the ECS [manifest in (1.6)] implies that the volume,  $V$ , enclosed by the surface defined by (1.6) is given by  $V = \lambda^{-1/D} V_w$ . Hence it follows from (1.5) that

$$F_0 = \lambda D V = D V^{(D-1)/D} V_w^{1/D}. \quad (1.9)$$

If the ECS is smooth at the point  $\mathbf{R}(\hat{\mathbf{r}})$ , where the normal is  $\hat{\mathbf{m}}$ , then Wulff planes close by, with  $\hat{\mathbf{m}}' = \hat{\mathbf{m}} + \delta \hat{\mathbf{m}}$ , must all intersect at  $\mathbf{R}(\hat{\mathbf{r}})$  in the limit as  $\delta \hat{\mathbf{m}} \rightarrow 0$ . The condition for these planes to intersect is just

$$\frac{\Gamma(\hat{\mathbf{m}} + \delta \hat{\mathbf{m}})}{(\hat{\mathbf{m}} + \delta \hat{\mathbf{m}}) \cdot \hat{\mathbf{r}}} - \frac{\Gamma(\hat{\mathbf{m}})}{\hat{\mathbf{m}} \cdot \hat{\mathbf{r}}} = \delta \hat{\mathbf{m}} \cdot \nabla_{\hat{\mathbf{m}}} \left( \frac{\Gamma(\hat{\mathbf{m}})}{\hat{\mathbf{m}} \cdot \hat{\mathbf{r}}} \right) = 0, \quad (1.10)$$

provided  $\Gamma(\hat{\mathbf{m}})$  is differentiable.<sup>†</sup> Since (1.10) must hold for any  $\delta\hat{\mathbf{m}}$ , we have

$$^t\nabla_{\hat{\mathbf{m}}} \left( \frac{\Gamma(\hat{\mathbf{m}})}{\hat{\mathbf{m}} \cdot \hat{\mathbf{r}}} \right) = \frac{1}{\hat{\mathbf{m}} \cdot \hat{\mathbf{r}}} \left( \nabla_{\hat{\mathbf{m}}} - [\hat{\mathbf{r}} - \hat{\mathbf{m}} (\hat{\mathbf{m}} \cdot \hat{\mathbf{r}})] \right) \Gamma(\hat{\mathbf{m}}) = 0, \quad (1.11)$$

which defines  $\hat{\mathbf{r}}$  as a function of  $\hat{\mathbf{m}}$ , and is just the analytical form of the  $\min_{\hat{\mathbf{m}}(\cdot)}$  function of Eq. (1.6) in the case of differentiable  $\Gamma(\hat{\mathbf{m}})$ . Decomposing  $\mathbf{R}[\hat{\mathbf{r}}(\hat{\mathbf{m}})] = \mathbf{R}(\hat{\mathbf{m}})$  into vectors parallel and perpendicular to  $\hat{\mathbf{m}}$  and using (1.11), we may write the ECS as a parametric function of  $\hat{\mathbf{m}}$ , i.e.,

$$\lambda \mathbf{R}(\hat{\mathbf{m}}) = (\hat{\mathbf{m}} + \nabla_{\hat{\mathbf{m}}}) \Gamma(\hat{\mathbf{m}}), \quad (1.12)$$

for those parts of the ECS constructed from differentiable parts of the Wulff plot.

In our derivation above, we found a particular solution for which  $F[S]$  is stationary. However, it is far from obvious that there are no other solutions for which  $F[S]$  is smaller yet. If we represent the ECS as a function  $\mathbf{R}(\hat{\mathbf{r}})$  as in the preceding discussion, Eq. (1.2) may be written as

$$\Phi[S] = \int_S d\Omega \left( \frac{\Gamma(\hat{\mathbf{m}})}{\hat{\mathbf{m}} \cdot \mathbf{R}} - \frac{(D-1)\lambda}{D} \right) R^D. \quad (1.13)$$

Variations  $\mathbf{R} \rightarrow \mathbf{R} + \delta\mathbf{R}$  induce variations in  $\Phi$  which must be zero for a stationary solution. When  $\Gamma(\hat{\mathbf{m}})$  is differentiable, our argument for the derivation of the Wulff construction amounts to nothing more than to writing these variations as (Zia, 1984)

$$\delta\Phi[S] = \int_S d\Omega \left[ (D-1) \left( \frac{\Gamma(\hat{\mathbf{m}})}{\hat{\mathbf{m}} \cdot \mathbf{R}} - \lambda \right) + \frac{\delta\hat{\mathbf{m}}}{\delta\mathbf{R}} \cdot \nabla_{\hat{\mathbf{m}}} \left( \frac{\Gamma(\hat{\mathbf{m}})}{\hat{\mathbf{m}} \cdot \hat{\mathbf{r}}} \right) \right] R^{D-1} \delta\mathbf{R} = 0. \quad (1.14)$$

---

<sup>†</sup> The transverse gradient,  $\nabla_{\hat{\mathbf{m}}}$ , is defined by  $[\nabla_{\hat{\mathbf{m}}} f(\hat{\mathbf{m}})]^\mu = (\delta^{\mu\nu} - \zeta^\mu \zeta^\nu / \zeta^2) \zeta^\nu \frac{\partial}{\partial \zeta^\nu} f\left(\frac{\zeta^k}{\zeta}\right)$   
 $\equiv \tau^{\mu\nu} \zeta^\nu \frac{\partial}{\partial \zeta^\nu} f\left(\frac{\zeta^k}{\zeta}\right)$  with  $\zeta \equiv \sqrt{\zeta_p \zeta^p}$ . In two-dimensional polar coordinates,  $\nabla_{\hat{\mathbf{m}}} = \theta \frac{\partial}{\partial \theta}$ .



Evidently,  $\delta\Phi[S] = 0$  when Eqs. (1.6) and (1.11) are satisfied. Clearly, however, there may be other solutions in which the sum of the two terms in the integrand of (1.14) is zero but the individual terms are not. A priori, it is not even clear that the ECS can be represented by a single valued function  $R(\hat{\mathbf{r}})$ . Furthermore, our tacit assumption that the interface may be represented by equivalent infinitesimal spherical caps of a common centre of curvature does, in principle (while being physically very plausible and, as it turns out, correct), also require proof.

Dinghas' ingenious proof and its successive refinements and extensions (Herring, 1953; Taylor<sup>†</sup>, 1974, 1978) put all these worries to rest by proving that the Wulff solution gives the absolute minimum of  $F[S]$  at fixed volume. In their most general and powerful form, the proof and, indeed, the statement of the theorem itself, requires the technology of geometric measure theory (Taylor, 1974). We will content ourselves here with a more simple version.

At the heart of the proof of the Wulff theorem lies the Brunn-Minkowski inequality (e.g., Minkowski, 1911; Federer, 1969), which states the following (see Fig. 1.6): Let the "bodies"  $B_1$  and  $B_2$  be nonempty subsets of  $\mathbb{R}^D$  having volumes  $V_1$  and  $V_2$ , respectively. Let  $X_c \in B_2$  and call it the centre of  $B_2$ . Define a third body  $\bar{B}$  as the subset of  $\mathbb{R}^D$  which is swept out with  $B_2$  as the centre of  $B_2$  is placed at all points of  $B_1$  keeping fixed the orientation of both  $B_1$  and  $B_2$ . If we denote the volume of  $\bar{B}$  by  $\bar{V}$ , then the theorem states that

$$\bar{V} \geq (V_1^{1/D} + V_2^{1/D})^D, \quad (1.15)$$

with the equality holding if and only if  $B_1$  and  $B_2$  are geometrically similar.

---

<sup>†</sup> Taylor (1978) will tell you how to catch fish with the Wulff construction!

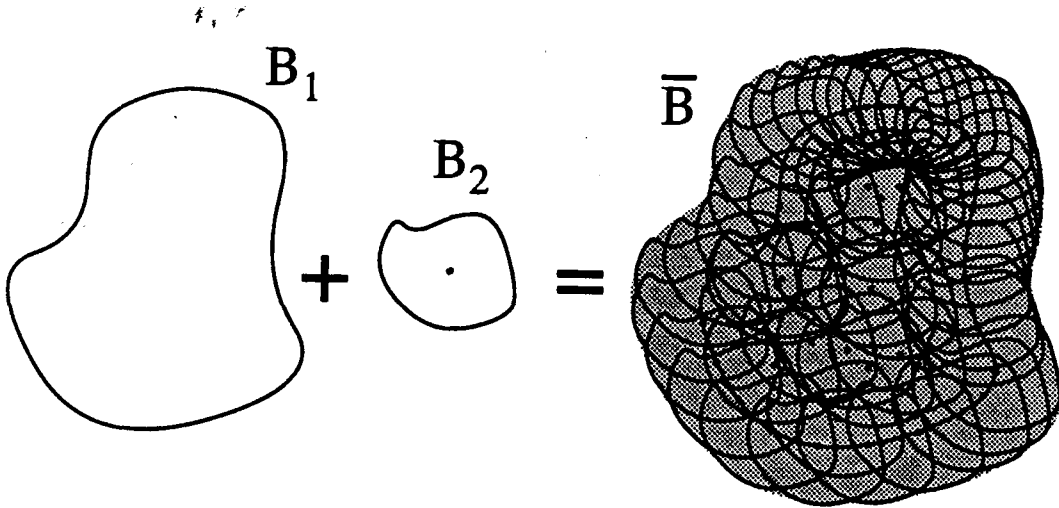


FIG. 1.6: The geometrical construct of the Brunn-Minkowski theorem for two compact “bodies”  $B_1$  and  $B_2$ . The (arbitrary) centre of  $B_2$  is indicated by a dot. The volume swept out by placing the centre of  $B_2$  at every point of  $B_1$  generates the body  $\bar{B}$  as indicated. The volumes of the three bodies obey the Brunn-Minkowski inequality, Eq. (1.15), which is an equality if and only if  $B_1$  and  $B_2$  are geometrically similar.

The proof of Wulff’s theorem now goes as follows: Let  $B_1$  be the body whose surface,  $S_1$ , is being investigated as a candidate for being an absolute minimum of the functional (1.1) subject to the constraint that  $V_1$  be fixed. We define a third body  $B_\epsilon$  (of volume  $V_\epsilon$ ) as the union of  $B_1$  and the set of points swept out by moving each point of  $S_1$  out by a vector  $\epsilon \hat{m} \Gamma(\hat{m})$ , for every point of  $S_1$  for which a surface normal  $\hat{m}$  is defined (see Fig. 1.7). We then have

$$\lim_{\epsilon \rightarrow 0} \frac{V_\epsilon - V_1}{\epsilon} = \int_{S_1} dS_1 \Gamma(\hat{m}) . \quad (1.16)$$

Let  $B_2$  be the body of the ECS obtained by the Wulff construction with scale factor  $\epsilon$  so that  $V_2 = \epsilon^D V_w$ . Let  $X_c \in B_2$  be the origin of the polar coordinate system used in the Wulff

construction, and form the body  $\bar{B}$  as described above. Since the Wulff construction guarantees that  $B_2$  has no points outside the plane perpendicular to and through  $\varepsilon \hat{m} \Gamma(\hat{m})$  [see Fig. 1.7], we have the inequality

$$\lim_{\varepsilon \rightarrow 0} \frac{V_\varepsilon - V_1}{\varepsilon} \geq \lim_{\varepsilon \rightarrow 0} \frac{\bar{V} - V_1}{\varepsilon} \quad (1.17)$$

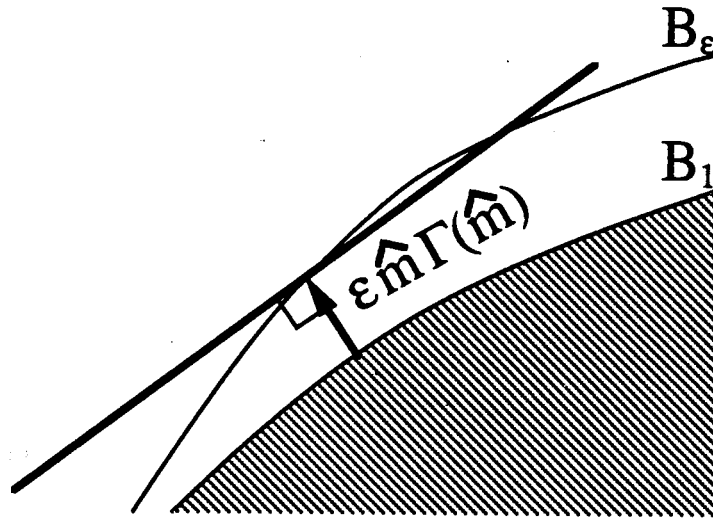


FIG. 1.7. The geometrical construct for Dinghas' proof.  $B_\varepsilon$  is constructed from  $B_1$  by moving every point of the surface of  $B_1$  out along the surface normal  $\hat{m}$  by a distance  $\varepsilon \Gamma(\hat{m})$ . The heavy straight line indicates the plane normal to and through  $\varepsilon \hat{m} \Gamma(\hat{m})$ .

Applying the Brunn-Minkowski inequality (1.15) to the right hand side, evaluating the resulting limit, and substituting for the left hand side from (1.16) one obtains

$$F[S_1] = \int_{S_1} dS_1 \Gamma(\hat{m}) \geq \lim_{\varepsilon \rightarrow 0} \frac{\bar{V} - V_1}{\varepsilon} \geq \lim_{\varepsilon \rightarrow 0} \frac{(V_1^{1/D} + \varepsilon V_w^{1/D})^D - V_1}{\varepsilon} = D V_1^{(D-1)/D} V_w^{1/D} \quad (1.18)$$

Thus,  $D V_1^{(D-1)/D} V_w^{1/D}$  is a lower bound for  $F[S_1]$ . When  $B_1$  and  $B_2$  are geometrically similar, all inequalities in Eq. (1.18) become equalities [cf. Eq. (1.9)], which proves that the surface obtained from the Wulff construction is the absolute minimum of  $F[S]$ .

The fact that the Wulff construction gives the ECS as the interior envelope of planes strongly suggests that a Legendre transform may be involved (e.g., Callen, 1960). That this is, indeed, the case was first recognized by Andreev in 1982 (81 years after Wulff!). The fact that  $R(\hat{\mathbf{r}})$  is the Legendre transform of  $\Gamma(\hat{\mathbf{m}})$  is most clearly visible when the ECS is described in Cartesian coordinates as  $z(\mathbf{x})$ ,  $\mathbf{x}=(x,y)$ . It is then natural to describe the orientation of the interface in terms of its slope  $\mathbf{p} \equiv \frac{\partial z}{\partial \mathbf{x}}$  and in terms of the interfacial free energy per unit projected area in the x-y plane, given by  $f(\mathbf{p}) = \Gamma(\hat{\mathbf{m}})\sqrt{1+\mathbf{p}^2}$ , with  $\hat{\mathbf{m}}(\mathbf{p}) = (-p_x, -p_y, 1)/\sqrt{1+\mathbf{p}^2}$ . Transcribing Eq. (1.6) to Cartesian coordinates, one obtains

$$z(\mathbf{x}) = \frac{1}{\lambda} \tilde{f}(-\lambda \mathbf{x}), \quad (1.19)$$

with

$$\tilde{f}(\boldsymbol{\eta}) \equiv f(\mathbf{p}) - \boldsymbol{\eta} \cdot \mathbf{p}. \quad (1.20)$$

$\boldsymbol{\eta}$  and  $\mathbf{p}$  are conjugate variables related by<sup>†</sup>

$$\boldsymbol{\eta} = \frac{\partial f(\mathbf{p})}{\partial \mathbf{p}} \quad (1.21)$$

and

$$\mathbf{p} = -\frac{\partial \tilde{f}(\boldsymbol{\eta})}{\partial \boldsymbol{\eta}}, \quad (1.22)$$

provided  $f(\mathbf{p})$  is differentiable at  $\mathbf{p}$ . Eqs. (1.20-22) clearly express  $\tilde{f}(\boldsymbol{\eta})$  and  $f(\mathbf{p})$  as Legendre-transform-conjugate pairs.

Since the Legendre transform is nothing more than a change of variables, the normalized ECS, as obtained from the Wulff construction, is itself a free energy surface! This is, perhaps, the most astonishing result of ECS theory. The Wulff plot describes the anisotropic interfacial free energy in terms of the independent variable  $\hat{\mathbf{m}}$  (or  $\mathbf{p}$ ), whereas the ECS does the same in terms of the conjugate variable  $\hat{\mathbf{r}}$  (or  $\boldsymbol{\eta}$ ). That the ECS and the

---

<sup>†</sup> Eq. (1.21) may be recognized as a transcription of (1.12) by using the fact that  $[(\nabla_{\hat{\mathbf{m}}})_x, (\nabla_{\hat{\mathbf{m}}})_y] = -\sqrt{1+\mathbf{p}^2} \frac{\partial}{\partial \mathbf{p}}$ .

interfacial free energy are different representations of the same physical quantity is already apparent from the Wulff construction, itself, since the Wulff plot may be reconstructed from the ECS via the inverse relation (1.8).<sup>†</sup> Legendre transform conjugacies are ubiquitous in thermodynamics, and the conjugacy between  $\Gamma(\hat{\mathbf{m}})$  and  $R(\hat{\mathbf{r}})$  is precisely analogous to any other such conjugacy commonly encountered. For example, the Helmholtz free energy density of a magnetic system,  $f(m)$ , gives the free energy in terms of the system's magnetization density,  $m$ . Via the Legendre transform, one obtains the corresponding Gibbs free energy density  $g(h)$  as  $g(h)=f(m)-mh$ , with  $-m=\partial g/\partial h$  and  $h=\partial f/\partial m$ , which describes the system in terms of the conjugate field variable  $h$  (which in this case is literally the applied field). To remind ourselves of the analogy with such more familiar cases, we call  $\hat{\mathbf{m}}$  (or  $\mathbf{p}$ ) the *density* variable, and  $\hat{\mathbf{r}}$  (or  $\boldsymbol{\eta}$ ), the *field* variable.

The loci of singularities of a free energy (hyper)surface are (by definition) phase boundaries. Thus, the ECS may be considered to be a constant-T cut through the three-dimensional  $(\hat{\mathbf{r}}, T)$  phase diagram of the crystal/anything interface (Rottman and Wortis, 1984; Wortis, 1988). Flat regions (or *facets*) and rounded regions of the ECS (see Fig. 1.1) may be identified as different phases. If the facet is connected smoothly to the adjacent rounded region, the facet edge corresponds to a second-order phase boundary. Correspondingly, the facet edge is associated with universal exponents and critical behaviour (e.g. Pokrovsky and Talapov, 1979; Jayaprakash et al., 1984b). Slope discontinuities and sharp features of the ECS correspond to first order phase boundaries.

---

<sup>†</sup> If there are parts of the Wulff plot that do not contribute to the ECS, the corresponding directions  $\hat{\mathbf{m}}$  are not thermodynamically stable and hence not defined in equilibrium (Herring's theorem, Herring, 1951). They can only show up in the Wulff plot as a result of a mean-field calculation or via some other approximation procedure (see also Rottman and Wortis, 1984a).

## 1.2 Formulations of Statistical Mechanics: Canonical and Grand Canonical Descriptions of the ECS

In the previous section we took the interfacial free energy per unit area,  $\Gamma(\hat{\mathbf{m}})$ , as a given thermodynamic quantity. In this Sub-section, we discuss the thermodynamic definition of  $\Gamma(\hat{\mathbf{m}})$  and, from that, give a microscopic definition in terms of a Boltzmann sum (trace) over a “canonical” ensemble of microscopic configurations. We will then make use of the Legendre transform duality between the ECS,  $R(\hat{\mathbf{r}})$ , and  $\Gamma(\hat{\mathbf{m}})$  to formulate the ECS directly in terms of a “grand canonical” trace.

Let the two phases under consideration be labelled by (+) and (-) and let our box have wall area  $A_w$ . When we put just the right amount of material in our box so that we sit at phase coexistence with only the pure (+)-phase filling the box (e.g., point A in Fig. 1.2), the sample free energy,  $F^{++}$ , contains contributions from the bulk and from the boundaries of the sample. We may write

$$F^{++} = V f_b^{++} + A_w f_w^{++} + (\text{rest})^{++}, \quad (1.23)$$

where

$$f_b^{++} \equiv \lim_{V \rightarrow \infty} \frac{F^{++}}{V} \quad (1.24)$$

and

$$f_w^{++} \equiv \lim_{A_w \rightarrow \infty} \frac{F^{++} - V f_b^{++}}{A_w}. \quad (1.25)$$

The thermodynamic limits (1.24) and (1.25) are to be taken so that the system size goes uniformly to infinity, i.e., every linear coordinate is multiplied by a constant  $C$  which goes to infinity and the number of particles is taken to be proportional to the volume. By  $(\text{rest})^{++}$  we simply mean contributions to  $F^{++}$  which either do not scale at all with  $C$  or scale like  $C^v$  with  $v < 2$ . These limits [and, therefore, the expansion (1.23)] exist for

sufficiently short ranged microscopic forces (e.g., Fisher and Caginalp, 1977; Caginalp and Fisher, 1979). Eqs. (1.24) and (1.25) define the bulk free energy,  $f_b^{++}$ , and the wall free energy per unit area,  $f_w^{++}$ , respectively. Similarly, we define  $f_b^-$  and  $f_w^-$  for the (-) phase.

We now add more material to the box so that the net density is made to sit in the forbidden region (point B in Fig 1.2), and both phases are present inside the box. When the volumes of the two phases are comparable, we can have a (macroscopically) planar interface between the two phases. (If one of the volumes is much less than the other, we will get a small crystalline inclusion with curved interfaces and many macroscopic surface normals will be present.) Let the volume of the (+) phase be denoted by  $V^{++}$  and the volume of the (-) phase by  $V^- = (V_B - V^{++})$ . We can, for example, imagine controlling the orientation of the interface by an appropriate choice of boundary condition as follows: Cut the box into two with a plane of the desired orientation,  $\hat{\mathbf{m}}$ , such that one half of the box has volume  $V^{++}$ . Now, somehow, treat the the walls of the half with volume  $V^{++}$  (and wall area  $A_w^{++}$ ) so that, energetically, they prefer to be in contact with the (+) phase, and treat the walls of the other half (with wall area  $A_w^- = A_w - A_w^{++}$ ), so that they prefer to be in contact with the (-) phase. In equilibrium this will then force an interface into the system of the desired orientation, provided, of course, such an interface is thermodynamically stable.<sup>†</sup> If the interface has area  $A$ , the sample free energy,  $F_{\hat{\mathbf{m}}}^{+-}$ , will have an expansion

$$F_{\hat{\mathbf{m}}}^{+-} = (V^{++} f_b^{++} + V^- f_b^-) + (A_w^{++} f_w^{++} + A_w^- f_w^-) + A \Gamma(\hat{\mathbf{m}}) + (\text{rest})^{+-}, \quad (1.26)$$

---

<sup>†</sup> We have in mind, of course, an Ising model. For an Ising model, the described procedure can be implemented by simply fixing the signs of the boundary spins (see Section 2).

where

$$\begin{aligned} \Gamma(\hat{\mathbf{m}}) &\equiv \\ &\equiv \lim_{A \rightarrow \infty} \frac{1}{A} \left[ F_{\hat{\mathbf{m}}}^{+-} - (V^{++} f_b^{++} + V^{--} f_b^{--}) - (A_w^{++} f_w^{++} + A_w^{--} f_w^{--}) \right]. \end{aligned} \quad (1.27)$$

Eq. (1.27) is the thermodynamic definition of the interfacial free energy per unit area for an interface of orientation  $\hat{\mathbf{m}}$ . In this thesis, we will be dealing exclusively with systems which have the simplifying property that the bulk and wall free energies ( $f_b$  and  $f_w$ ) of the two phases are the same. Restricting ourselves from now on to systems with such symmetric phases, we obtain the more manageable expression

$$\Gamma(\hat{\mathbf{m}}) \equiv \lim_{A \rightarrow \infty} \frac{1}{A} \left( F_{\hat{\mathbf{m}}}^{+-} - V f_b - A f_w \right), \quad (1.28)$$

or equivalently,

$$\Gamma(\hat{\mathbf{m}}) \equiv \lim_{A \rightarrow \infty} \frac{1}{A} \left( F_{\hat{\mathbf{m}}}^{+-} - F^{++} \right). \quad (1.29)$$

It is now straightforward to write down Eq. (1.29) as a trace over microscopic configurations. If only the pure bulk phase fills the box, denote the Hamiltonian of the system by  $\mathcal{H}^{++}$ . If both phases fill the box and an interface of orientation  $\hat{\mathbf{m}}$  has been enforced, denote the Hamiltonian of the system by  $\mathcal{H}_{\hat{\mathbf{m}}}^{+-}$ . The free energies  $F^{++}$  and  $F_{\hat{\mathbf{m}}}^{+-}$  are then given by

$$\beta F^{++} = - \ln Z^{++} \quad (1.30)$$

and

$$\beta F_{\hat{\mathbf{m}}}^{+-} = - \ln Z_{\hat{\mathbf{m}}}^{+-}, \quad (1.31)$$

where  $Z^{++}$  and  $Z_{\hat{\mathbf{m}}}^{+-}$  are the partition functions

$$Z^{++} = \text{Tr} \exp(-\beta \mathcal{H}^{++}) \quad (1.32)$$

and

$$Z_{\hat{\mathbf{m}}}^{+-} = \text{Tr} \exp(-\beta \mathcal{H}_{\hat{\mathbf{m}}}^{+-}), \quad (1.33)$$



where  $\beta \equiv (k_B T)^{-1}$ , with  $k_B$  Boltzmann's constant. In terms of these partition functions, Eq. (1.29) becomes

$$\beta\Gamma(\hat{\mathbf{m}}) \equiv -\lim_{A \rightarrow \infty} \frac{1}{A} \ln \left( \frac{Z_{\hat{\mathbf{m}}}^{+-}}{Z^{++}} \right). \quad (1.34)$$

We shall regard (1.34) as the “canonical” description of the interfacial free energy, because the trace is carried out at *fixed* macroscopic orientation  $\hat{\mathbf{m}}$  in analogy with the fixed density or magnetization constraint of more familiar canonical ensembles. Correspondingly, we regard the description of the ECS which instructs us first to calculate  $\Gamma(\hat{\mathbf{m}})$  via (1.34) and then to obtain the ECS via the Wulff construction, to be the “canonical” description of the equilibrium crystal shape problem. So far we have put “canonical” and “grand canonical” in quotation marks to emphasize that we do not mean the standard canonical and grand canonical ensemble of particles. Since from now on we will only speak of ensembles of interfaces in this thesis, we will drop the quotes.

Eqs. (1.20) and (1.22) tell us how to arrive at a grand canonical description of the ECS. Substituting the definition of  $\Gamma(\hat{\mathbf{m}})$ , Eq. (1.34), into the definition of  $\beta\mathcal{F}(\boldsymbol{\eta})$ , Eq. (1.20), we obtain

$$\beta\mathcal{F}(\boldsymbol{\eta}) = \lim_{A_{xy} \rightarrow \infty} \frac{1}{A_{xy}} \left[ -\ln \text{Tr} e^{-\beta(\mathcal{H}_{\hat{\mathbf{m}}}^{+-} - \boldsymbol{\eta} \cdot \mathbf{p}(\hat{\mathbf{m}})A_{xy})} - \beta F^{++} \right], \quad (1.35)$$

where  $A_{xy} \equiv A/\sqrt{1+\mathbf{p}^2}$ . Since we can expect the term  $\text{Tr} \exp[-\beta(\mathcal{H}_{\hat{\mathbf{m}}}^{+-} - \boldsymbol{\eta} \cdot \mathbf{p}(\hat{\mathbf{m}})A_{xy})]$  to be a sharply peaked function of  $\hat{\mathbf{m}}$  in the limit  $A_{xy} \rightarrow \infty$  (an explicit example will be given in Section 2), we can extend the trace of (1.35) to a trace over a grand canonical ensemble of systems. Each member of this ensemble is contained in a box of base area  $A_{xy}$  on which boundary conditions have been imposed to enforce a macroscopically planar interface of orientation  $\hat{\mathbf{m}}$  as described above. Each member has Hamiltonian  $\mathcal{H}_{\hat{\mathbf{m}}}^{+-}$  and may be labelled

by its orientation  $\hat{\mathbf{m}}^\dagger$ . Summing over this ensemble, we obtain the grand canonical expression for the ECS,

$$\beta\mathcal{F}(\boldsymbol{\eta}) = \lim_{A_{xy} \rightarrow \infty} \frac{1}{A_{xy}} \left\{ - \ln \sum_{\hat{\mathbf{m}}} \text{Tr} e^{-\beta[\mathcal{H}_{\hat{\mathbf{m}}}^{\dagger-} - \boldsymbol{\eta} \cdot \mathbf{p}(\hat{\mathbf{m}}) A_{xy}] - \beta F^{++}} \right\} \quad (1.36)$$

$$= - \lim_{A_{xy} \rightarrow \infty} \frac{1}{A_{xy}} \ln \sum_{\hat{\mathbf{m}}} \left( \frac{Z_{\hat{\mathbf{m}}}^{\dagger-}}{Z^{++}} \right) e^{\beta \boldsymbol{\eta} \cdot \mathbf{p}(\hat{\mathbf{m}}) A_{xy}}, \quad (1.37)$$

where  $\mathbf{p}(\hat{\mathbf{m}})$  is the slope of the plane used in enforcing the boundary conditions for each member of the ensemble. The field term,  $\exp[\beta \boldsymbol{\eta} \cdot \mathbf{p}(\hat{\mathbf{m}}) A_{xy}]$ , is a fugacity for the slope,  $\mathbf{p}(\hat{\mathbf{m}})$ , and, therefore, controls the orientation of the interface.

It is sometimes useful to enlarge the ensemble further to include systems which have arbitrary macroscopic interfaces (of macroscopically planar topology but not necessarily planar) running across the box (we can, for example, imagine defining the boundary conditions by dividing the walls of the box into two *arbitrary*, simply connected parts). Denoting microscopic quantities from now on by script letters, we replace the field term,  $\boldsymbol{\eta} \cdot \mathbf{p} A_{xy}$ , with  $\boldsymbol{\eta} \cdot \int_{A_{xy}} \mathbf{p}(\mathbf{x}) dx dy = -(\eta_x \hat{x} + \eta_y \hat{y}) \cdot \int_S \hat{\mathbf{m}} dS$ . (When the interface is forced to have edges which all lie in a plane of slope  $\mathbf{p}$ , the replacement becomes an identity, since the integral of  $\hat{\mathbf{m}}$  over a closed surface vanishes.) In this larger ensemble we may, thus, write

---

<sup>†</sup> If we want this ensemble to contain interfaces of large slopes  $|\mathbf{p}|$ , the ratio (box height)/ $\sqrt{A_{xy}}$  is to be chosen sufficiently large so that the projected area of the interface remains  $A_{xy}$ , i.e., so that steep interfaces do not "cut off" corners of the box.

$$\beta\bar{f}(\eta) = \lim_{A_{xy} \rightarrow \infty} \frac{1}{A_{xy}} \left\{ -\ln \sum_{\{\hat{m}\}} \text{Tr} e^{-\beta[\mathcal{H}_{\{\hat{m}\}}^{\dagger} + (\eta_x \hat{x} + \eta_y \hat{y}) \cdot \int_S \hat{m} dS] - \beta F^{++}} \right\}, \quad (1.38)$$

where the notation  $\{\hat{m}\}$  indicates that arbitrary interfaces are included in the ensemble. Eq. (1.38) is particularly useful when pure interface models (such as the SOS model) are being considered, since (1.38) then allows an unrestricted sum over interface configurations (e.g., Jayparakash et al., 1983). Since in our box geometry  $\hat{x} \cdot \int_S \hat{m} dS = A_{xy}$  for any configuration, we may bring  $\beta\bar{f}(\eta) = \ln\{\exp[\beta A_{xy} \bar{f}(\eta)]\}/A_{xy}$  to the right hand side of Eq. (1.38) and write

$$\lim_{S \rightarrow \infty} \frac{1}{S} \left\{ \ln \sum_{\{\hat{m}\}} \text{Tr} e^{-\beta[\mathcal{H}_{\{\hat{m}\}}^{\dagger} - \lambda R(\hat{r}) \hat{r} \cdot \int_S \hat{m} dS] + \beta F^{++}} \right\} = 0, \quad (1.39)$$

which provides a coordinate independent grand canonical description of the ECS in which  $R(\hat{r})$  appears as an implicitly determined quantity.

Eq. (1.38) gives the correct expression, Eq. (1.22), for the expectation value of the slope:

$$\frac{\partial \bar{f}(\eta)}{\partial \eta} = -\langle \mathbf{p} \rangle = -\mathbf{p}. \quad (1.40)$$

The fluctuations in the slope are calculated as

$$\lim_{A_{xy} \rightarrow \infty} \left\{ A_{xy} \left[ \langle p_i p_j \rangle - \langle p_i \rangle \langle p_j \rangle \right] \right\} = -\frac{1}{\beta} \frac{\partial^2 \bar{f}(\eta)}{\partial \eta_i \partial \eta_j} = \frac{1}{\beta} \sqrt{1 + \mathbf{p}^2} K_{ij}, \quad (1.41)$$

where  $K_{ij}$  is the curvature tensor of the normalized ECS (for a more complete discussion on this tensor, see Zia, 1984; Akutsu and Akutsu, 1987a). The eigenvalues of  $K_{ij}$  are  $1/R_1$

and  $1/R_2$ , where  $R_1$  and  $R_2$  are the principal radii of curvature. Therefore, where the ECS has well defined curvature with  $R_1$  and  $R_2$  finite, the fluctuations in the slope go to zero like  $1/A_{xy}$  in the thermodynamic limit  $A_{xy} \rightarrow \infty$  and the grand canonical trace does, indeed, select a sharp slope  $\mathbf{p}$  according to the Wulff prescription (1.40). At sharp edges and corners corresponding to first order surface phase coexistence,  $K_{ij}$  is defined arbitrarily close to the discontinuity and the fluctuations in the slope vanish in the thermodynamic limit. Fluctuations would presumably be divergent at a second order (surface) critical feature which has divergent radii of curvature. For lattice gas models, bulk coexistence ends in a critical point at  $T=T_c$ . Thus, as  $T_c$  is approached in these models, the interfacial free energy goes to  $0^+$  since the critical point may be characterized by unbounded proliferation of interfacial area. Correspondingly, the normalized ECS, and, hence, the principal radii of curvature, shrink to zero, so the fluctuations become divergent when the critical point is approached, as we would expect.

## 1.3 Organization and Motivation

In the remainder of this thesis we shall apply the concepts developed above to two model calculations.<sup>†</sup> In Section 2, we derive new exact solutions for the ECS's of two-dimensional (2D) free-fermion models. These models include planar Ising models, and also the modified KDP model which is not in the Ising universality class. In Section 3, we focus on the thermal evolution of the equilibrium facet shape associated with the ECS of the three-dimensional (3D) Ising model. We will derive low-temperature expansions for the facet shape and its conjugate quantity, the anisotropic step free energy per unit length, i.e., the free energy associated with the creation of a single step on an otherwise flat crystal surface. These expansions are naturally structured as perturbation expansions about the exact result for the 2D square Ising model derived in Section 2. To date our low temperature expansion is the only analytical calculation of the facet shape and step free energy for a full interface model, i.e., a model which includes overhanging and bulk excitations.

A unifying motivation for much of the work presented in this dissertation was the following remarkable fact, which was first pointed out by van Beijeren and Nolden, and also by Akutsu and Akutsu (1987b), in 1987, and will be derived in Section 3: Whenever the facet edge is a second order phase boundary, it follows from the geometry of the Wulff construction that the conjugacy between the ECS and the interfacial free energy per unit area contains a precisely analogous conjugacy between the equilibrium facet shape and the step free energy per unit length. This means that *we may think of facets as 2D ECS's which are embedded in the surface of a 3D ECS!*

---

<sup>†</sup> Sections 2 and 3 are adaptations to thesis format of research articles either already published (Holzer and Wortis, 1989; Holzer, 1990a) or submitted for publication (Holzer, 1990b).

## 2. A General, Exact Solution for Equilibrium Crystal Shapes in Two Dimensions for Free-Fermion Models

### 2.1 Introductory Remarks

As a first application of the concepts discussed in Section 1, we will now derive an exact solution for the ECS's of 2D planar Ising models. This solution immediately generalizes to the somewhat larger class of so-called free-fermion models, which includes non-Ising models and is the class of all models for which the bulk free energy may be found exactly by the Feynman<sup>†</sup>-Vdovichenko (FV) method (Feynman, 1972; Vdovichenko, 1965; see also Landau and Lifshitz, 1968; Morita, 1986) [or equivalently by the Pfaffian method (Temperley and Fisher, 1961; Kasteleyn, 1961, 1963; see also McCoy and Wu, 1973)].

There are a number of reasons to study 2D Ising models: The Ising model in zero magnetic field and below the bulk transition temperature ( $T_c$ ) is the simplest model describing a full two-phase system [as opposed to a pure "interface" model such as the SOS model (e.g., Leamy et al., 1975; the SOS model is also discussed in Section 3)]. The two-dimensional (2D) Ising model is particularly interesting for at least two reasons: 1.) Exact solutions are possible (Onsager, 1944) and 2.) as we shall see in Section 3, these exact solutions are valuable in approximating the shapes of facets of 3D Ising ECS's. Since some real crystals, such as noble gas crystals, may possibly be approximated by an appropriate 3D Ising model, 2D Ising ECS's may also have some relevance to the analysis

---

<sup>†</sup> Feynman's solution for the bulk free energy of the Ising model predates Vdovichenko's (see Sherman, 1960) but was apparently not published until 1972. His solution is only slightly different from Vdovichenko's.

of experimental facet-shape data. Finally, we mention, that prior to this work, exact ECS's were known (from calculations conceptually completely different from ours) for the rectangular (Rottman and Wortis, 1981; Avron et al., 1982; Zia and Avron, 1982), triangular and honeycomb lattices (Zia, 1986) only.<sup>†</sup>

Our calculation is formulated in the grand canonical description and makes use of an exact mapping of the interface onto a FV "random" walker. This mapping makes possible the exact evaluation of the grand canonical trace in the thermodynamic limit. Before presenting the derivation, let us first state the simple solution, so it will clear what our aim is: If the "momentum-space" FV lattice-walk matrix for a lattice  $\mathcal{L}^*$  (the dual of the direct lattice  $\mathcal{L}$ ) is denoted by  $\Lambda(k_x, k_y)$ , then the ECS for the dual model on  $\mathcal{L}$ , represented in Cartesian coordinates as  $Y(X)$ , is given by

$$\text{Det} \left\{ \mathbf{1} - \Lambda[k_x = i\beta\lambda Y, k_y = -i\beta\lambda X; \{\omega\}] \right\} = 0, \quad T < T_c, \quad (2.1)$$

where  $\{\omega\}$  denotes the set of Boltzmann weights associated with the steps of the lattice walk. The matrix  $\Lambda$  is a finite dimensional  $q \times q$  matrix, where  $q$  is even and, in the simplest cases, just equal to the coordination number of the lattice. Since the bulk partition function of free-fermion models can be expressed in terms of an integral of the form  $\int dk_x dk_y \ln \text{Det}(\mathbf{1} - \Lambda)$  [e.g., Landau and Lifshitz, 1968 and also below], the ECS for these models may, in fact, be read off from the analytic form of the bulk free energy!

The FV method and its refinements have a venerable history. The root of the FV method may be considered to be an unpublished conjecture by Feynman which was proved by Sherman in 1960 (the Sherman theorem, see also Sherman, 1963; Burgoyne, 1963).

---

<sup>†</sup> In the symmetry directions, the interfacial free energies for these lattices were first published by Fisher and Ferdinand in 1967.

Feynman re-interpreted the seminal work of Kac and Ward (1952) on a combinatorial solution of the Ising model in terms of an identity between lattice-path sums and the graphical expansion of the Ising model. Making implicit use of the Sherman theorem, Vdovichenko gave an elegant, intuitive solution to the Onsager problem in 1965. The first application of these methods to Ising interfaces was recently reported by Calheiros, Johannesen, and Merlini in 1987. The FV has now been textbook material (notably Landau and Lifshitz, 1968) for some twenty years but appears not to be as well and widely appreciated as perhaps it should be. We shall explain the method in detail below.

The remainder of this Section is organized as follows: In Sub-section 2.2, we derive equation (2.1), discuss its range of validity and give some examples of previously unknown Ising ECS's. In Sub-section 2.3, we explore, in some detail, a pedagogical example of a non-Ising case for which Eq. (2.1) is also valid. We apply the FV method to the free-fermion cases of the eight-vertex model (Fan and Wu, 1969,1970; Sutherland, 1970). The coexisting phases of the model are identified, and Eq. (2.1) is shown to give the correct ECS of the corresponding dual models even for the non-Ising case of the modified KDP model (Wu, 1967, 1968).

## 2.2 Derivation

For definiteness consider an Ising model with ferromagnetic interactions. The generalization to other free-fermion models will be made at the end of this Sub-section. Let the 2D Ising system be defined on a rectangular strip  $\Omega$  (our "box") of a planar lattice  $\mathcal{L}$ , i.e., a lattice with non-crossing bonds. The strip  $\Omega$  has a geometric dual, the strip  $\Omega^*$  of the dual lattice  $\mathcal{L}^*$ . Without loss of generality, we take the lattice to have basis vectors  $\hat{x}$  and  $\hat{y}$ , and we align the strip with the y-axis. (It is always possible to choose a coordinate



system in which the basis vectors of the lattice are orthogonal unit vectors.) We take the width of  $\Omega^*$  to be  $N$  and think of the length of  $\Omega^*$  as finite but tending toward infinity (Fig. 1). At zero magnetic field and  $T < T_c$ , a phase of predominantly “up” (+) spins can coexist with a phase of predominantly “down” (–) spins. The microscopic configurations of the system can of course be described in terms of the spins on  $\Omega$ ; but, in the present context it is much more useful to think in terms of the bonds of  $\Omega^*$  dual to the “broken” bonds of  $\Omega$ , which connect spins of opposite sign (see Fig. 2.1). We consider these bonds to be elementary microscopic interfaces of microscopic normal  $\hat{m}$  which we take to point from – to +. If the coupling between spins at sites  $i$  and  $j$  of  $\Omega$  is  $K_{ij}$ , the creation of an elementary interface between them costs energy  $2K_{ij}/\beta$  and is, therefore, associated with a Boltzmann factor of  $\omega_{ij} = \exp(-2K_{ij})$ .

A macroscopic interface between the (+)-phase and the (–)-phase can be forced into the system as follows: Divide the boundary of  $\Omega$  into two connected (1D) regions and fix the boundary spins in one region to be + and in the other region to be –. As shown in Fig. 2.2, this forces an interface to run across the strip<sup>†</sup> from the dual spin  $\sigma_{(0,0)}^*$  at  $(0,0)$  to the dual spin  $\sigma_{(N,M)}^*$  at  $(N,M)$  on the boundary of  $\Omega^*$ . With this (+–) choice of boundary condition, denote the Hamiltonian of the system by  $\mathcal{H}_{N,M}^{+-}$  and its partition function by  $Z_{N,M}^{+-} = \text{Tr} \exp[-\beta \mathcal{H}_{N,M}^{+-}]$ . If all boundary spins are fixed to be +, denote the Hamiltonian of the system by  $\mathcal{H}^{++}$  and its partition function by  $Z^{++} = \text{Tr} \exp[-\beta \mathcal{H}^{++}]$ . In this latter case, there can be no macroscopic interface across the strip, which now contains only the pure (+) phase. The sample free energy  $\beta F^{+-} = -\ln Z_{N,M}^{+-}$  contains contributions from the bulk, from the boundaries, and from the interface running from  $(0,0)$  to  $(N,M)$ . The sample free energy  $\beta F^{++} = -\ln Z^{++}$  contains contributions from the bulk and from the boundaries,

---

<sup>†</sup> Because Ising models at  $T < T_c$  in zero field are at two-phase coexistence, boundary conditions automatically adjust the net magnetization (total particle density) in addition to orienting the interface.

only. Since the Ising model is invariant under overall change of sign of the spins, the extensive (order  $N+M$ ) boundary contributions are the same whether  $(+-)$ - or  $(++)$ -boundary conditions are imposed. The interfacial free energy per unit length for an interface of macroscopic orientation  $\hat{\mathbf{m}}$  is therefore given by the 2D version of Eq. (1.34) as

$$\beta\Gamma(\hat{\mathbf{m}}) \equiv -\lim_{L \rightarrow \infty} \frac{1}{L} \ln \left( \frac{Z_{N,M}^{+-}}{Z^{++}} \right), \quad (2.2)$$

where  $L \equiv \sqrt{N^2 + M^2}$ ,  $\hat{\mathbf{m}} = (-M, N)/L$ . We will use the convention that  $N > 0$  ( $N < 0$ ) corresponds to the upper (lower) half of the strip being in the  $(+)$ -phase and the lower (upper) half in the  $(-)$ -phase.

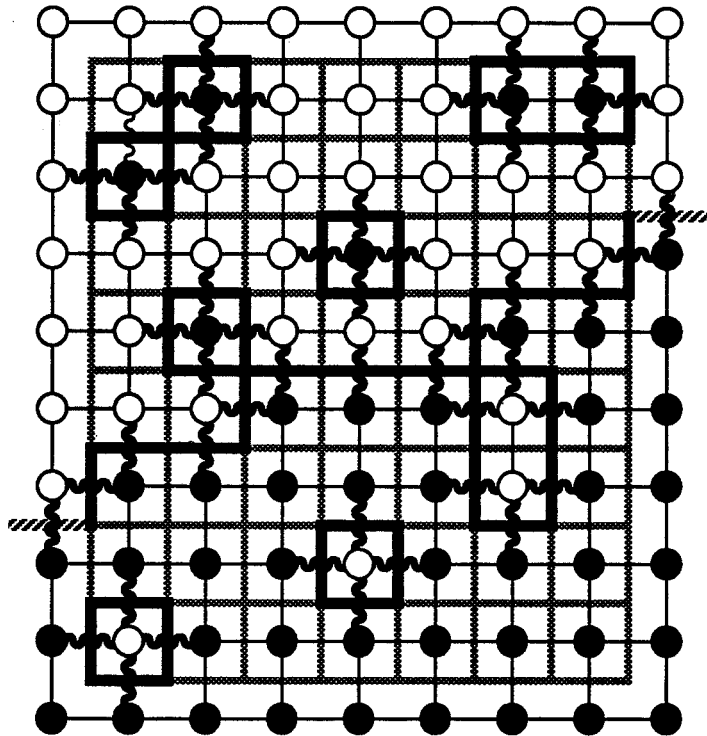


FIG. 2.1. A configuration of a ferromagnetic Ising model defined on the square lattice of thin black lines. A spin of sign  $+1$  is denoted by a white circle; a spin of sign  $-1$ , by a black circle. The dual lattice is drawn in grey. We call the bonds between spins of opposite sign “broken bonds”. Broken bonds are drawn as wavy lines. We consider the bonds dual to broken bonds to be elementary interfaces. Elementary interfaces are indicated by heavy black lines.

$\Gamma(\hat{\mathbf{m}})$  is related to the high-T correlation length of the dual system in the  $\hat{\mathbf{u}}$  direction,  $\xi^*(\hat{\mathbf{u}})$ , via the well-known duality relation (e.g., Watson, 1968; Fisher, 1969; Zia, 1978; Fradkin et al., 1978)

$$\beta\Gamma(\hat{\mathbf{m}}) = -\lim_{L \rightarrow \infty} \frac{1}{L} \ln \langle \sigma_{(0,0)}^* \sigma_{(N,M)}^* \rangle = 1/\xi^*(\hat{\mathbf{u}}), \quad (2.3)$$

where  $\hat{\mathbf{u}} = (N, M)/L$ , with  $\hat{\mathbf{m}} \cdot \hat{\mathbf{u}} = 0$ . Eq. (2.3) forms the basis of all solutions to the 2D ECS problem which were known prior to our result Eq. (2.1): A calculation of the dual-lattice correlations  $\langle \sigma_{(0,0)}^* \sigma_{(N,M)}^* \rangle$  in the thermodynamic limit,  $N, M \rightarrow \infty$ , with  $\hat{\mathbf{m}}$  ( $\hat{\mathbf{u}}$ ) fixed, gives  $\gamma(\hat{\mathbf{m}})$ , from which the ECS is determined via the Wulff construction.

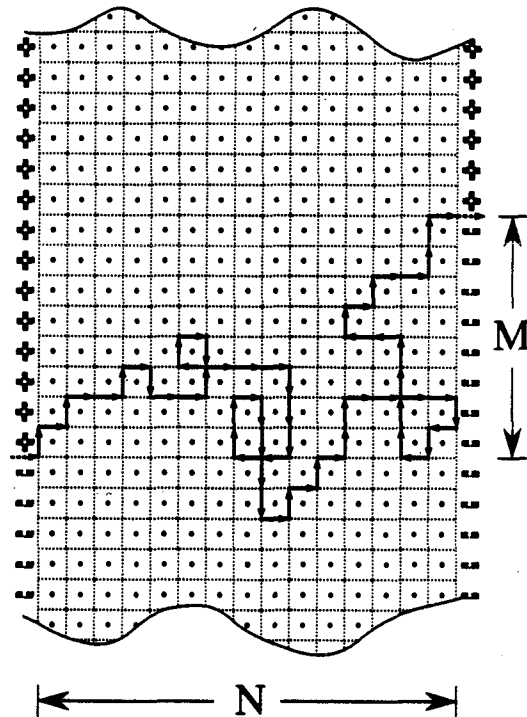


FIG. 2.2. The boundary conditions considered in the derivation of the exact 2D solution, illustrated on a rectangular lattice: The strip  $\Omega$  of the square lattice  $\mathcal{L}$  is defined by the heavy dots, and the spins on its boundary are forced to be either "up" (+) or "down" (-) as shown. Its dual, the strip  $\Omega^*$  of the dual lattice  $\mathcal{L}^*$ , is indicated by the grid of dotted lines. The (+-) boundary conditions force an interface into the system, which runs from dual spin  $\sigma_{(0,0)}^*$  to dual spin  $\sigma_{(N,M)}^*$ . The lattice walk shown illustrates a term in the sum, Eq. (2.9).

Here we shall calculate the ECS directly in the grand canonical ensemble, without going first through the auxiliary function  $\Gamma(\hat{\mathbf{m}})$ . If the ECS is represented in 2D Cartesian coordinates as  $Y(X)$ , Eq. (1.38) becomes, in the variables of the present problem,

$$\beta\lambda Y(X) = \lim_{|N| \rightarrow \infty} \frac{1}{|N|b_x} \left[ -\ln \sum_M \text{Tr} e^{-\beta \left( \mathcal{Z}_{N,M}^{+-} - \lambda X \hat{x} \cdot \sum_i \hat{\mathbf{m}}_i d_i \right)} - \beta F^{++} \right], \quad (2.4)$$

where the sum in the exponential extends over all microscopic interfaces whose segment lengths and normals are denoted by  $d_i$  and  $\hat{\mathbf{m}}_i$ . In Eq. (2.4) the sum over  $M$  sums over an ensemble of systems of all possible macroscopic interface orientations. We take each system of this ensemble to be defined on  $\Omega$  with  $+-$  boundary conditions labeled by  $M$ . Because  $X$  is constant,  $\sum_i \hat{\mathbf{m}}_i d_i$  vanishes for microscopic interfaces forming closed loops. Thus, the only contributions to the field term in the exponent arise from the line from  $(0,0)$  to  $(N,M)$ , and that contribution is  $-\lambda X \hat{x} \cdot \sum_i \hat{\mathbf{m}}_i d_i = \lambda XM$ , independent of the particular path traced out by the line. [This simplification is a manifestation of the fact that in two dimensions there is no distinction between the ensembles Eq. (1.36) and Eq. (1.38).] Thus, Eq. (2.5) becomes

$$\beta\lambda Y(X) = - \lim_{|N| \rightarrow \infty} \frac{1}{N} \ln \sum_M e^{-\beta\lambda XM} \left( \frac{Z_{N,M}^{+-}}{Z^{++}} \right). \quad (2.5)$$

We now evaluate  $Z_{N,M}^{+-}/Z^{++}$  using the Vdovichenko-Feynman “random walker” method.

To see what the interface has to do with “walkers”, consider the standard low-T expansions of  $Z_{N,M}^{+-}$  and  $Z^{++}$  (Kramers and Wannier, 1941):

$$Z^{++} = e^{-\beta E_0} \sum_{\{G\}_{++}} W(G) \equiv e^{-\beta E_0} \Sigma_{++} \quad (2.6)$$

$$Z_{N,M}^{+-} = e^{-\beta E_0} \sum_{\{G\}_{+-}} W(G) \equiv e^{-\beta E_0} \Sigma_{+-}. \quad (2.7)$$

In Eqs. (2.6) and (2.7),  $E_0$  is the ground state energy of the system with the  $(++)$  boundary condition,  $\{G\}_{++}$  is the set of graphs which can be drawn on  $\Omega^*$  such that each graph is equivalent to a configuration of elementary interfaces when the  $(++)$  boundary condition is imposed,  $\{G\}_{+-}$  is the corresponding set of graphs for the  $(+-)$  boundary condition, and each graph is summed with weight  $W(G)$ . Since each link of a graph  $G$  corresponds to an elementary interface, the weight of  $G$  is given by  $W(G) = \prod_{\text{links}} \omega_{ij}$ , where the product is taken over all the links of  $G$ . The set  $\{G\}_{++}$  contains closed polygons (loops) only. The set  $\{G\}_{+-}$  contains loops and, in addition, open graphs connecting  $(0,0)$  and  $(N,M)$ . If  $(O)$  denotes the sum of  $W(G)$  over all single closed loops,  $(O \sim O)$  the sum over all pairs of closed loops,  $(\text{---})$  the sum over the open graphs,  $(\text{---} \sim O)$  the sum over open graphs in the presence of single closed loops, etc., we can write symbolically

$$\Sigma_{++} = 1 + (O) + (O \sim O) + \dots$$

$$\Sigma_{+-} = (\text{---}) + (\text{---} \sim O) + (\text{---} \sim O \sim O) + \dots$$

Instead of evaluating the sums over closed loops, it turns out to be easier, following Feynman and Vdovichenko, to sum over closed *directed* lattice paths (lattice walks). Give weight  $W(\underline{G}) = (-1)^S \prod_{\text{steps}} \omega_{ij}$  to each single directed closed path  $\underline{G}$ , where  $S$  is the number of self-intersections of the path and the product is over the steps (directed links) of the path. The upshot of the Sherman theorem, which holds for any planar embedded lattice with non-crossing bonds, is that  $\Sigma_{++} = \exp(\mathcal{G})$ , where  $(\mathcal{G})$  denotes the sum of  $W(\underline{G})$  over all possible  $\underline{G}$ . The crucial point here is that the  $n$ -loop term of the directed paths has uncoupled into  $(\mathcal{G})^n/n!$ . Hence, if  $(\text{---})$  denotes the sum over open graphs which are counted using directed paths weighted in the same manner as the closed paths of  $(\mathcal{G})$ , one is led to expect that  $(\text{---})$  uncouples from the  $(\mathcal{G})$ 's, so that,  $Z_{N,M}^{+-} = (\text{---})Z^{++}$ . Calheiros, Johannesen and Merlini showed that, indeed, this follows rigorously from the Sherman

theorem by considering the closed-loop expansion with an auxiliary bond  $J_a^*$  external to  $\mathcal{L}^*$  connecting the dual sites  $(0,0)$  and  $(N,M)$ . In the limit  $J_a^* \rightarrow 0$ , one finds that<sup>†</sup>

$$\frac{Z_{N,M}^{+-}}{Z^{++}} = \sum_{(0,0) \rightarrow (N,M)} (-1)^S \prod_{\text{Steps}} \omega_{ij}, \quad (2.8)$$

where the sum extends over all directed paths from  $(0,0)$  to  $(N,M)$ , the product is over all directed links or steps of the path, and  $S$  is the number of self intersections of the path.

*[He] flung himself upon his horse  
and rode madly off in all directions.*

S. LEACOCK

By following Feynman and Vdovichenko, the sum Eq. (2.8) can now easily be evaluated, at least in the thermodynamic limit, as  $|N| \rightarrow \infty$ . Let  $\{\mathbf{d}_\mu\}$ , with  $\mu \in \{1, 2, \dots, q\}$ , be the set of vectors which correspond to all possible distinct directed bonds of  $\mathcal{L}^*$ . If  $\mathcal{L}^*$  is a Bravais lattice,  $q$  is the coordination number; otherwise,  $q$  is the sum of the coordination numbers for each site of the unit cell. (Since for each  $\mathbf{d}_\mu$  there is a  $\mathbf{d}_\nu = -\mathbf{d}_\mu$ ,  $q$  is even.) Imagine the paths from  $(0,0)$  to  $(N,M)$  to be generated by a lattice walker and denote by  $\mathbf{d}_\mu(n)$  the  $n$ th step of the walk. With each change of the walker's direction we associate a phase factor  $\exp(i\phi_{\mu\nu}/2)$ , where  $\phi_{\mu\nu}$  is the angle ("of turn") from  $\mathbf{d}_\nu(n)$  to  $\mathbf{d}_\mu(n+1)$ , defined such that  $|\phi_{\mu\nu}| < \pi$ . ( $|\phi_{\mu\nu}| = \pi$  will be excluded explicitly.) This keeps track of the parity of self-intersections because the product of these phase factors over a

---

<sup>†</sup> This expression is exact if the interface problem is formulated as done here for a system with fixed boundary conditions such as the strip  $\Omega$ . If, alternatively, one formulates the interface problem for a system with a pair of "frustrated" plaquettes joined by a "seam" of reversed bonds, additional terms appear; however, these additional terms do not contribute to interfacial (order  $L$ ) properties in the thermodynamic limit, as the separation between the frustrated plaquettes becomes macroscopic.

single closed loop gives  $-(-1)^S$ , a topological property of planar embedded loops (Whitney, 1937). Let  $\Psi_{\mu\kappa}(x,y ; n)$  be the sum over all weighted walks (including the phase factors) which step onto the origin with  $\mathbf{d}_\kappa(0)$  and  $n$  steps later, onto site  $(x,y)$  with  $\mathbf{d}_\mu(n)$ . These  $\Psi_{\mu\kappa}(x,y ; n)$ , then, obey a recursion equation which, in the limit as the strip width  $|N| \rightarrow \infty$  and full translational symmetry is restored, can be diagonalized via a Fourier transform to obtain (e.g., Landau and Lifshitz, 1968)

$$\Psi_{\mu\kappa}(\mathbf{k}_x, \mathbf{k}_y ; n+1) = \sum_{\nu} \Lambda_{\mu\nu}(\mathbf{k}_x, \mathbf{k}_y) \Psi_{\nu\kappa}(\mathbf{k}_x, \mathbf{k}_y ; n) . \quad (2.9)$$

The  $\Lambda_{\mu\nu}$  are the elements of the  $q \times q$  matrix  $\Lambda$  and have the form

$$\Lambda_{\mu\nu}(\mathbf{k}_x, \mathbf{k}_y ; \omega_{ij}) = \omega_{ij} e^{i\phi_{\mu\nu}/2} e^{-i\mathbf{k} \cdot \mathbf{d}_\mu} (1 - \delta_{\mathbf{d}_\mu, -\mathbf{d}_\nu}) , \quad (2.10)$$

where  $\mathbf{k}=(k_x, k_y)$ . The Kronecker  $\delta$  in (2.10) ensures that walks cannot immediately backtrack ( $|\phi_{\mu\nu}|=\pi$ ). The sum over all paths from  $(0,0)$  to  $(N,M)$ , Eq. (2.8), can now be written in terms of  $\Lambda$  as<sup>†</sup>

$$\frac{Z_{N,M}^{+-}}{Z^{++}} = \iint_{-\pi}^{\pi} \frac{dk_x dk_y}{(2\pi)^2} e^{i(k_x N + k_y M)} \sum_{m=0}^{\infty} [\Lambda^m]_{\mu_{\text{out}} \nu_{\text{in}}} . \quad (2.11)$$

In principle, the strip  $\Omega$  should be chosen such that  $\mu_{\text{out}}=\nu_{\text{in}}$ , so self-intersections are properly accounted for; however, in the thermodynamic limit this is not important, since we can then replace  $[\Lambda^m]_{\mu_{\text{out}} \nu_{\text{in}}}$  with  $\text{Tr}(\Lambda^m)$ .

---

<sup>†</sup> To walk from  $(0,0)$  to  $(N,M)$  a minimum number of  $N_0(N,M)$  steps is necessary. In the original presentation of this work [Holzer (1990a)], the first  $N_0(N,M)$  terms of the sum  $\sum_{m=0}^{\infty} \Lambda^m$  were, therefore, explicitly omitted. However, since  $\int dk_x \int dk_y \exp[i(k_x N + k_y M)] \Lambda^P$  is identically zero if  $P < N_0(N,M)$  [ $\Psi_{\mu\kappa}(x,y ; n)=0$  if  $n < N_0(N,M)$ ], we may sum over all non-negative powers of  $\Lambda$ , thus obtaining a slightly more aesthetic expression for the ECS.

The FV method gives us an intuitive picture of a walker, described by the step-to-step transition matrix  $\Lambda$ , generating all possible interface configurations. While  $\Lambda$  cannot keep track of the microscopic interface orientations, the field term of Eq. (2.5) can be incorporated into  $\Lambda$  because it depends only on the y-coordinate  $M$  of the final step of the walk. Since with every transition to a step  $\mathbf{d}_\mu$  the walker's y-coordinate changes by  $\hat{\mathbf{y}} \cdot \mathbf{d}_\mu$ , we can associate with this transition a field term  $\exp(-\beta\lambda X \hat{\mathbf{y}} \cdot \mathbf{d}_\mu)$  in addition to the topological phase factor and the Boltzmann weight. The product of these field-term factors over the path from  $(0,0)$  to  $(N,M)$  gives a total field term of  $\exp(-\beta\lambda XM)$ . Diagonalizing the corresponding recursion equations, one arrives (trivially) at the same form of  $\Lambda$  as in the case  $X=0$  except that, where we used to have just  $k_y$ , we now have  $k_y - i\beta\lambda X$ . Thus,  $(Z_{N,M}^{+-}/Z^{++}) \exp(-\beta\lambda XM)$  is simply given by the right hand side of (2.11) except that  $\Lambda(k_x, k_y)$  is replaced with  $\Lambda(k_x, k_y - i\beta\lambda X)$ . Substituting this form of  $(Z_{N,M}^{+-}/Z^{++}) \times \exp(-\beta\lambda XM)$  into Eq. (2.5), we obtain<sup>†</sup>

$$\beta\lambda Y(X) = - \lim_{|N| \rightarrow \infty} \frac{1}{N} \ln \left\{ \sum_{M=-\infty}^{+\infty} \iint_{-\pi}^{\pi} \frac{dk_x dk_y}{(2\pi)^2} e^{i(k_x N + k_y M)} \text{Tr}(\mathbf{1} - \Lambda)^{-1} \right\}, \quad (2.12)$$

---

<sup>†</sup> It may be noticed that the same integrand as in Eq. (2.12) is obtained by substituting Eq. (2.11) into Eq. (2.5) and making a change of variable to  $k'_y = k_y + i\beta\lambda X$ . We then get the same integrand as a function of  $k'_y$  as that which is obtained as a function of  $k_y$  by incorporating the field term into  $\Lambda$  from the beginning, except that the integration over  $k'_y$  is from  $-\pi + i\beta\lambda X$  to  $\pi + i\beta\lambda X$ . That this is consistent with Eq. (2.12) follows simply from the translational invariance of the lattice, which implies that the integrand is invariant under  $\text{Re}(k_x, k_y) \rightarrow \text{Re}(k_x, k_y) + (2\pi n, 2\pi m)$ , with  $n, m$  integers. Thus, if we integrate in the  $k'_y$ -plane along the contour  $C = C_1 \cup C_2 \cup C_3$ , where  $C_1$  is the straight line from  $i\beta\lambda X$  to  $-\pi$ ,  $C_2$  the straight line from  $-\pi$  to  $\pi$ , and  $C_3$  the straight line from  $\pi$  to  $i\beta\lambda X$ , the contributions from  $C_1$  and  $C_3$  cancel, leaving only the integration along the real axis, Eq. (2.12).



where  $\Lambda = \Lambda(k_x, k_y - i\beta\lambda X)$  and  $X$  must be bounded such that  $\Lambda^P \rightarrow 0$  as  $P \rightarrow \infty$ . Summing over  $M$ , using the identity  $\sum_{M=-\infty}^{+\infty} \exp(ik_y M) = 2\pi \sum_{n=-\infty}^{+\infty} \delta(k_y - 2\pi n)$ , and then integrating over  $k_y$ , we obtain

$$\beta\lambda Y(X) = - \lim_{|N| \rightarrow \infty} \frac{1}{N} \ln \left[ \int_{-\pi}^{\pi} \frac{dk_x}{2\pi} e^{ik_x N} \frac{\sum_{i=1}^q \prod_{j \neq i}^q (1 - \lambda_j)}{\text{Det}(1 - \Lambda)} \right], \quad (2.13)$$

where  $\Lambda = \Lambda(k_x, -i\beta\lambda X)$  and  $\lambda_i$ , with  $i \in \{1, \dots, q\}$ , denote the eigenvalues of  $\Lambda$ . In the thermodynamic limit  $|N| \rightarrow \infty$ , only the saddle point contributes to the integral of Eq. (2.13). With  $\Lambda$  of the form (2.10), the condition for the integrand of (2.13) to have a saddlepoint<sup>†</sup> is given by  $\text{Det}(1 - \Lambda) = 0$ , which is approached asymptotically like  $1/N$ , i.e.,  $\text{Det}(1 - \Lambda) \rightarrow 0$  like  $1/N$  as  $|N| \rightarrow \infty$ . Thus, (2.13) is simply evaluated as

$$\beta\lambda Y(X) = -i\bar{k}_x, \quad (2.14)$$

where  $\bar{k}_x$  is the solution to  $\text{Det}[1 - \Lambda(\bar{k}_x, -i\beta\lambda X)] = 0$  which may be expressed succinctly in the form of Eq. (2.1). The propagator for lattice paths is defined as the amplitude for the walker to arrive after any number of steps, i.e., as  $\sum_{n=0}^{\infty} \Lambda^n = (1 - \Lambda)^{-1}$ . Eq. (2.1), therefore, expresses the ECS as the locus of purely imaginary poles of the determinant of the propagator for lattice paths.

---

<sup>†</sup>  $\Lambda$  is a matrix of exponentials and, therefore,  $\text{Det}(1 - \Lambda)$  and  $C(\Lambda) \equiv \sum_{i=1}^q \prod_{j \neq i}^q (1 - \lambda_j)$  are analytic functions of  $k_x$  and  $k_y$ . The saddlepoint condition for (14) is, thus, found as usual by differentiating  $ik_x N + \ln C(\Lambda) - \ln \text{Det}(1 - \Lambda)$  and setting the result equal to zero. That the saddle point is given by  $\text{Det}(1 - \Lambda) = 0$  is also clear from the fact that the form of  $\Lambda$ , combined with the translational invariance of the lattice, implies that  $C(\Lambda)$  and  $\text{Det}(1 - \Lambda)$  must be polynomials of order  $\sim q$  in  $z$  and  $1/z$ , where  $z = \exp(ik_x)$ . The only contributions to the integral can come from the zeros of  $\text{Det}(1 - \Lambda)$ .

An alternative way of evaluating (2.12) is to make use the fact that replacing  $\text{Tr}(\mathbf{1}-\mathbf{\Lambda})^{-1}$  with  $1/\text{Det}(\mathbf{1}-\mathbf{\Lambda})$  in the integrand of (2.12) does not change the saddle point in the thermodynamic limit  $|N| \rightarrow \infty$ . This allows us to obtain further insight into the analytical structure of solution (2.1). Replacing  $\text{Tr}(\mathbf{1}-\mathbf{\Lambda})^{-1}$  with  $1/\text{Det}(\mathbf{1}-\mathbf{\Lambda})$ , summing over  $M$ , integrating over  $k_y$ , and making the change of variable  $e^{ik_x} = z$  leaves us with the contour integral,

$$\beta\lambda Y(X) = - \lim_{|N| \rightarrow \infty} \frac{1}{N} \ln \left\{ \oint \frac{dz}{2\pi i} \frac{z^N}{z \text{Det}(\mathbf{1}-\mathbf{\Lambda})} \right\}, \quad (2.15)$$

where  $\mathbf{\Lambda} = \mathbf{\Lambda}(k_x, 0 - i\beta\lambda X)$  and the contour of integration is counter clockwise around the unit circle  $|z|=1$ . Since for matrices  $\mathbf{\Lambda}$  of the form (2.10) translational invariance of the lattice implies that  $\text{Det}(\mathbf{1}-\mathbf{\Lambda})$  is just a polynomial in  $z$  and  $1/z$ , the result, Eq. (2.14), follows immediately. For all the Ising models for which the exact (bulk) solution is known (e.g., I. Syozi, 1972 and references therein), the poles of the integral of Eq. (2.15) have a very simple structure: For all these models  $z\text{Det}(\mathbf{1}-\mathbf{\Lambda})$  is of the form  $[z-z_1(X)][z-z_2(X)]$  for appropriate orientation of the axes. The roots  $z_1(X)$  and  $z_2(X)$  are real and positive for  $X \in [X_{\min}, X_{\max}]$  and  $T < T_c$ . For a range of the field variable  $X \in [X_A, X_B] \subset [X_{\min}, X_{\max}]$ ,  $z_1(X) \leq 1$  and  $z_2(X) \geq 1$ . Thus, for  $X \in [X_A, X_B]$ , Eq. (2.15) is evaluated as  $\beta\lambda Y(X) = -\ln[z_1(X)]$ , if  $N > 0$ , and as  $-\ln[z_2(X)]$ , if  $N < 0$ . Since the outward normal of the interface is  $\hat{\mathbf{m}} = (-\langle M \rangle(X), N)/L$ ,  $N > 0$  ( $N < 0$ ) corresponds to the ‘‘upper (lower) half’’ of the ECS. If  $X_A \neq X_{\min}$  and  $X_B \neq X_{\max}$ , and  $X \in [X_{\min}, X_A] \cup [X_B, X_{\max}]$ , then (by definition) either both or neither of the poles  $z_1, z_2$  lie inside  $|z|=1$ . In this case we find that  $\mathbf{\Lambda}^P(k_x, k_y - i\beta\lambda X)$  no longer converges for all  $(k_x, k_y)$  as  $P \rightarrow \infty$ . Hence, for  $X \in [X_{\min}, X_A] \cup [X_B, X_{\max}]$ , the substitution  $\mathbf{\Lambda}(k_x, k_y) \rightarrow \mathbf{\Lambda}(k_x, k_y - i\beta\lambda X)$ , which incorporates the field term of Eq. (2.5) into the matrix  $\mathbf{\Lambda}$ , is no longer well founded mathematically for a purely real integration path in the  $k_x$ -plane. However, since the ECS of any 2D system with finite, short-range forces is

smooth<sup>†</sup> for  $0 < T < T_c$ , it follows from *analytical continuity* that the upper half of the ECS must be given by  $-\ln[z_1(X)]$  and the lower half, by  $-\ln[z_2(X)]$  for the *entire* range of field  $X \in [X_{\min}, X_{\max}]$ . This analytical continuation amounts to deforming the integration contour of Eq. (2.15) to include the relevant pole, thereby avoiding regions in the  $z$ -plane ( $k_x$ -plane) where the modulus of one or more eigenvalues of  $\Lambda(k_x, -i\beta\lambda X)$  is greater or equal to unity [two explicit examples are given in Appendix A]. (In writing down the integral as its saddle point as in Eq. (2.14), this analytical continuation is implicit.) In general, the ECS problem is defined for those fields  $X$  that allow a path in the  $k_x$ -plane from  $-\pi$  to  $\pi$  along which the modulus of every eigenvalue of  $\Lambda(k_x, -i\beta\lambda X)$  remains less than unity. To summarize, we have for  $T < T_c$  and  $X_{\min} \leq X \leq X_{\max}$

$$\beta\lambda Y(X) = \begin{cases} -\ln z_1, & \text{if } \hat{\mathbf{m}} \cdot \hat{\mathbf{y}} \geq 0 \quad (\text{upper half}) \\ -\ln z_2, & \text{if } \hat{\mathbf{m}} \cdot \hat{\mathbf{y}} \leq 0 \quad (\text{lower half}) \end{cases}, \quad (2.16)$$

which can, again, be expressed succinctly in the form of Eq. (2.1).

The problem of calculating the ECS has been reduced to the problem of finding the purely imaginary zeros of  $\text{Det}(\mathbf{1} - \Lambda)$ . While it is straightforward to construct the matrix  $\Lambda$  for a given lattice, this is not necessary if the analytic form of the bulk free energy of the Ising system defined on either  $\mathcal{L}$  or  $\mathcal{L}^*$  is known. Using the FV method to evaluate  $\Sigma_{++}$  [cf. Eq. (2.6)], which is what the method was originally designed for, one finds that the bulk free energy per unit cell of the model defined on  $\mathcal{L}$  is given by

$$\beta f_b = \beta \epsilon_0 - \frac{1}{2} \int_{-\pi}^{\pi} \int_{-\pi}^{\pi} \frac{dk_x dk_y}{(2\pi)^2} \ln \text{Det} \{ \mathbf{1} - \Lambda_{\mathcal{L}^*}[k_x, k_y; \exp(-2K_{ij})] \} \quad (2.17)$$

---

<sup>†</sup> We argued in the Introduction that singular features of the ECS correspond to phase boundaries. Here, the interface is a one-dimensional object and, as such, it can have phase transitions only at  $T=0$ .

In Eq. (2.17)  $\epsilon_0$  is the ground state energy per unit cell, the factor of 1/2 comes from the fact that directed paths may be traversed in two directions, and the subscript  $\mathcal{L}^*$  emphasizes that  $\Lambda$  describes a walk representing the interface on the dual lattice  $\mathcal{L}^*$ . Thus, the ECS for the Ising system can simply be read off from the analytic form of the bulk free energy!<sup>†</sup> This is a remarkable result because, naively, at least, one would not expect the analytic form of the *bulk* free energy to contain complete information on the surface thermodynamics. The bulk free energy is normally given in terms of  $\Lambda_{\mathcal{L}}$  because the FV walker problem is traditionally formulated in terms of high-T ( $\tanh K$ ) graphs on the direct lattice  $\mathcal{L}$ . The corresponding form of the free energy is

$$\beta f_b = -\ln 2^{\ell} \prod \cosh K_{ij} - \frac{1}{2} \int_{-\pi}^{\pi} \int_{-\pi}^{\pi} \frac{dk_x dk_y}{(2\pi)^2} \ln \text{Det} [1 - \Lambda_{\mathcal{L}}(k_x, k_y; \tanh K_{ij})] \quad , \quad (2.18)$$

where  $\ell$  is the number of sites per unit cell and the product is over all the bonds of the unit cell. As a direct consequence of the duality between the systems on  $\mathcal{L}$  and  $\mathcal{L}^*$ , Eq. (2.18) can be obtained simply from (2.17) by expressing  $\exp(-2K_{ij})$  as  $(1 - \tanh K_{ij}) / (1 + \tanh K_{ij})$ . Thus, equivalent expressions for the ECS of an Ising model on lattice  $\mathcal{L}$  are

$$\text{Det} \{1 - \Lambda_{\mathcal{L}^*}[k_x, k_y; \exp(-2K_{ij})]\} \quad \text{and} \quad \text{Det} [1 - \Lambda_{\mathcal{L}}(k_x, k_y; \tanh K_{ij})] = 0. \quad (2.19)$$

On the other hand, if the bulk free energy of the dual system on  $\mathcal{L}^*$  is known in terms of an integral over  $\ln \text{Det} \{1 - \Lambda_{\mathcal{L}}[k_x, k_y; \exp(-2K_{ij}^*)]\}$  (low-T graphs) or  $\ln \text{Det} [1 - \Lambda_{\mathcal{L}^*}(k_x, k_y$

---

<sup>†</sup>Reading off the equilibrium crystal shape from the bulk free energy will, of course, lead to an ECS for a lattice which has the same basis vectors  $\mathbf{a}$  and  $\mathbf{b}$  as the lattice on which the bulk problem was solved. Let the resulting ECS be given by  $\text{Det}[1 - \Lambda_b(\mathbf{X})] = 0$ , with  $\mathbf{X} = (X, Y)$ . If we are interested in a lattice  $\mathcal{L}'$  which has basis vectors  $\mathbf{a}' = \mathbf{M} \mathbf{a}$  and  $\mathbf{b}' = \mathbf{M} \mathbf{b}$ , where  $\mathbf{M}$  is the matrix of the appropriate linear transformation, then the ECS for the system on  $\mathcal{L}'$  is given by  $\text{Det}[1 - \Lambda_b(\mathbf{X}')] = 0$ , with  $\mathbf{X}' = \mathbf{M}^{-1} \mathbf{X}$ .

;  $\tanh K_{ij}^*$ ] (high-T graphs), the expressions (2.19) [and, of course, also (2.17) and (2.18)] may be obtained via the duality transformation  $\exp(-2K_{ij}^*) \rightarrow \tanh K_{ij}$ .

Once one has obtained the ECS from Eq. (2.1), one can use the inverse of the Wulff construction to determine the corresponding interfacial free energy per unit length  $\Gamma(\theta)$ , or equivalently, the inverse of the (anisotropic) high-T correlation length  $\xi^*(\theta+\pi/2)$  of the dual system [cf. Eq. (2.3)]. Once the ECS is known in the form  $Y(X)$ , the (2D) analytical form of the inverse Wulff construction is given by

$$\Gamma(\theta) = 1/\xi^*(\theta+\pi/2) = \lambda X \sin\theta + \lambda Y \cos\theta ; \quad \tan \theta \equiv -\frac{\partial Y}{\partial X} . \quad (2.20)$$

Eq. (2.20) is easily derived by expressing (1.12) in 2D polar coordinates and solving for  $\Gamma(\theta)$  and  $\partial Y/\partial X$ . With appropriate choice of basis vectors [ $\mathbf{a}=\hat{\mathbf{x}}$  and  $\mathbf{b}=\hat{\mathbf{y}}$  for the ECS's of Table 2.I (see also Fig. 2.5)], Eqs. (2.20) give two polynomials in  $\cosh(\beta\lambda X)$  and  $\cosh(\beta\lambda Y)$ . Since these two polynomials generally combine to give a polynomial in a single variable of order higher than 4 $th$ , it is generically not possible to obtain an analytic, closed form expression for  $\Gamma(\theta)$ . An exception is the rectangular lattice (see Appendix B). Of course, Eq. (2.20) can always be implemented numerically to obtain  $\Gamma(\theta)$  to arbitrary accuracy.

Figures 2.3 and 2.4 show two examples of ECS's and corresponding interfacial free energies typical of ferromagnetic Ising models. These shapes display the following universal features of 2D Ising ECS's (Zia, 1986): 1) The ECS becomes a circle as  $T \rightarrow T_c^-$ . For less symmetric lattices the ECS becomes an ellipse as  $T \rightarrow T_c^-$  (see Fig. 2.10). This is a result of the fact that the lattice anisotropy is a marginal variable (in the renormalization-group sense). 2) The ECS, as obtained from Eq. (2.1) for fixed  $\lambda$ , vanishes in all directions linearly with  $t \equiv (T_c - T)$  as  $t \rightarrow 0^+$ , i.e., the  $R(\theta, T) = \sqrt{x^2 + y^2} \sim t^\mu$  with the surface critical exponent  $\mu=1$  (and with a  $\theta$ -dependent amplitude in the generic case of an

asymptotically elliptical ECS). That  $\mu=1$  follows immediately from the duality relation (2.3) since the bulk correlation length  $\xi$  diverges like  $t^{-\nu}$  and we know that  $\nu=1$  from the exact bulk solution.  $\mu=1$  is consistent with the hyperscaling relation  $\mu=(D-1)\nu$  (Widom, 1965). In Table 2.I we give, for convenience of the reader, the analytical form for the ECS of the Ising model defined on a number of commonly encountered lattices (Fig. 2.5). The results for the ECS of the square, triangular, and honeycomb lattices have been obtained previously via the canonical formulation [see Eq. (2.3)] from the known direction dependent correlation lengths of these lattices (rectangular lattice: Cheng and Wu, 1967; see also McCoy and Wu, 1973; triangular/honey comb lattice: Vaidya, 1976). We obtained the equations for the Kagomé and “Union Jack” lattices and their duals by explicit construction of the matrix  $\Lambda$ . For the special cases,  $K_1=K_4$ ,  $K_2=K_3$ , and  $K_5=K_6$  for the Kagomé lattice and  $K_1=K_2=K_3=K_4$  and  $K_5=K_6$  for the “Union Jack” lattice, our result for  $\text{Det}(\mathbf{1}-\Lambda)$  reduces to that which can be read off from the bulk free energy as obtained by Kano and Naya in 1953 and by Vaks et al. in 1966, respectively.

In the derivation above, we had ferromagnetic Ising models in mind. However, the properties of the model crucial for our derivation are satisfied for a wider class of models. Hurst and Green showed in 1960 (see also Hurst, 1966) that the FV method is equivalent to the Pfaffian method, which can be used to solve any model which can be written as a free fermion field theory, i.e., a field theory which is quadratic in fermionic operators. The factors of  $(-1)$  which appear in the FV method are directly related to the  $(-1)$ 's of fermion anticommutators, and the uncoupling of directed graphs, necessary for the FV method to work, is precisely due to the field theory being free. The upshot of this equivalence is that we know the ECS for *any* model solvable by the Pfaffian or FV method in the form of the poles of the determinant of the free-fermion propagator, Eq. (2.1), provided that the FV walk can be identified with an interface between coexisting phases.

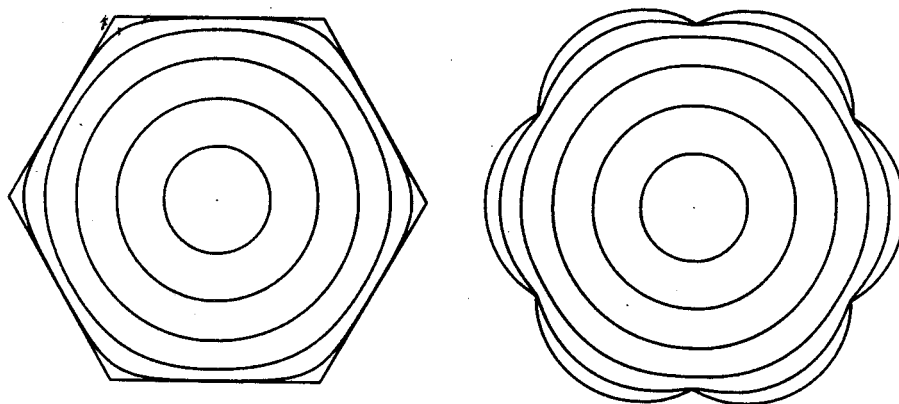


FIG. 2.3. The ECS (left) and corresponding Wulff plot (right) of the diced lattice (Fig. 2.5c) for equal, ferromagnetic couplings. The Wulff plot [polar plot of the interfacial free energy per unit length,  $\Gamma(\theta)$ ] was obtained numerically from Eq. (2.20). Different curves correspond to different temperatures, spaced equally from 0 (polygon) to  $T_c$  (dot at centre) at intervals of  $T_c/6$ .

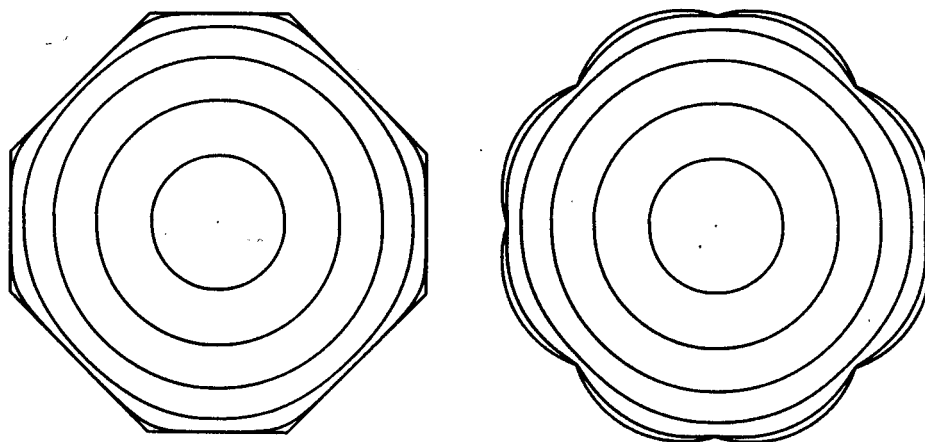


FIG. 2.4. Same as Fig. 2.3 for the 4-8 lattice with ferromagnetic couplings  $K_1=K_2=K_3=K_4$  and  $K_5=K_6$  as indicated in Fig. 2.5d with  $K_1/K_5=3/2$ . The horizontal and vertical faces at  $T=0$  are associated with  $K_5$ ; the diagonal ones, with  $K_1$ .

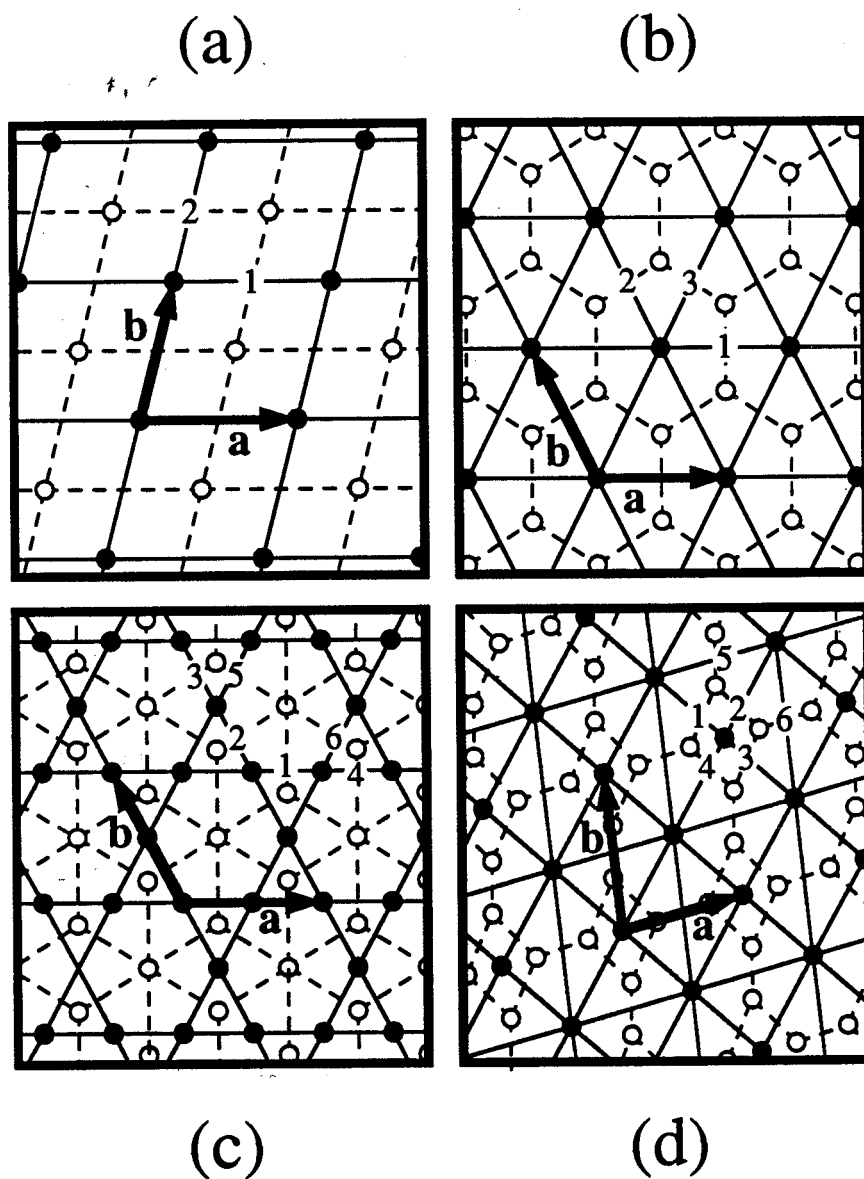


FIG. 2.5. The lattices of Table 2.I in duality pairs: (a) rectangular lattice (self-dual); (b) triangular and honeycomb lattices; (c) Kagomé lattice (solid) and diced lattice (dashed); (d) "Union Jack" lattice (solid) and 4-8 lattice (dashed). The labeling of bonds and the definition of basis vectors correspond to those used in Table 2.I. The position of sites within the unit cell, defined by the basis vectors  $a$  and  $b$ , is arbitrary. In the figure these sites were placed at symmetric positions for aesthetic reasons.



**Table 2.I**  
Examples of Exact Equilibrium Crystal Shapes

$$A - B \cosh(\beta \lambda a \cdot \hat{Y}) - C \cosh(\beta \lambda b \cdot \hat{Y}) - D \cosh[\beta \lambda (a+b) \cdot \hat{Y}] - E \cosh[\beta \lambda (a-b) \cdot \hat{Y}] = 0$$

$$Y \equiv (-Y, X); \quad c_i \equiv \cosh 2K_i, \quad s_i \equiv \sinh 2K_i$$

Rectangular D=E=0	
A	$c_1 c_2$
B	$s_1$
C	$s_2$

Triangular E=0	
A	$c_1 c_2 c_3 + s_1 s_2 s_3$
B	$s_1$
C	$s_2$
D	$s_3$

Honeycomb E=0	
A	$c_1 c_2 c_3 + 1$
B	$s_2 s_3$
C	$s_1 s_3$
D	$s_1 s_2$

Kagomé E=0	
A	$(c_1 c_3 c_5 + s_1 s_3 s_5)(s_2 s_4 s_6 + c_2 c_4 c_6) + c_1 c_4 + c_2 c_3 + c_5 c_6$
B	$c_4 s_1 s_2 s_6 + c_1 s_3 s_4 s_5 + s_1 s_4 (c_2 c_6 + c_3 c_5)$
C	$c_2 s_3 s_4 s_6 + c_3 s_1 s_2 s_5 + s_2 s_3 (c_1 c_5 + c_4 c_6)$
D	$c_5 s_1 s_3 s_6 + c_6 s_2 s_4 s_5 + s_5 s_6 (c_1 c_3 + c_2 c_4)$

Diced E=0	
A	$c_5 c_6 (c_1 c_2 c_3 c_4 + s_1 s_2 s_3 s_4) + s_5 s_6 (c_1 c_4 s_2 s_3 + c_2 c_3 s_1 s_4) + c_1 c_3 c_5 + c_2 c_4 c_6 + 1$
B	$s_2 s_6 (c_1 + c_3 c_5) + s_3 s_5 (c_4 + c_2 c_6)$
C	$s_4 s_6 (c_3 + c_1 c_5) + s_1 s_5 (c_2 + c_4 c_6)$
D	$s_2 s_4 (c_5 + c_1 c_3) + s_1 s_3 (c_6 + c_2 c_4)$

"Union Jack"	
A	$c_5 c_6 (c_1 c_2 c_3 c_4 + s_1 s_2 s_3 s_4 + 1) + s_5 c_6 (c_1 c_2 s_3 s_4 + s_1 s_2 c_3 c_4) + c_5 s_6 (c_1 c_4 s_2 s_3 + s_1 s_4 c_2 c_3) + s_5 s_6 (c_1 c_3 s_2 s_4 + s_1 s_3 c_2 c_4)$
B	$s_5 (c_1 c_2 + c_3 c_4) + c_5 (s_1 s_2 + s_3 s_4)$
C	$s_6 (c_1 c_4 + c_2 c_3) + c_6 (s_1 s_4 + s_2 s_3)$
D	$s_2 s_4$
E	$s_1 s_3$

4-8	
A	$c_5 c_6 (c_1 c_2 c_3 c_4 + s_1 s_2 s_3 s_4) + c_5 (c_1 c_4 + c_2 c_3) + c_6 (c_1 c_2 + c_3 c_4) + c_1 c_3 + c_2 c_4 + c_5 c_6$
B	$s_1 s_2 s_6 (c_3 c_4 + c_5) + s_3 s_4 s_6 (c_1 c_2 + c_5)$
C	$s_2 s_3 s_5 (c_1 c_4 + c_6) + s_1 s_4 s_5 (c_2 c_3 + c_6)$
D	$s_1 s_3 s_5 s_6$
E	$s_2 s_4 s_5 s_6$

Table. 2.I. The analytic expressions for the ECS's of the lattices indicated. The labeling of the interactions and the basis vectors **a** and **b** are defined in Fig. 2.5.

## 2.3 An example of non-Ising free-fermion crystal shapes: The modified KDP model.

We will now demonstrate the validity of Eq. (2.1) for the modified KDP model, a non-Ising free-fermion model. To be precise, we shall show that the purely imaginary poles of the determinant of the free-fermion propagator of the modified KDP model will correctly give the ECS of the dual model. The dual model turns out to be the limit of an antiferromagnetic Ising model on a triangular lattice as the interactions become infinite. The resulting ECS's have sharp corners for any  $T < T_c$ . The interface configurations of this model are extremely simple, so the solutions obtained from (2.1) can be confirmed via an independent elementary calculation. Historically, the 3D KDP model was originally proposed by Slater in 1941 as a model having the characteristics of the ferroelectric potassium dihydrogen phosphate (KDP)  $\text{KH}_2\text{PO}_4$ . The 2D version of the Slater KDP model was solved by Lieb, and independently by Sutherland, in 1967. The modified KDP model is a special (more simple) version of the KDP model in which a certain configuration has been suppressed but which still has many of the essential features of the full KDP model (Lieb and Wu, 1972).

The modified KDP model is a special case of the eight-vertex model. The square-lattice eight-vertex model is defined by eight types of vertices, as shown in Fig. 2.6, which must be placed on the vertices of a square lattice, such that arrows from different vertices sharing the same bond point in the same direction. Each vertex carries a Boltzmann weight  $\omega_i = \exp(-\beta e_i)$ ,  $i=1,2,\dots,8$ . When these weights satisfy the so-called free-fermion condition (Hurst and Green, 1960; Hurst, 1966; Lieb and Wu, 1972),

$$\omega_1\omega_2 + \omega_3\omega_4 = \omega_5\omega_6 + \omega_7\omega_8 \quad , \quad (2.21)$$

the square lattice eight-vertex model is solvable by the Pfaffian method and, therefore, by the FV method. Eq. (2.21) is satisfied by any eight-vertex model at one particular temperature. When the weights  $\omega_i$  are chosen such that (2.21) is satisfied at all temperatures, the model is known as *the* free-fermion model (Lieb and Wu, 1972). Depending on the particular choices for the  $\omega_i$ , the free-fermion model can be shown to be either trivial (decoupled 1D chains), equivalent to the Ising model on a triangular lattice, or, in a certain limiting case (see below), equivalent to the modified KDP model, which in turn turns out to be equivalent to the close-packed dimer model on a hexagonal lattice (Wu, 1968).

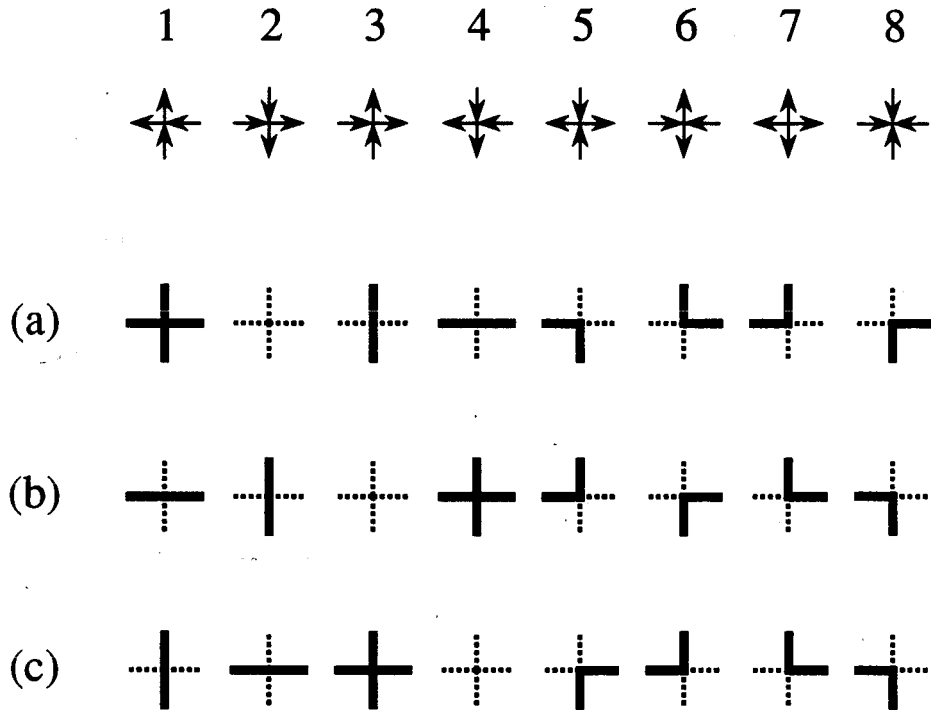


FIG. 2.6. The eight vertex configurations of the eight-vertex model. As an alternative to representing vertex configurations by arrows, one can represent them by “bond arrangements”. These bond arrangements are constructed from the arrow representation by first choosing (arbitrarily) a vertex which corresponds to no bonds (no bold lines), the basis. Other bond configurations are then constructed from the basis by drawing a bond for every arrow pointing in a direction opposite to that of the corresponding arrow of the basis vertex. (a), (b), and (c) show three of the eight possible bond arrangements based on the vertices 2, 3, and 4, respectively.

We shall first show how the free-fermion model is solved by the FV method. Specializing to the modified KDP model, we will then identify the corresponding walk with microscopic interface configurations separating coexisting phases of the dual model. The FV method was used by Ryazanov in 1971 to calculate the bulk free energy of the modified KDP model in zero (electric) field. It is straightforward to generalize this particular solution to the general free-fermion model. To identify the “random” walker counting problem, it is convenient to represent the vertices as “bond arrangements” (e.g., Lieb and Wu, 1972). There are eight possible bond arrangements, three of which are shown in Fig. 2.6. In the absence of macroscopic interfaces, allowed vertex configurations correspond to closed loops of bonds, and calculating the partition function reduces to the problem of counting all possible loop configurations. Since the loop counting is done on a square lattice, the appropriate walking matrix  $\Lambda$  is  $4 \times 4$  and schematically given by

$$\Lambda = \begin{pmatrix} \begin{array}{c} \vdots \\ \uparrow \\ \vdots \end{array} & \begin{array}{c} \vdots \\ \uparrow \\ \vdots \end{array} & 0 & \begin{array}{c} \uparrow \\ \vdots \end{array} \\ \begin{array}{c} \vdots \\ \leftarrow \\ \vdots \end{array} & \begin{array}{c} \vdots \\ \leftarrow \\ \vdots \end{array} & \begin{array}{c} \vdots \\ \leftarrow \\ \vdots \end{array} & 0 \\ 0 & \begin{array}{c} \vdots \\ \downarrow \\ \vdots \end{array} & \begin{array}{c} \vdots \\ \downarrow \\ \vdots \end{array} & \begin{array}{c} \downarrow \\ \vdots \end{array} \\ \begin{array}{c} \vdots \\ \rightarrow \\ \vdots \end{array} & 0 & \begin{array}{c} \vdots \\ \rightarrow \\ \vdots \end{array} & \begin{array}{c} \rightarrow \\ \vdots \end{array} \end{pmatrix}. \quad (2.22)$$

This matrix involves only six vertices. The remaining two, corresponding to no bonds and intersecting bonds, are automatically taken into account correctly by virtue of the free-fermion condition (2.21). With the choice of bond arrangement (a) of Fig. 2.6,  $\Lambda$  becomes [cf. Eq. (2.10)]

$$\Lambda = \frac{\omega_1}{\omega_2} \begin{pmatrix} \omega_3 e_{-y} & \alpha^{-1} \omega_6 e_{-y} & 0 & \alpha \omega_7 e_{-y} \\ \alpha \omega_5 e_x & \omega_4 e_x & \alpha^{-1} \omega_7 e_x & 0 \\ 0 & \alpha \omega_8 e_y & \omega_3 e_y & \alpha^{-1} \omega_5 e_y \\ \alpha^{-1} \omega_8 e_{-x} & 0 & \alpha \omega_6 e_{-x} & \omega_4 e_{-x} \end{pmatrix}, \quad (2.23)$$

where vertex energy is measured with respect to vertex 2 (Fig. 2.6), which corresponds to no bonds, and  $\alpha \equiv e^{-i\pi/4}$ ,  $e_{\pm x} \equiv e^{ik_{\pm x}}$ , and  $e_{\pm y} \equiv e^{ik_{\pm y}}$ . Eq. (2.23) yields the same bulk free energy as obtained by Hurst and Green in 1960 and by Fan and Wu in 1969 and 1970 via other methods. We find [making use of (2.21)]

$$\text{Det}(\mathbf{1}-\Lambda) = a + 2b \cos k_x + 2c \cos k_y + 2f \cos(k_x - k_y) + 2g \cos(k_x + k_y), \quad (2.24)$$

where  $a = \omega_1^2 + \omega_2^2 + \omega_3^2 + \omega_4^2$ ,  $b = \omega_1 \omega_3 - \omega_2 \omega_4$ ,  $c = \omega_1 \omega_4 - \omega_2 \omega_3$ ,  $f = \omega_3 \omega_4 - \omega_5 \omega_6$ , and  $g = \omega_3 \omega_4 - \omega_7 \omega_8$ . The bulk free energy of the free-fermion model is independent of the choice of "bond arrangement", because the integral of  $\text{Det}(\mathbf{1}-\Lambda)$  is invariant under change of arrangement. However, crystal shapes are obtained from  $\text{Det}(\mathbf{1}-\Lambda)$ , itself, which *does* depend on the choice of "bond arrangement". As we shall see, it is necessary to identify the coexisting phases for which we wish to calculate the ECS, before the correct bond arrangement can be chosen.

We define the modified KDP model as the limit of the free-fermion eight-vertex model

$$\begin{aligned} e_1 & & e_2 = h+v & & e_3 = \varepsilon-h+v & & e_4 = \varepsilon+h-v \\ e_5 = e_6 = \varepsilon & & e_7 = \frac{e_1}{2} + h & & e_8 = \frac{e_1}{2} + v, \end{aligned} \quad (2.25)$$

as  $e_1 \rightarrow \infty$ . The variables  $h$  and  $v$  correspond to horizontal and vertical electric fields in the original KDP model. In the limit  $e_1 = \infty$ , analysis of the bulk free energy (Fan and Wu, 1970) shows that this model has a second-order phase transition which is *not* of the Ising type. As  $T \rightarrow T_c^+$ , the specific heat has a  $(T - T_c)^{-1/2}$  divergence instead of the  $\ln|T - T_c|$  divergence of the Ising model. The critical temperature is given by the condition  $\omega_2 + \omega_3 + \omega_4 = 2\max(\omega_2, \omega_3, \omega_4)$ , which divides the  $h$ - $v$  plane into three distinct regions:  $h < \varepsilon/2$  and  $v < \varepsilon/2$  defines the region  $\mathfrak{R}_2$ , where  $\omega_2$  is largest;  $h > \varepsilon/2$  and  $v < h$  defines the region  $\mathfrak{R}_3$ , where  $\omega_3$  is largest;  $h < v$  and  $v > \varepsilon/2$  defines the region  $\mathfrak{R}_4$ , where  $\omega_4$  is largest.

The identification of the walk described by the matrix  $\Lambda$  of Eq. (2.22) with a microscopic interface configuration separating coexisting phases is most easily accomplished in the familiar language of the Ising model by making use of the following duality (Fan and Wu, 1969; see also Lieb and Wu, 1972): Any eight-vertex model on a square lattice is dual to an Ising model on the dual lattice with four-spin interactions and (crossing-bond) next-nearest-neighbour interactions. In terms of this equivalent Ising model, the free-fermion condition is the condition that the four-spin interaction and one of the next-nearest-neighbour interactions be zero. The free-fermion eight-vertex model (2.25) is, therefore, dual to an "Ising" model on a triangular lattice (at least for finite  $e_1$ ) which is calculated to have interaction energies (e.g., Lieb and Wu, 1972),

$$J_1 = \frac{1}{4}(-e_1 + 3h - v) \quad J_2 = \frac{1}{4}(-e_1 + 3v - h) \quad J_3 = \frac{1}{4}(-e_1 + 2\varepsilon - h - v) \quad , \quad (2.26)$$

where  $J_i > 0$  corresponds to ferromagnetic coupling. In terms of these Ising energies, the vertex weights become

$$\begin{aligned} e_1 + J_0 &= -J_1 - J_2 - J_3 & e_2 + J_0 &= J_1 + J_2 - J_3 & e_3 + J_0 &= -J_1 + J_2 + J_3 \\ e_4 + J_0 &= J_1 - J_2 + J_3 & e_5 + J_0 &= e_6 + J_0 = J_3 & e_7 + J_0 &= e_8 + J_0 = -J_3 \quad , \quad (2.27) \end{aligned}$$

where the overall constant  $J_0 = \frac{1}{4}(-e_1 - 2\varepsilon - h - v)$ .

Since we are interested in the limit  $e_1 \rightarrow \infty$ , we focus on the completely antiferromagnetic sector of the model (2.26), where  $e_1$  is finite but large enough to make all Ising couplings negative. This sector is defined for  $e_1 > \varepsilon > 0$  and consists of a triangular region in the  $h$ - $v$  plane (see Fig. 2.7). Within this triangular region, we identify the same three regions of the  $h$ - $v$  plane as those for the modified KDP model. The interior of each region is characterized by one bond being weaker than the others. The weakest bond in  $\mathfrak{R}_2$ ,  $\mathfrak{R}_3$ , and  $\mathfrak{R}_4$  is  $J_3$ ,  $J_1$ , and  $J_2$ , respectively. On the boundaries where regions meet, two bond energies are equal and weaker than the third, except at the point  $h=v=\varepsilon/2$  where all couplings are equal. We can now identify the nature of the phases in the interior of each region and on the boundaries. In the interior of each region is a  $2 \times 1$  phase which consists of rows of predominantly aligned spins. The rows are along the direction of the weakest bond, and the sign of the alignment of the spins alternates from row to row. Within each region, the  $2 \times 1$  phase has two degenerate realizations, related by an overall change of sign, which constitute the two phases which can coexist in zero magnetic field below  $T_c$  (see Fig. 2.8). The ECS is thus well defined in the interior of each region,  $\mathfrak{R}_2$ ,  $\mathfrak{R}_3$ , and  $\mathfrak{R}_4$ , and corresponds to the shape of a macroscopic inclusion of an appropriately oriented  $2 \times 1$  phase coexisting with a  $2 \times 1$  phase of the same orientation but opposite overall sign.<sup>†</sup> On the

---

<sup>†</sup>This is slightly different from the traditional picture of an Ising crystal. In the traditional picture, a ferromagnetic Ising model is interpreted as a lattice-gas model of the solid/fluid system for which the ECS problem was originally formulated. (The volume constraint of the ECS problem becomes a constraint on the magnetization.) However, there is nothing sacred about solid/fluid coexistence. The problem of finding the shape of a macroscopic inclusion of one phase in another is well defined whenever the inclusion and the surrounding medium coexist in equilibrium. The problem is particularly interesting

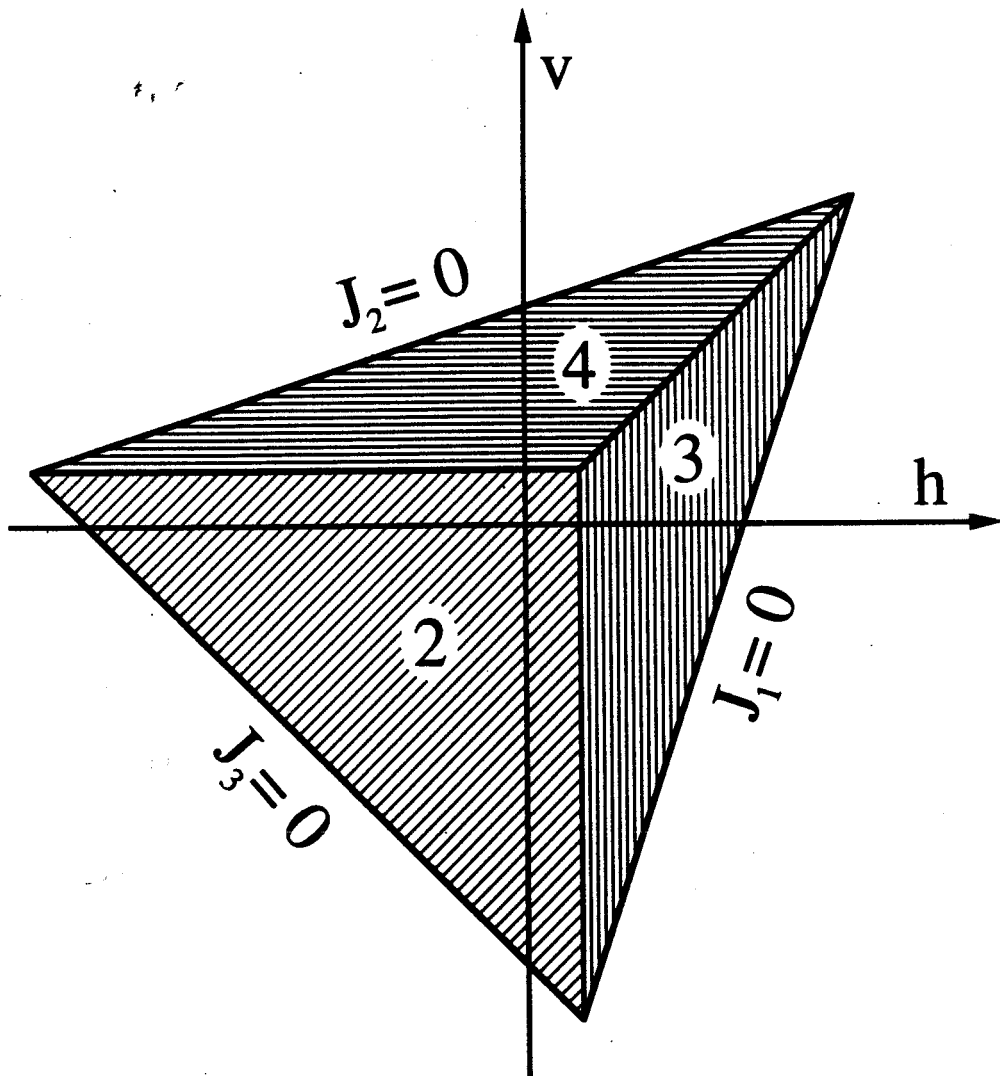


FIG. 2.7. The antiferromagnetic sector of the free-fermion model, defined by the vertex weights of Eq. (2.26), in the  $h$ - $v$  plane of horizontal and vertical (electric) fields. In the regions, 2, 3, and 4, the ground state of the model is given by vertices 2, 3, and 4. In terms of the equivalent Ising couplings, the regions, 2, 3, and 4, are characterized by  $2 \times 1$  phases aligned along bonds  $J_3$ ,  $J_1$ , and  $J_2$ , respectively. As  $e_1 \rightarrow \infty$ , the modified KDP model is approached, and the boundaries of the antiferromagnetic sector are pushed off to infinity.

---

when there is crystalline anisotropy, as is the case for coexisting  $2 \times 1$  phases on the triangular lattice.

[For the  $2 \times 1$  phases, the volume constraint of the ECS problem becomes a constraint on the sublattice (staggered) magnetization.]



boundaries where regions meet, the ground state is macroscopically degenerate and there is no ordered phase at any temperature.

The walk of the FV method can now easily be identified as a microscopic interface configuration: The bold lines of bond arrangements correspond to composite elementary interfaces on the hexagonal lattice dual to the triangular Ising system (2.26), as shown in Fig. 2.9. Depending on which bond arrangement is chosen, these interface configurations carry different vertex weights  $e_i$  [Fig. 2.6]. To interpret these energies as the energies needed to create the composite interfaces of Fig. 2.9 from the ground state configuration, we must first identify the ground-state energy per vertex. It follows from Eqs. (2.27) that the energy for the the  $2 \times 1$  ground state of  $\mathfrak{R}_2$ ,  $\mathfrak{R}_3$ , and  $\mathfrak{R}_4$  corresponds to the energy of vertex 2, 3, and 4, respectively. Subtracting the ground state energies, one can now easily identify the vertex energies of bond arrangements (a), (b), and (c) as precisely the energies needed to create the corresponding broken bonds *per vertex* from the  $2 \times 1$ -phase ground states of regions  $\mathfrak{R}_2$ ,  $\mathfrak{R}_3$ , and  $\mathfrak{R}_4$ , respectively (see Fig's 2.6 and 2.9). Different bond arrangements result in different weights for the entries of the matrix  $\Lambda$  [cf. Eq. (2.22)], which leads to different functions  $\text{Det}(\mathbf{1}-\Lambda)$ . It is now clear that the matrix  $\Lambda$  based on bond arrangement (a), with vertex 2 describing the ground state, can describe elementary interfaces of the antiferromagnetic triangular Ising model only in  $\mathfrak{R}_2$ . To obtain the ECS in  $\mathfrak{R}_3$  and  $\mathfrak{R}_4$ ,  $\Lambda$  must be based on bond arrangements (b) and (c), respectively.  $\text{Det}(\mathbf{1}-\Lambda)$  for  $\mathfrak{R}_3$  is obtained from Eq. (2.24) by making the substitutions  $(b,f,g) \rightarrow (-b,-f,-g)$ , and for  $\mathfrak{R}_4$ , by making the substitutions  $(c,f,g) \rightarrow (-c,-f,-g)$ .

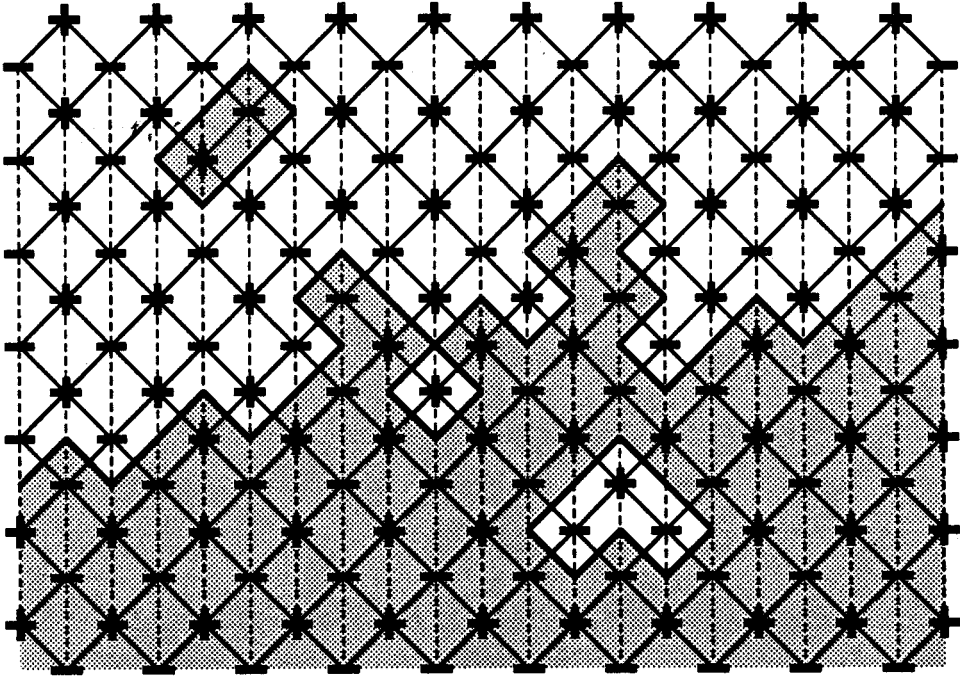


FIG. 2.8. An interface between two degenerate  $2 \times 1$  phases of the antiferromagnetic triangular Ising model. The dashed bond is weaker than the others so that the ground state corresponds to spins aligned in rows along the dashed lines.

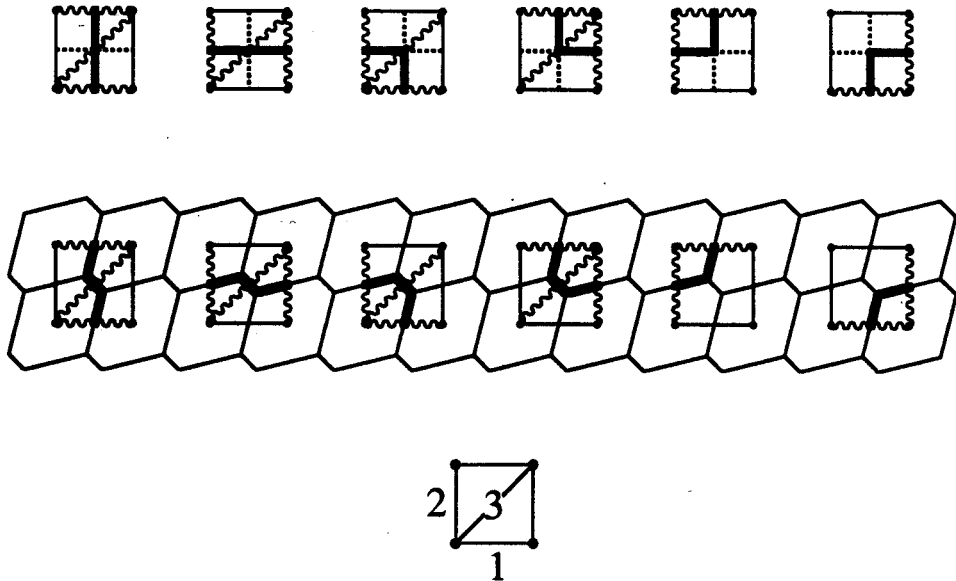


FIG. 2.9. The one-to-one correspondence between vertex configurations of the eight-vertex model and composite elementary interfaces on the hexagonal lattice. The wavy lines correspond to broken bonds of the triangular dual lattice, which has interactions  $J_1$ ,  $J_2$ , and  $J_3$ , as shown.

Before we take the limit  $e_1 \rightarrow \infty$ , let us look at the kind of shapes one obtains with bond arrangement (a) for finite  $e_1$ . In Fig. 2.10 we show the shapes obtained from Eq. (2.24) with the vertex weights (2.25) at  $h=v=0$  for increasing values of  $e_1$ . For  $e_1/\epsilon < 2$ ,  $J_3 > 0$ , and we are outside the antiferromagnetic sector. The signs of  $J_1$  and  $J_2$  may be reversed by symmetry, so that, for these couplings, the model is equivalent to the triangular ferromagnetic Ising model. The value  $e_1/\epsilon = 2$  corresponds to sitting on the boundary of the antiferromagnetic sector with  $J_3 = 0$ . This is equivalent to an antiferromagnetic rectangular Ising model, which (again, by symmetry) is identical to a ferromagnetic rectangular Ising model. For  $e_1/\epsilon > 2$ , we are in region  $\mathfrak{R}_2$  of the antiferromagnetic sector of the triangular Ising model and the coexisting phases are  $2 \times 1$  phases aligned along the direction of bond  $J_3$ . Note that, with increasing  $e_1$ , the corners “pointing” in the direction perpendicular to the weakest bond  $J_3$  become increasingly sharp.

Setting  $e_1 = \infty$  in Eqs. (2.26) shows that the modified KDP model is dual to an antiferromagnetic “Ising” model on a triangular lattice with infinite interactions differing from each other by a finite amount. The infiniteness of these interactions severely restricts the possible interface configurations, because any interface must make maximal use of the weakest bonds. Thus, the walker generating the interface performs a very simple walk: After a step along the easiest elementary interface (along the bond dual to the weakest bond of the triangular lattice) he can either step to the right or to the left. Next, he is forced to again take a step along the easiest elementary interface, and so on. The simplicity of this walk is reflected in the structure of the matrix  $\mathbf{\Lambda}$ , which becomes the direct sum of two  $2 \times 2$  matrices, when  $\omega_1 = \omega_7 = \omega_8 = 0$ . The determinant of the propagator factors, therefore, into two simple expressions. One describes the upper half of the crystal shape; the other, the lower. For  $\mathfrak{R}_2$ , one finds for the ECS the simple expression

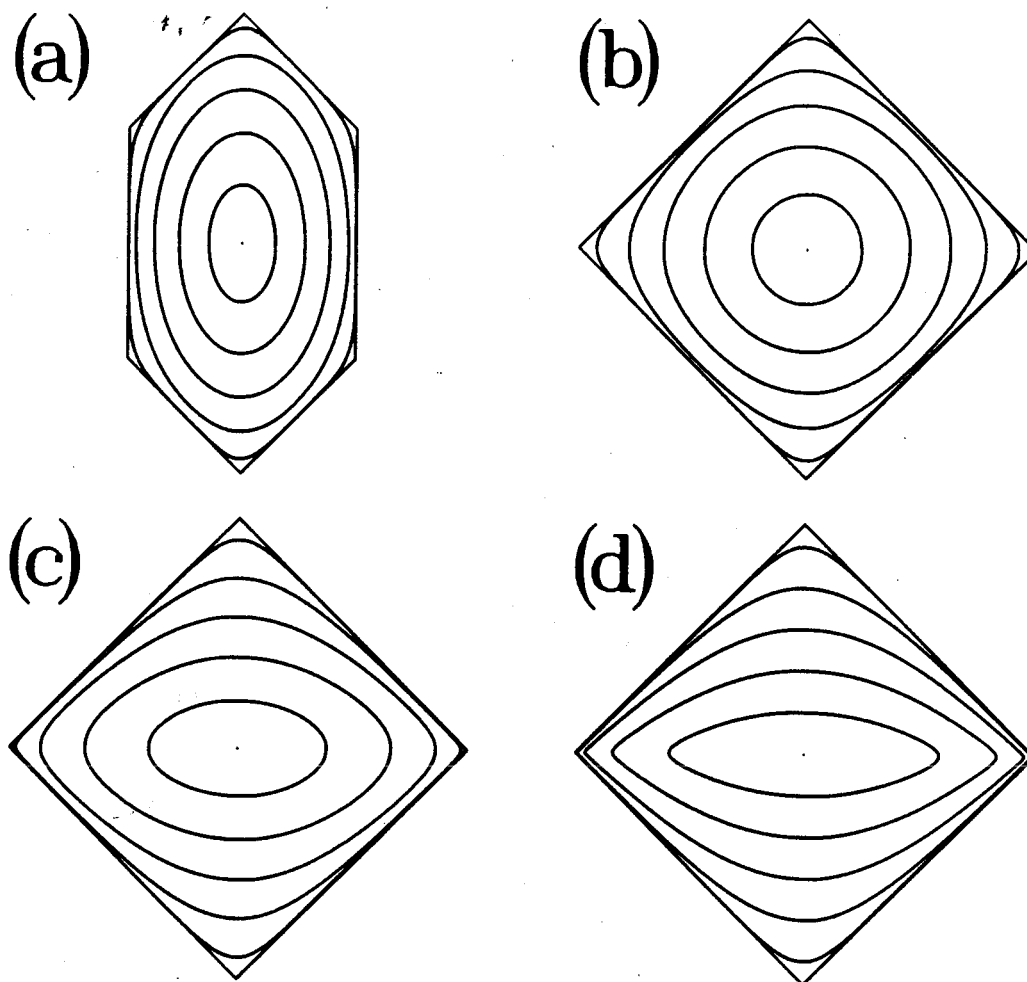


FIG. 2.10. Equilibrium crystal shapes of the free-fermion model defined by the vertex weights of Eq. (2.25) at  $h=v=0$  and for various values of  $e_1/\epsilon$ : (a)  $e_1/\epsilon=1$ ; (b)  $e_1/\epsilon=2$ ; (c)  $e_1/\epsilon=4$ ; (d)  $e_1/\epsilon=8$ . In each case, the ECS has been plotted at temperatures equally spaced from 0 to  $T_c$  at intervals of  $T_c/6$ . The lattice of the model was chosen to have the same basis and orientation as shown in Fig. 2.8, with the weakest bond in the horizontal direction. The shapes (a) and (b) are the ECS's of a macroscopic inclusion of "up" phase in a sea of "down" phase for the ferromagnetic triangular and square Ising models, respectively. The shapes (c) and (d) are the ECS's of a macroscopic inclusion of  $2 \times 1$  phase in another of opposite (staggered) magnetization (see Fig. 2.87). With increasing value of  $e_1/\epsilon$ , the modified KDP model ( $e_1/\epsilon=\infty$ ) is approached, and the corners "pointing" in the direction perpendicular to the weakest bond become increasingly sharp.

$$\omega_3 e^{-\beta\lambda X} + \omega_4 e^{-\beta\lambda Y} - \omega_2 = 0 \quad \text{and} \quad (X, Y) \rightarrow (-X, -Y), \quad (h, v) \in \mathfrak{R}_2. \quad (2.28)$$

The corresponding equations for  $\mathfrak{R}_3$  and  $\mathfrak{R}_4$  are obtained from Eq. (2.28) by making the substitutions  $\omega_4 \rightarrow -\omega_4$  and  $\omega_3 \rightarrow -\omega_3$ , respectively. Notice that the pair of functions (2.28), (and the corresponding ones in  $\mathfrak{R}_3$  and  $\mathfrak{R}_4$ ) describe curves of infinite extent and that the ECS is to be interpreted as the convex region enclosed by the two functions for  $T < T_c$ . Where the pair of curves intersect, the ECS has a sharp corner which moves toward the origin like  $(T_c - T)^{1/2}$ , as  $T \rightarrow T_c^-$ . In all other directions the ECS vanishes linearly with  $T$ , as  $T \rightarrow T_c^-$ . The sharp corners and the fact that the crystal shape appears to be analytically continued beyond the convex region<sup>†</sup> are unusual features of the ECS and are a direct result of the infiniteness of the interactions. To gain further insight into the physical origin of these features, we make use of the simplicity of the interface configurations to calculate - in a very direct and elementary manner - the interfacial free energy and the crystal shape.

Consider the infinite-interaction “Ising” model dual to the KDP model on an arbitrary triangular lattice, so that the corresponding FV walk takes place on an arbitrary hexagonal lattice. Let the easiest steps on the hexagonal lattice be denoted by  $\mathbf{d}_w$  and  $-\mathbf{d}_w$  and denote the steps to the right and left of  $\mathbf{d}_w$  by  $\mathbf{d}_r$  and  $\mathbf{d}_l$  respectively. Because of the

---

<sup>†</sup> In the antiferromagnetic sector, there are real, unbounded solutions  $Y(X)$  to  $\text{Det}[1 - \Lambda(X, Y)] = 0$  for  $X \in [-\infty, X_L] \cup [X_R, \infty]$  even for finite  $e_1$ . We believe that these solutions have no physical significance, at least not in the context of ECS's. The expression for  $Y(X)$  in terms of a sum over  $\Lambda$ 's [cf. Eq. (2.12)] becomes formally divergent for  $X \in [-\infty, X_L] \cup [X_R, \infty]$ . When  $e_1 = \infty$ ,  $X_L$  and  $X_R$  coincide with the “boundaries”  $X_{\min}$  and  $X_{\max}$  of the ECS. (For purely ferromagnetic Ising models, no such real, unbounded solutions exist.)

infiniteness of the interactions, the walker actually performs a walk on a rectangular lattice with the composite steps  $\pm \mathbf{d}_1$  and  $\pm \mathbf{d}_2$ , where  $\mathbf{d}_1 = \mathbf{d}_w + \mathbf{d}_r$  and  $\mathbf{d}_2 = \mathbf{d}_w + \mathbf{d}_f$ . Since a step  $\pm \mathbf{d}_1$  or  $\pm \mathbf{d}_2$  of given sign must be followed by a step of the same sign, the only interfaces available to the (say) upper half of the ECS must have tangent vectors which lie between  $\mathbf{d}_1$  and  $\mathbf{d}_2$  (see Fig. 2.11). It is precisely the absence of other interface orientations which causes the sharp corners of the ECS. The zero-temperature character of the infinite interactions manifests itself in the fact that the entropy of a walk from the origin to the point  $\mathbf{R} = n \mathbf{d}_1 + m \mathbf{d}_2$ , ( $m, n > 0$ ) is simply given by the zero-temperature entropy,  $\ln[(n+m)! / (n! m!)]$ , at all temperatures. If  $E_1$  and  $E_2$  denote the costs in energy of taking steps  $\pm \mathbf{d}_1$  and  $\pm \mathbf{d}_2$ , we can immediately write down the corresponding free energy per unit length,  $\Gamma(\theta)$ , as

$$\Gamma(\theta) = \tilde{n} E_1 + \tilde{m} E_2 - \frac{1}{\beta} [(\tilde{n} + \tilde{m}) \ln(\tilde{n} + \tilde{m}) - \tilde{n} \ln \tilde{n} - \tilde{m} \ln \tilde{m}], \quad \theta \in [0, \theta_{\max}] \cup [\pi, \pi + \theta_{\max}], \quad (2.29)$$

where  $\tilde{n} \equiv n/R$ ,  $\tilde{m} \equiv m/R$ ,  $\theta$  is measured clockwise from the  $\hat{\mathbf{z}} \times \mathbf{d}_2$  direction, and  $\cos \theta_{\max} = \mathbf{d}_1 \cdot \mathbf{d}_2 / (d_1 d_2)$ . For other directions,  $\Gamma(\theta)$  is infinite. Explicitly, we find  $\tilde{m} = (\cos \theta - \sin \theta \cot \theta_{\max}) / d_2$  and  $\tilde{n} = \sin \theta / (d_1 \sin \theta_{\max})$ . Performing the Wulff construction for each of the two branches of  $\Gamma(\theta)$  *separately* (i.e., separately for  $\theta \in [0, \theta_{\max}]$  and for  $\theta \in [\pi, \pi + \theta_{\max}]$ ), one finds that the envelope of the Wulff lines for each branch produces an infinitely extended curve. The pair of curves thus obtained is given by

$$e^{\frac{\beta}{2} [E_1 + E_2 + (\mathbf{d}_1 + \mathbf{d}_2) \cdot \mathbf{Y}]} = 2 \cosh \left\{ \frac{\beta}{2} [E_1 - E_2 + (\mathbf{d}_1 - \mathbf{d}_2) \cdot \mathbf{Y}] \right\} \quad \text{and} \quad (\mathbf{d}_1, \mathbf{d}_2) \rightarrow (-\mathbf{d}_1, -\mathbf{d}_2), \quad (2.30)$$

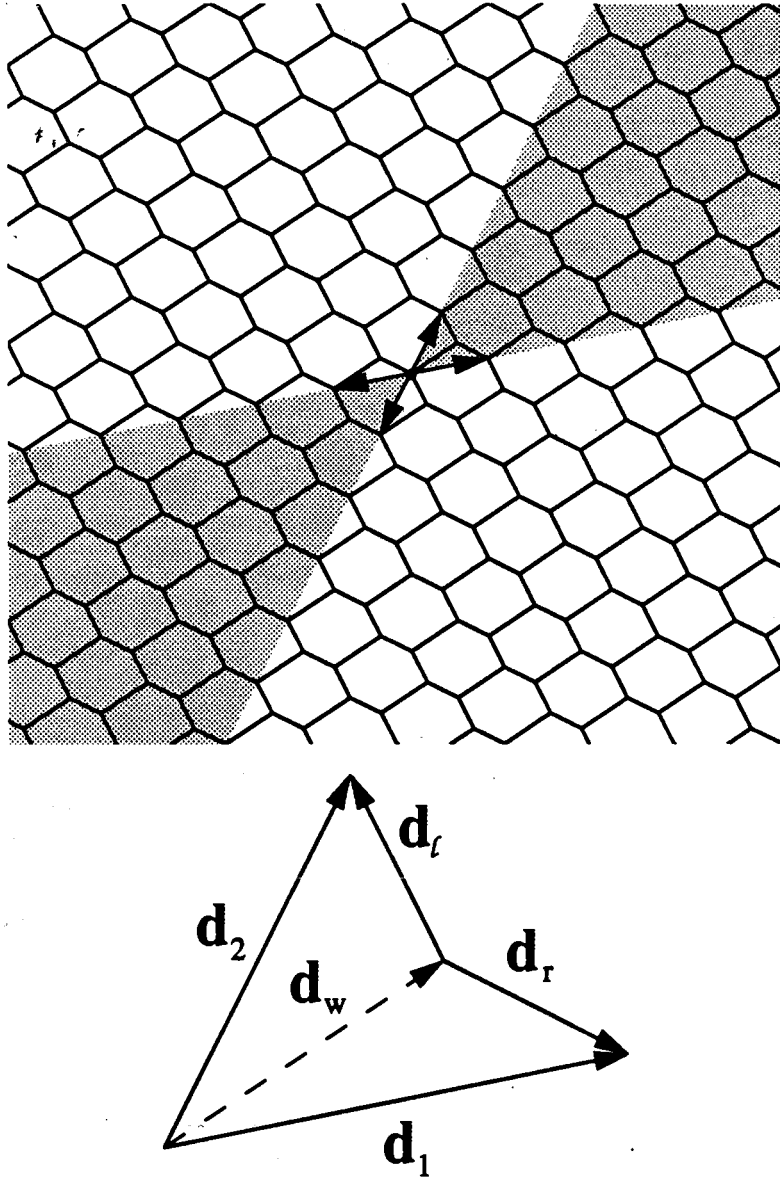


FIG. 2.11. The Feynman-Vdovichenko walker for the modified KDP model performs a very simple walk on the honeycomb lattice: The infiniteness of the interactions forces the walker to make maximal use of the lowest-energy step, which we take to be  $\pm d_w$ . Every step  $d_w$  is followed by a step  $d_r$  or  $d_l$ , which must be followed again by a step  $d_w$ , and so on. Thus, the walk takes place effectively on a square lattice with the composite steps  $\pm d_1$  and  $\pm d_2$ . Since every composite step must be followed by a composite step of the same sign, only the shaded regions are accessible to a walker starting out at a given lattice site. The fact that directions outside the shaded regions are forbidden is what causes the sharp corners of the ECS of the modified KDP model and gaps in the corresponding Wulff plot.

where  $\mathbf{Y} \equiv (-Y, X)$ . Eqs. (2.28) and the corresponding equations in  $\mathfrak{R}_3$  and  $\mathfrak{R}_4$  are special cases of (2.30) corresponding to  $(\hat{\mathbf{d}}_1, \hat{\mathbf{d}}_2)$  equal to  $(-\hat{\mathbf{y}}, \hat{\mathbf{x}})$ ,  $(\hat{\mathbf{x}}, \hat{\mathbf{x}} + \hat{\mathbf{y}})$ , and  $(\hat{\mathbf{x}} + \hat{\mathbf{y}}, \hat{\mathbf{y}})$ , respectively, and are just rotations and linear distortions of one another. The interior envelope of *all* Wulff planes is just the convex region enclosed by both curves and results in a ECS with sharp corners (see Fig. 2.12).<sup>†</sup>

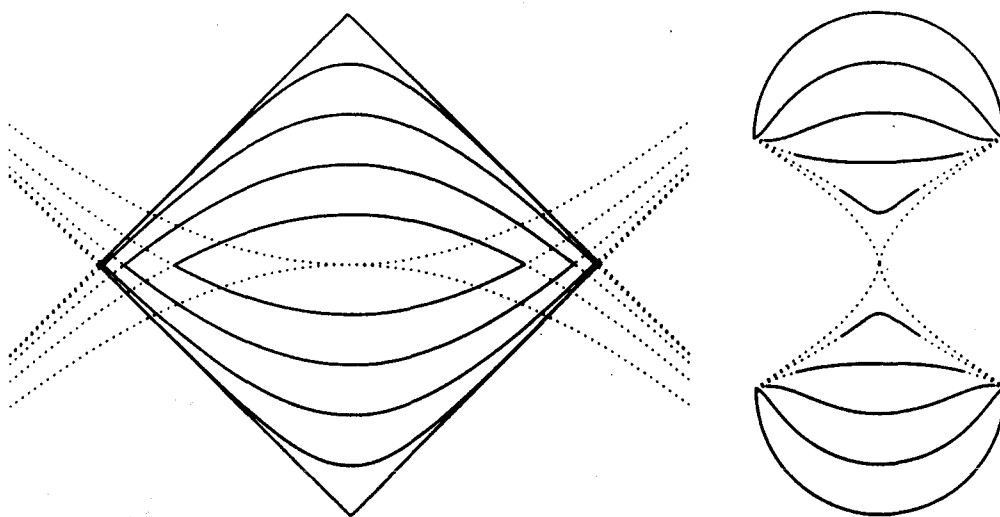


FIG. 2.12. The ECS of the modified KDP model (solid lines, left) and the corresponding Wulff plot (right) for  $h=v=0$ . The curves have been plotted at temperatures equally spaced from 0 to  $T_c$  at intervals of  $T_c/5$ . The dual lattice for the model has been chosen to have the basis and orientation shown in Fig. 2.8. At finite  $T$ , those orientations corresponding to the dashed lines do not contribute to the ECS and are, therefore, thermodynamically unstable.

<sup>†</sup> For those orientations  $\theta$  for which the function  $\Gamma(\theta)$  defined in Eq. (2.29) does not contribute to the ECS,  $\Gamma(\theta)$  is not an interfacial free energy. If  $\mathbf{R}=(n,m)$  is not tangent to the ECS, an interface from  $(0,0)$  to  $(n,m)$  will consist of two macroscopically linear segments in accordance with the lever rule [e.g., M. Wortis (1988)]. The *single* sharp corner thus generated (costing infinite energy but having zero thermodynamic weight) is strictly disallowed in the calculation leading to (2.29). Thus, only for orientations tangent to the ECS does (2.29) have meaning as the interfacial free energy of the modified KDP model.



For completeness we mention that the ECS (2.30) can be calculated very simply by mapping the interface configurations of the modified KDP model onto a one-dimensional Ising model. This is very similar in spirit to the work of Shi and Wortis (1988). Each step of the walk can be in two “states”, along either  $\mathbf{d}_1$  or  $\mathbf{d}_2$  [ $(\downarrow)$  or  $(\uparrow)$ ]. Because successive steps do not interact in the case of the modified KDP model, the 1D Ising model reduces to a zero-dimensional model consisting of a single “spin”. By rearranging Eq. (2.5), one can express the ECS as<sup>†</sup>

$$1 = \text{Tr} \exp \left\{ -\frac{\beta}{2} [(E_{\downarrow} + E_{\uparrow}) + (E_{\downarrow} - E_{\uparrow}) \sigma] \right\}, \quad \sigma = \pm 1, \quad (2.31)$$

with

$$E_{\downarrow} = E_1 + \mathbf{d}_1 \cdot \mathbf{Y} \quad \text{and} \quad E_{\uparrow} = E_2 + \mathbf{d}_2 \cdot \mathbf{Y}, \quad (2.32)$$

which immediately yields Eq. (2.30) for the general ECS.

## 2.4 Conclusion

We have found a general, exact solution for the ECS's of free-fermion models. This solution was derived in a “grand canonical” ensemble of interface orientations and made use of an exact mapping of the interface onto a Feynman-Vdovichenko walker. This mapping is possible, because free-fermion models allow bulk fluctuations to be effectively uncoupled from interface fluctuations via the inclusion of appropriate minus signs into the Boltzmann weights. The ECS of free-fermion models turns out to be remarkably simple: The ECS is given by the locus of purely imaginary poles of the determinant of the lattice-

---

<sup>†</sup> This is essentially just the implicit grand canonical form of the ECS, Eq. (1.39), in two dimensions with  $F^{++}=0$ . Because of the noninteracting nature of the Hamiltonian here, the thermodynamic limit  $S \rightarrow \infty$  of (1.39) is trivial and simply divides out the number of spins, yielding (2.31).

path propagator. Because the bulk free energy of these models is usually expressed as an integral over this determinant, the ECS can simply be read off from the analytic form of the bulk free energy.

2D Ising models without crossing bonds are free-fermion models. Prior to the work presented in this Section, the only known exact 2D Ising ECS's were those of the rectangular, triangular and honeycomb lattices. New Ising results are easily obtained either by explicitly constructing the FV matrix or by reading off  $\text{Det}(\mathbf{1}-\Lambda)$  from the analytic form of the bulk free energy (if already known). As examples of new solutions, we give in Table 2.1 the ECS's of the Kagomé and "Union Jack" lattices and their duals, the diced and 4-8 lattices, respectively (see also Fig's. 2.3 and 2.4).

From a study of the free-fermion case of the eight-vertex model (*the free-fermion model*), we demonstrated that one must generally be careful in reading off the ECS from the bulk free energy. While many different forms of the FV matrix give the same bulk free energy, these different matrices represent interfaces between different coexisting phases and, therefore, result in different ECS's. The modified KDP model is a special case of the free-fermion model which is not in the Ising universality class. The ECS of the modified KDP model is the limit of the ECS defined for coexisting  $2 \times 1$  phases of a triangular antiferromagnet in the limit of infinite interactions differing by a finite amount. The ECS of the modified KDP model is lenticular and has, as a consequence of the infinite interactions, sharp corners. The infinite interactions greatly simplify the interface configurations possible and allow elementary calculation of the ECS, which confirms the result obtained from the general solution.

### 3. Low-Temperature Expansions For The Step Free Energy and Facet Shape of the Simple-Cubic Ising Model

#### 3.1 Background and Introductory Remarks

We now return to 3D ECS's. At the outset, it is useful to have in mind a picture of the thermal evolution of a 3D ECS for the full temperature range  $0 \leq T < T_{\text{triple}}$ . We will be interested here in the simplest case, for which all microscopic forces are short-ranged and attractive [so-called "type-A" crystals (Rottman and Wortis, 1984)]. A typical scenario for the temperature evolution of such a crystal is shown in Fig. 3.1. This picture is based on current theoretical understanding (e.g., Rottman and Wortis, 1984a) and on experiments, particularly those on  $^4\text{He}$  (e.g., Balibar and Castaing, 1980; Landau et al., 1980; Keshishev et al. 1981; Wolf et al., 1983).<sup>†</sup> At  $T=0$ , the ECS is strictly faceted even in the presence of quantum fluctuations (Fisher and Weeks, 1983; Fradkin, 1983). The  $T=0$  Wulff plot consists of sections of spheres (Herring, 1951), so that an infinite number of Wulff planes pass through the edges and corners of the  $T=0$  ECS. As a result of this degeneracy, all edges and corners become rounded as soon as  $T$  is nonzero. Above  $T=0$  the facets join the rounded regions without any slope discontinuity. With increasing  $T$ , each facet shrinks and eventually disappears at its faceting (or roughening) temperature  $T_R$ . Generally  $T_R$  is different for facets of different crystal symmetry. For temperatures above the highest  $T_R$ , the ECS is completely rounded (but still anisotropic!). Depending on the particular substance involved, the disappearance of facets may be preempted by bulk melting at the triple point. -- In this Section we will focus on a quantitative calculation of the temperature dependent shape of equilibrium facets for a simple model.

---

<sup>†</sup>  $^4\text{He}$  crystal shapes equilibrate within seconds because of the efficient mass transport due to the surrounding superfluid.

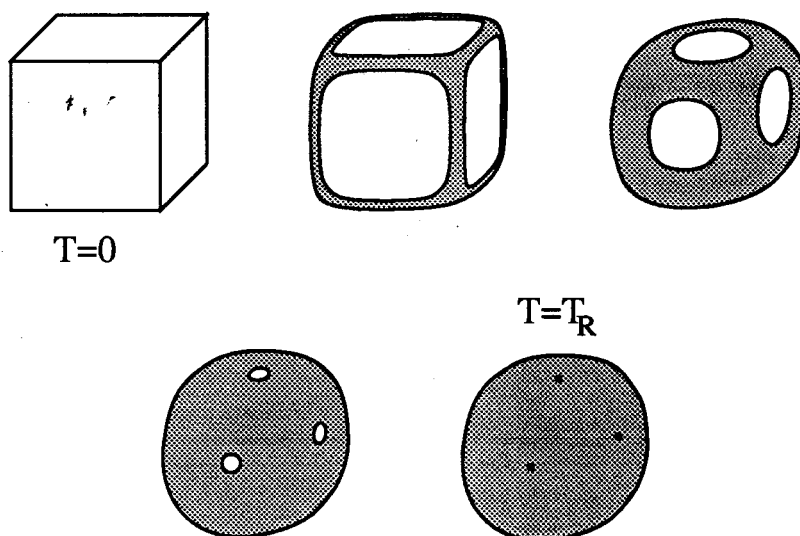


FIG. 3.1. Sketch of the thermal evolution of a ("type A") ECS of cubic symmetry. At  $T=0$  the ECS is strictly faceted. At finite  $T$  all edges and corners become rounded. The facets connect to the rounded regions without slope discontinuity. They shrink with increasing  $T$  and vanish at the faceting or roughening temperature  $T_R$ .

One of the most basic quantities characterizing a 2D crystalline interface is the anisotropic step free energy,  $\gamma(\theta)$ , the excess free energy per unit length associated with the creation of a single step on an otherwise macroscopically flat facet (Burton et al., 1951). It turns out, as we shall show below, that the step free energy per unit length (SFE) is Legendre-transform conjugate to the equilibrium facet shape (EFS),  $y(x)$ . At  $T_R$ , the disappearance of the facet corresponds to the vanishing of the SFE. The corresponding phase transition is the roughening transition. The roughening transition has been studied extensively (e.g, Weeks, 1980). Here, we will give only a brief account of those aspects immediately relevant to this Section.

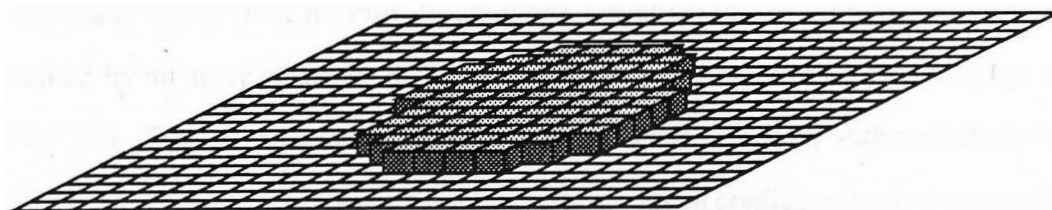


FIG. 3.2. An *island* excitation on an otherwise flat crystalline interface (atoms have been coarse grained into bricks). The island is bounded by a *step*. When the step free energy per unit length vanishes at  $T=T_R$ , there is no longer a free energy barrier for the creation of islands. The character of the crystalline interface becomes fluid-like as large islands of all sizes, as well as islands on islands, can form freely.

The basic physics of the roughening transition is that, when the SFE vanishes, islands [i.e., raised (or lowered) patches surrounded by a step (see Fig. 3.2)] of all sizes can proliferate without bound, so that the interface loses memory of the reference plane, which for  $T < T_R$  was the facet plane. For  $T > T_R$ , the interface thus becomes fluid-like or *rough* at long length scales, with the interfacial width diverging with the system size ( $L$ ) like  $\log(L)$ . The phase below  $T_R$  is known as *smooth*; the phase above  $T_R$ , as *rough*. Correspondingly, the curved and faceted regions of the ECS are identified with the rough and smooth phases, respectively. The fact that some parts of the ECS are rounded for all  $T > 0$ , simply means that  $T_R = 0$  for planar interfaces with orientations of the corresponding tangent planes. For short ranged forces,  $T_R$  is non-zero only for a finite (and usually small) number of interface orientations which correspond to low-Miller-index, high-density facets. Close to  $T_R$ , the SFE/EFS is expected to have universal temperature dependence.

The model which has been very useful to study the universal character of the roughening transition is the so-called solid-on-solid (SOS) model. The SOS model is a pure interface model (i.e., no bulk fluctuations are allowed), in which the interface is represented by an array of stacks of “solids”, the solids being cubes in the simplest case (see Fig. 3.3). The  $i$ th stack consists of cubes up to some height  $h_i$ , with no cubes above  $h_i$  and no vacancies below  $h_i$  (hence the term SOS). A given configuration is then specified by the set of heights  $\{h_i\}$ . The energy of a given configuration is taken to be a function of the area of the “exposed” cube surfaces so that  $\mathcal{H}_{\text{SOS}} = \sum_{\langle ij \rangle} V(|h_i - h_j|)$ , where the sum is over nearest neighbour pairs and  $V(x)$  is an increasing function of  $x$  (common choices are  $x$  and  $x^2$ ). It is often a useful simplification to restrict the difference of the heights of neighbouring stacks to be within a small range [e.g., for the body centred cubic restricted SOS model, the difference is restricted to be  $\pm$  one solid (van Beijeren, 1977)]. The resulting model is called the “restricted” SOS (RSOS) model. The SOS and RSOS models are believed to capture the universal features of the roughening transition. While the SOS model neglects bulk fluctuations (also called “bubbles” in this context), overhangs, and handles (see Fig. 3.3), these excitations can in principle be integrated out with renormalization flow to long length scales, because the bulk correlation length remains finite at  $T_R$  if  $T_R < T_c$  (Huse et al., 1985). The SOS model is dual to the XY model (Chui and Weeks, 1976; van der Erdern and Knops, 1978; Swendsen, 1978). In precise analogy to the duality statement of Eq. (2.3), the SFE,  $\gamma(\theta, T)$ , is just given by the inverse of the XY correlation length, i.e.,

$$\gamma(\theta, T) \rightarrow \text{Be}^{-C/\sqrt{T_R - T}} \quad \text{as} \quad T \rightarrow T_R^- \quad (3.1)$$

Thus, as  $T \rightarrow T_R^-$ , the SFE vanishes with a Kosterlitz-Thouless singularity (Kosterlitz and Thouless, 1973). The functional form of (3.1) is universal; the parameters (“roughening amplitudes”)  $B$ ,  $C$ , and  $T_R$  depend on the details of the model.<sup>†</sup>

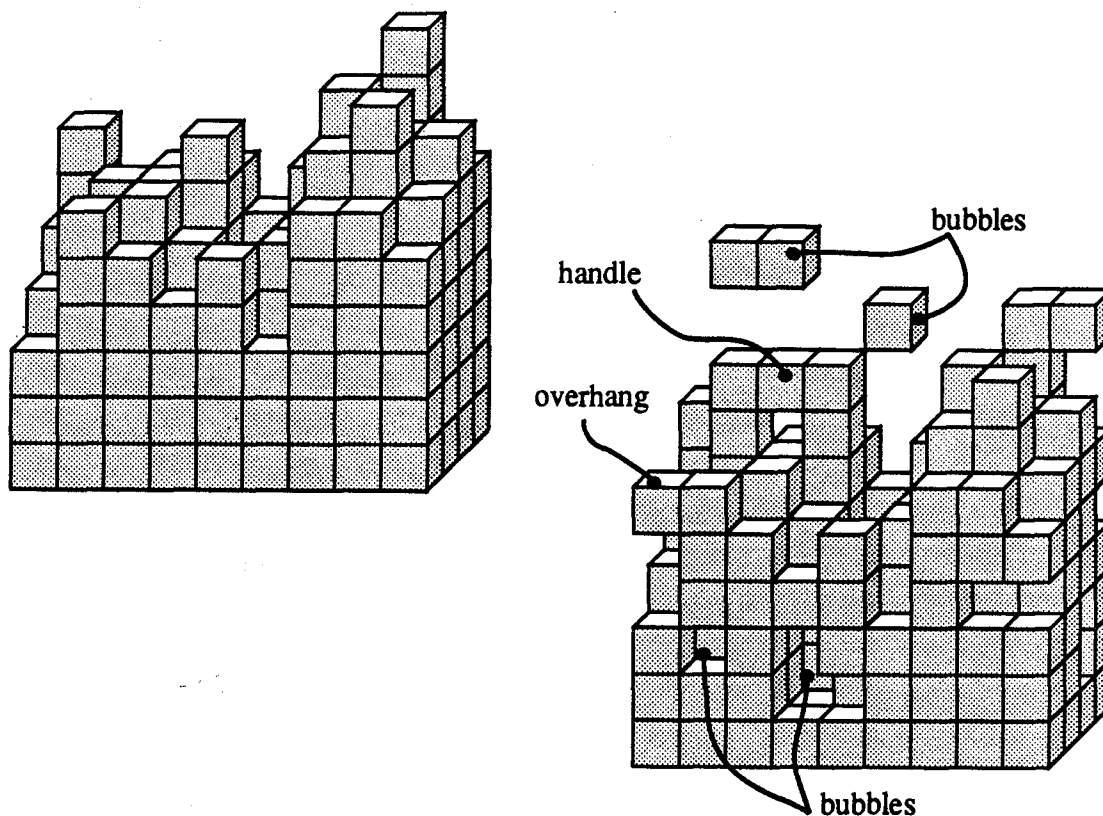


FIG. 3.3. Top: The SOS model. The interface is represented by an array of stacks of cubes. Bottom: A lattice-gas version of the interface. Overhangs, bubbles, and handles are present.

<sup>†</sup> For high-symmetry facets, the facet shape becomes circular as  $T \rightarrow T_R^-$  and  $B$  is independent of  $\theta$ . For lower-symmetry facets, we expect the facet shape to become elliptical as  $T \rightarrow T_R^-$  because of the marginality of the 2D lattice anisotropy. The argument is the same as that for the asymptotically elliptical ECS of 2D Ising models (Zia, 1986). If the facet shape is asymptotically elliptical with eccentricity  $\epsilon$ , then it follows from Legendre conjugacy that the step free energy must be of the form  $\gamma(\theta, T) = f(T) \sqrt{\sin^2 \theta + (1 - \epsilon^2) \cos^2 \theta}$ . The only Kosterlitz-Thouless form compatible with this angular dependence corresponds to  $B = B_0 \sqrt{\sin^2 \theta + (1 - \epsilon^2) \cos^2 \theta}$  and  $C$  a constant (independent of  $\theta$ ).

Exact solutions for the SFE/EFS exist for RSOS models isomorphic to the 6-vertex model (van Beijeren, 1977; Jayaprakash, et al., 1983; Jayaprakash and Saam, 1984a; Kotecký, 1988). While these models show the expected universal XY-dual behaviour at the roughening transition, they do not realistically model a true interface at lower temperatures because of the neglect of overhangs and bubbles. These excitations, although irrelevant in a renormalization-group sense, will alter the detailed, non-universal temperature evolution of the SFE/EFS. An analytical calculation of  $\gamma(\theta, T)$  for a more realistic model which includes these excitations had not been performed prior to the work presented here.

In this Section we develop a systematic low-temperature expansions of the SFE and EFS for the simple-cubic (sc) nearest-neighbour Ising model. These expansions will allow us to study in detail the effects of the excitations neglected in the SOS model. Our expansion will make explicit use of the conjugacy between the SFE and the EFS. We develop two expansions, one directly for the SFE (in the canonical ensemble) and one for the EFS (in the grand canonical ensemble). The expansion for the SFE,  $\gamma(\theta)$ , about its  $T=0$  cusps is divergent where the expansion of EFS is perfectly well behaved, and in that sense the two expansions complement each other.

We focus on the sc Ising model not only because of its simplicity and its fundamental importance to statistical mechanics but also because it allows us to make contact with the work of others. In addition to recent Monte Carlo data (Mon et al., 1988, 1989) for  $\gamma(\theta=0)$ , low-temperature expansions by Weeks et al. in 1973 (see also Leamy et al., 1975) for the (100) facet of the sc Ising and the associated SOS model allow the determination of the corresponding surface tensions  $\Gamma([100])$  (Shaw and Fisher, 1989) and roughening temperatures  $T_R$  (Adler, 1987). The expansions of Weeks et al. involve the combinatorics of finite clusters of adsorbed and/or desorbed atoms on an otherwise flat



interface. Here, we are faced with the more difficult problem of counting the configurations available to these excitations in the presence of a step running across the interface. Because of the interactions of these excitations with the step and the many degrees of freedom of the step itself, the complete combinatorics becomes exceedingly involved. Fortunately, however, a large subset of configurations is in one-to-one correspondence with those of the two-dimensional (2D) Ising ECS problem, for which we have calculated the exact solution in the previous Section. We exploit this fact by structuring the expansions for the SFE/EFS accordingly. While this simplifies our problem considerably, the remaining combinatorics is still non-trivial.

We generate *5th* and *11th* order series for the SFE and the EFS, respectively. We estimate convergence of these series for the symmetry directions to be better than 1% for  $T < 0.78T_R$ . Normalizing the step free energy to the surface free energy of the facet, we calculate the ratio of the facet diameter to the (100) diameter of the crystal. Below  $0.72T_R$ , we find that the facet shape is given to better than 1% by the 2D Ising ECS. Corrections due to overhangs and bubbles contribute less than 0.1% in this temperature region. Above  $0.72T_R$  the facet shape is essentially circular. From numerical extrapolations into the critical region we obtain estimates for the roughening temperature and for the critical amplitudes.

The remainder of this Section is organized as follows: In Sub-section 3.2 we give the conceptual framework on which our expansions are founded. We derive the Legendre-transform conjugacy between the SFE and the EFS, and show that the facet may be thought of as a 2D ECS. We obtain expressions for the SFE and EFS in terms of a canonical and grand canonical partition function, respectively. In Sub-section 3.3 we use the formalism of the previous Sub-section to calculate the step free energy and the shape of the (100) facet of the sc Ising model. In Sub-section 3.4 convergence estimates for the low-temperature

series are developed. The feasibility of extracting critical parameters from the series is discussed. The results of such extrapolations are shown to be consistent with the Monte Carlo estimates of Mon et al. (1988, 1989). We conclude in Sub-section 3.5.

### 3.2 Step free energies and facet shapes from interfacial free energies and equilibrium crystal shapes

As we have already seen in Fig 1.3, facets in the ECS arise from cusps of the Wulff plot . Not just any cusp will do, however. Let the cusp be in the  $\hat{z}$  direction and let  $\hat{m}$  be given in polar coordinates as shown in Fig. 3.4. Suppose that, *at fixed*  $\theta$ , the cusp has an expansion for small  $\phi$  given by

$$\Gamma(\theta, \phi) = \Gamma(\theta, 0) + \Gamma^{(1)}(\theta) \phi^\eta + (\text{higher order in } \phi), \quad (3.2)$$

where  $\eta > 0$ . Consider now the Wulff construction at fixed  $\theta$ . If the Wulff plane of the cusp (the facet plane) intersects with the Wulff plane of  $\Gamma(\theta, \phi)$  in the limit as  $\phi \rightarrow 0$  at a finite distance,  $x$ , from the cusp, then a facet with a smooth edge will be produced. From the similar triangles of Fig. 3.4 it follows that the distance  $x$  is given by

$$x = \Gamma^{(1)} \lim_{\phi \rightarrow 0} \left( \phi^{\eta-1} \right). \quad (3.3)$$

Thus, a facet of finite extent exists only if the cusp is linear, i.e., if  $\eta=1$ . This means that, if a cusp is to be conjugate to a facet with smooth edges,  $\Gamma(\theta, \phi)$  must have the Taylor expansion,

$$\Gamma(\theta, \phi) = \Gamma(\theta, 0) + \left( \lim_{\phi \rightarrow 0} \left. \frac{\partial \Gamma}{\partial \phi} \right|_{\theta} \right) \phi + (\text{higher order in } \phi). \quad (3.4)$$



$$\lim_{\phi \rightarrow 0} \left. \frac{\partial \Gamma}{\partial \phi} \right|_{\theta} = -k_B T \lim_{L \rightarrow \infty} \frac{1}{a} \lim_{L \rightarrow \infty} \frac{1}{L} \left( \ln \text{Tr} e^{-\beta \mathcal{H}_{\hat{z}} + \delta \hat{m}} - \ln \text{Tr} e^{-\beta \mathcal{H}_{\hat{z}}} \right) \quad (3.6a)$$

$$= \frac{1}{a} \lim_{L \rightarrow \infty} \frac{1}{L} \left( -k_B T \ln \text{Tr} e^{-\beta \mathcal{H}_{\hat{z}, \theta}} - A\Gamma(\hat{z}) - V f_b \right) \equiv \frac{\gamma(\theta)}{a}, \quad (3.6b)$$

where  $\mathcal{H}_{\hat{z}, \theta}$  denotes the Hamiltonian for a system with a single step of orientation  $\theta$  running across the facet of normal  $\hat{z}$ . Eq. (3.6) will be the starting point for our canonical expansion scheme for  $\gamma(\theta)$ . It emphasizes that the step free energy is defined in precise analogy to the interfacial free energy [cf. Eq. (1.28)].

A simple but important consequence of the linear cusp (3.4) is that the 3D Wulff construction for the ECS contains a 2D Wulff construction for the facet shape. Consider again a cut trough the 3D Wulff construction at fixed  $\theta$  (see Fig. 3.5). We saw that, in limit as  $\phi \rightarrow 0$ , the line of intersection of the Wulff plane belonging to  $\hat{m}(\theta, \phi)$  with the facet plane occurs at perpendicular distance  $\gamma(\theta)/a$  from the cusp. Since this is true for every angle  $\theta$ , these lines of intersection form a family of lines in the facet plane, each member of which is at perpendicular distance  $\gamma(\theta)/a$  from the cusp. The facet shape is the interior envelope of these lines because the ECS is the interior envelope of the corresponding planes. This shows explicitly that the EFS is obtained as the 2D Wulff construction of a polar plot of  $\gamma(\theta)/a$ . This remarkable fact, which allows us to think of facets as 2D ECS's embedded in the surface of 3D ECS's was first pointed out by van Beijeren and Nolden, and also by Akutsu and Akutsu (1987b), in 1987. The physical explanation is simple: Adjacent to the facet edge, the slope of the rounded region approaches zero, so steps become widely separated in the thermodynamic limit. Thus, the edge of the facet may be regarded microscopically as a single step encircling the (macroscopically) planar facet region. The minimum-free-energy configuration of this step is given by the 2D Wulff construction.

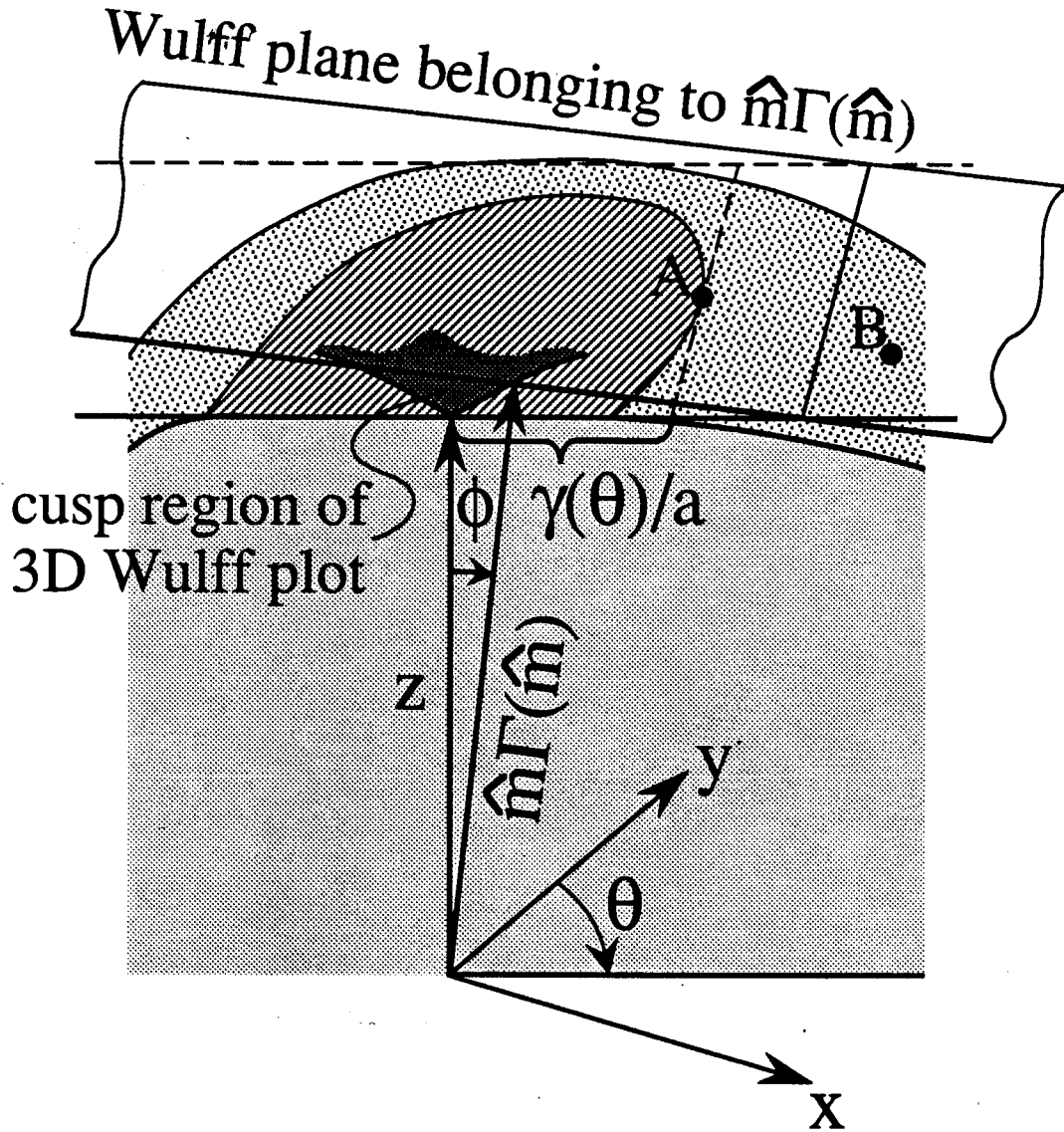


FIG. 3.5: Perspective view of a fixed- $\theta$  cut through the ECS and its Wulff plot as described in the text. The Wulff plane shown is tangent to the ECS at point B in the rounded or rough region of the ECS. In the limit as  $\phi \rightarrow 0$  ( $\hat{m} \rightarrow \hat{z}$ ) this plane intersects the facet plane, which is the Wulff plane of the cusp, along a line (dashed) which is at perpendicular distance  $\gamma(\theta)/a$  from the cusp and tangent to the facet at point A. The facet shape is obtained as the 2D Wulff construction of  $\gamma(\theta)/a$ .

The fact that the SFE and EFS are Legendre-transform-conjugate allows us to express the EFS in terms of a grand canonical trace. An argument paralleling the steps that led to Eq. (1.38) leads us to write the EFS, described in Cartesian coordinates as  $y_f(x_f)$ , as

$$y_f(x_f) = \frac{1}{\lambda a} \lim_{L_x \rightarrow \infty} \frac{1}{L_x} \left\{ -k_B T \ln \sum_{\theta} \text{Tr} e^{-\beta[\mathcal{H}_{\mathcal{L}, \theta} - \lambda a x_f \hat{\mathbf{x}} \cdot \int_{\mathcal{L}} \hat{\mathbf{n}} dL] - A\Gamma(\hat{\mathbf{z}}) - V f_b} \right\}. \quad (3.7)$$

In Eq. (3.7)  $L_x = L/\sqrt{1+s^2}$ , with  $s \equiv \partial y_f / \partial x_f$ , and  $\mathcal{L}$  is the line representing the microscopic step (see Fig. 3.6 and below),  $\hat{\mathbf{n}}$  is the (2D) normal of  $\mathcal{L}$ , and  $\sum_{\theta}$  sums over systems with all possible macroscopic step orientations  $\theta$ . Eq. (3.7) will form the basis of our grand canonical series expansion for  $y_f(x_f)$ .

To elucidate the content of Eq. (3.7), it is useful to derive it directly from the grand canonical formulation of the ECS. If we define  $\eta_f \equiv -\lambda x_f$ , then Eq. (1.38) implies that

$$\lim_{\eta \rightarrow \eta_f} \lim_{A_{xy} \rightarrow \infty} \frac{1}{A_{xy}} \left\{ -k_B T \ln \sum_{\{\hat{\mathbf{m}}\}} \text{Tr} e^{-\beta[\mathcal{H}_{\{\hat{\mathbf{m}}\}} + \eta \cdot \int_S \hat{\mathbf{m}} dS] - A_{xy} \tilde{f}(\eta_f) - V f_b} \right\} = 0, \quad (3.8)$$

where  $\eta \cdot \hat{\mathbf{m}}$  ( $\eta$  is a 2D vector,  $\hat{\mathbf{m}}$  is a 3D vector) is shorthand for  $(\eta_x \hat{\mathbf{x}} + \eta_y \hat{\mathbf{y}}) \cdot \hat{\mathbf{m}}$ . Through Eq. (3.8), the facet coordinates  $x_f$  are implicitly defined. If  $\mathbf{p}_f(\hat{\mathbf{m}}_f)$  denotes the expectation value for the slope of the facet (actually zero here, since we took the facet plane to be horizontal), we may write

$$\tilde{f}(\eta_f) = f(\mathbf{p}_f) - \eta_f \cdot \mathbf{p}_f = \frac{1}{A_{xy}} \left( A\Gamma(\hat{\mathbf{m}}_f) + k_B T \ln e^{\beta A \eta_f \cdot \hat{\mathbf{m}}_f} \right). \quad (3.9)$$

Substituting this into (3.8) we get

$$\lim_{\eta \rightarrow \eta_f} \lim_{A_{xy} \rightarrow \infty} \frac{1}{A_{xy}} \left\{ -k_B T \ln \sum_{\{\hat{\mathbf{m}}\}} \text{Tr} e^{-\beta[\mathcal{H}_{\{\hat{\mathbf{m}}\}} + \eta \cdot \int_S \Delta \hat{\mathbf{m}} dS] - A\Gamma(\hat{\mathbf{m}}_f) - V f_b} \right\} = 0, \quad (3.10)$$

where  $\Delta \hat{\mathbf{m}} \equiv \hat{\mathbf{m}} - \langle \hat{\mathbf{m}} \rangle = \hat{\mathbf{m}} - \hat{\mathbf{m}}_f$ . While the sum in (3.10) extends over systems with all possible interface configurations, only those with vicinal surfaces contribute in the limit  $\eta \rightarrow \eta_f$ . We can, therefore, restrict the ensemble to the subspace of systems which have a single step running across the facet of interest, i.e., we take  $\sum_{\{\hat{\mathbf{m}}\}} \rightarrow \sum_{\theta}$  and  $\mathcal{H}_{\{\hat{\mathbf{m}}\}} \rightarrow \mathcal{H}_{\frac{1}{2}, \theta}$ . A strip of the interface of such a system of width  $L_x$  is shown in Fig. 3.6, projected onto the  $xy$ -plane.  $\Delta \hat{\mathbf{m}} = 0$  everywhere on the interface except on the "cliffs" of height  $a$  (represented by lines in the figure). We may, therefore, write for the field term of Eq. (3.10)

$$\eta \cdot \int_S (\Delta m_x, \Delta m_y) dS = a\eta \cdot \int_{\mathcal{L}} d\mathcal{L} \hat{\mathbf{n}} = a\eta_y L_x + a\eta_x \hat{x} \cdot \int_{\mathcal{L}} d\mathcal{L} \hat{\mathbf{n}}, \quad (3.11)$$

where we have taken advantage of the fact that the integral  $\int_S \hat{\mathbf{m}} dS$  over a close surface vanishes. Substituting this into (3.10) and noting that the  $\eta_y$  term is independent of step configuration establishes (3.7) without any direct reference to  $\gamma(\theta)$ .

Eqs. (3.6) and (3.7) give the size of the facet at given  $\lambda$ . Experimentally, however, we would like to know the coordinates of the facet relative to the physical size of the crystal. As a theoretically convenient and experimentally well defined measure of the crystal size, we take the centre-of-crystal ("Wulff's point", Liebmann, 1914) to centre-of-facet distance, which is simply  $\Gamma(\hat{\mathbf{m}}_f)/\lambda$  [cf. Eq. (1.19)]. The relative facet coordinates  $(\xi_f, \eta_f)$  are, therefore, given by

$$(\xi_f, \eta_f) = \frac{\lambda}{\Gamma(\hat{\mathbf{m}}_f)} (x_f, y_f). \quad (3.12)$$

Finally, we remark that, for some intervals of  $\theta$ , the facet plane may be discontinuously truncated by Wulff planes from a part of the Wulff plot distant from the

facet's cusp. For such  $\theta$ , vicinal planes are thermodynamically unstable and  $\gamma(\theta)$  does not exist [i.e., the limits of Eq. (3.6) do not exist]. Where  $\gamma(\theta)$  does exist, the corresponding facet shape is (for short ranged forces) smooth for all  $0 < T < T_R$ , because the step is essentially a 1D object and can have phase transitions [i.e., cusps in  $\gamma(\theta)$ ] at  $T=0$  only.

We now turn to the problem of calculating explicitly low-temperature expansions for the SFE and the EFS of the sc Ising model.

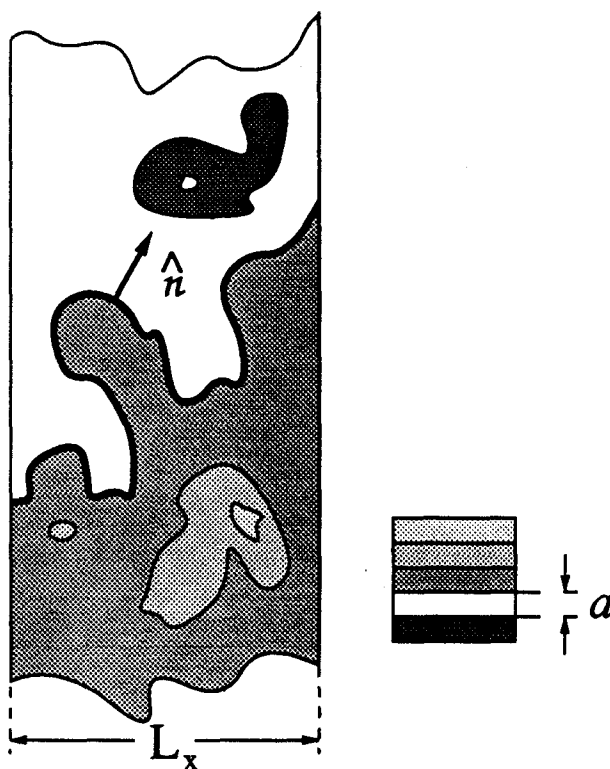


FIG. 3.6: A strip of vicinal surface projected onto the  $xy$  plane. The shading represents lattice planes of spacing  $a$  at different levels. The strip contains a "bare" step  $L$  (bold line) and excitations on the terraces to either side of the step (closed curves).  $\hat{n}$  is the 2D microscopic normal to the step in the  $xy$  plane. The field contribution to the grand canonical Hamiltonian,

$$\eta \cdot \int_S (\Delta m_x, \Delta m_y) dS = a\eta \cdot \int_{\text{all curves}} d\ell \hat{n},$$

vanishes around closed curves and, therefore, couples only to the "bare" step.



### 3.3 Low-Temperature Series for the SFE/EFS of the simple-cubic Ising model

The Hamiltonian of the nearest-neighbour sc Ising model is

$$\mathcal{H} = -J \sum_{\langle NN \rangle} \sigma_i \sigma_j, \quad (3.13)$$

where the "spins",  $\sigma_j = \pm 1$ , are located at the vertices of a simple-cubic lattice of lattice constant  $a$  and the sum is over nearest-neighbour pairs. To keep our equations uncluttered in the remainder of this Section, we shall set the overall scale factor  $\lambda a^3/J=1$  and measure lengths in units of  $a$ , temperature in units of  $J/k_B$ , and energy in units of  $J$ . (We shall also drop the subscripts on  $x_f$  and  $y_f$  from here on.) In the lattice-gas interpretation of (3.13),  $\sigma_j = +1$  means that site  $j$  is occupied (by an "atom");  $\sigma_j = -1$  means site that  $j$  is vacant. This model has a bulk phase transition at  $\beta_c = 0.221655$  (Pawley et al., 1984). For  $T < T_c$  there may be a first-order interface between a predominantly  $\sigma_j = +1$  phase and a predominantly  $\sigma_j = -1$  phase. The ECS is a cube at  $T=0$ . For  $0 < T < T_R$  all interface orientations are expected to be stable (Rottman and Wortis, 1984b). At  $T=0$  the (100) facet consists of a plane of bonds between spins of opposite sign. As  $T$  increases, fluctuations are excited as spins flip in the bulk (gas atoms and vacancies) and on the interface (ad- and desorbed atoms). Just as in Section 2, this is most easily visualized not in terms of broken bonds but in terms of their dual-lattice plaquettes. Each plaquette corresponds to a unit of interfacial area and costs energy 2 (i.e.,  $2J$ ).

In order to study a step on a (100) interface, we need to make appropriate changes in the Hamiltonian (3.13). Consider the Ising system as filling a box of volume  $V$  and height  $L_z$  in which (100) lattice planes of area  $A$  are stacked at  $z = \pm 1/2, \pm 3/2, \pm 5/2, \dots$ . To eliminate wall energies and to enforce a (100) interface, connect the box periodically in

the x and y directions and antiperiodically in the z direction. The (100) interface can be stabilized at  $z=0$  by applying an infinitesimal external symmetry breaking field, as described, for example, by Weeks et al. in 1973. The ground state of this interface is a plane of plaquettes at  $z=0$ . Let the coordinates of the dual lattice sites in this plane be given by two integers  $(n_x, n_y)$ . We now modify the lattice by piercing it with two screw dislocations of Burgers vector  $+\hat{z}$  at  $(0,0)$  and  $-\hat{z}$  at  $(N,M)$ . This forces a step into the interface running from  $(0,0)$  to  $(N,M)$  at average angle  $\theta = \arccos(N/L)$  with length  $L = \sqrt{N^2 + M^2}$ . Between the dislocations, this step divides the interface into an upper and a lower terrace. We choose to enforce the step in this manner (rather than by boundary conditions) for combinatorial reasons. We envision the ground state of the interface with this step to be planar everywhere except for the "tear" consisting of the  $|N| + |M| = K$  extra plaquettes constituting the shortest possible step from  $(0,0)$  to  $(N,M)$ . This state has degeneracy  $d_0(N,M) = \binom{K}{|M|}$ , because the step may stride  $|N|$  times in the x direction and  $|M|$  times in the y direction in any order (Fig. 3.7a). As T increases, atoms ad- and desorb on the facet and the step will begin to lengthen and to develop overhangs (Fig. 3.7b). The total free energy of this system will have contributions scaling like V from the bulk, like A from the (100) interface, like L from the step, and like  $L_z$  from the screw dislocations, plus end effects of order unity from the regions where the step terminates. Since we wish to extract the step free energy, we must also subtract the screw-dislocation contribution in addition to the bulk and surface terms already subtracted in Eqs. (3.6b) and (3.7). It turns out that the screw dislocations do not contribute to the orders considered in our calculation. Thus, we absorb them, for notational convenience, in the bulk free energy term, i.e.,  $f_b \rightarrow f_b + 2 \frac{L_z}{V} f_{\text{screw}}$ , where they can henceforth be ignored.

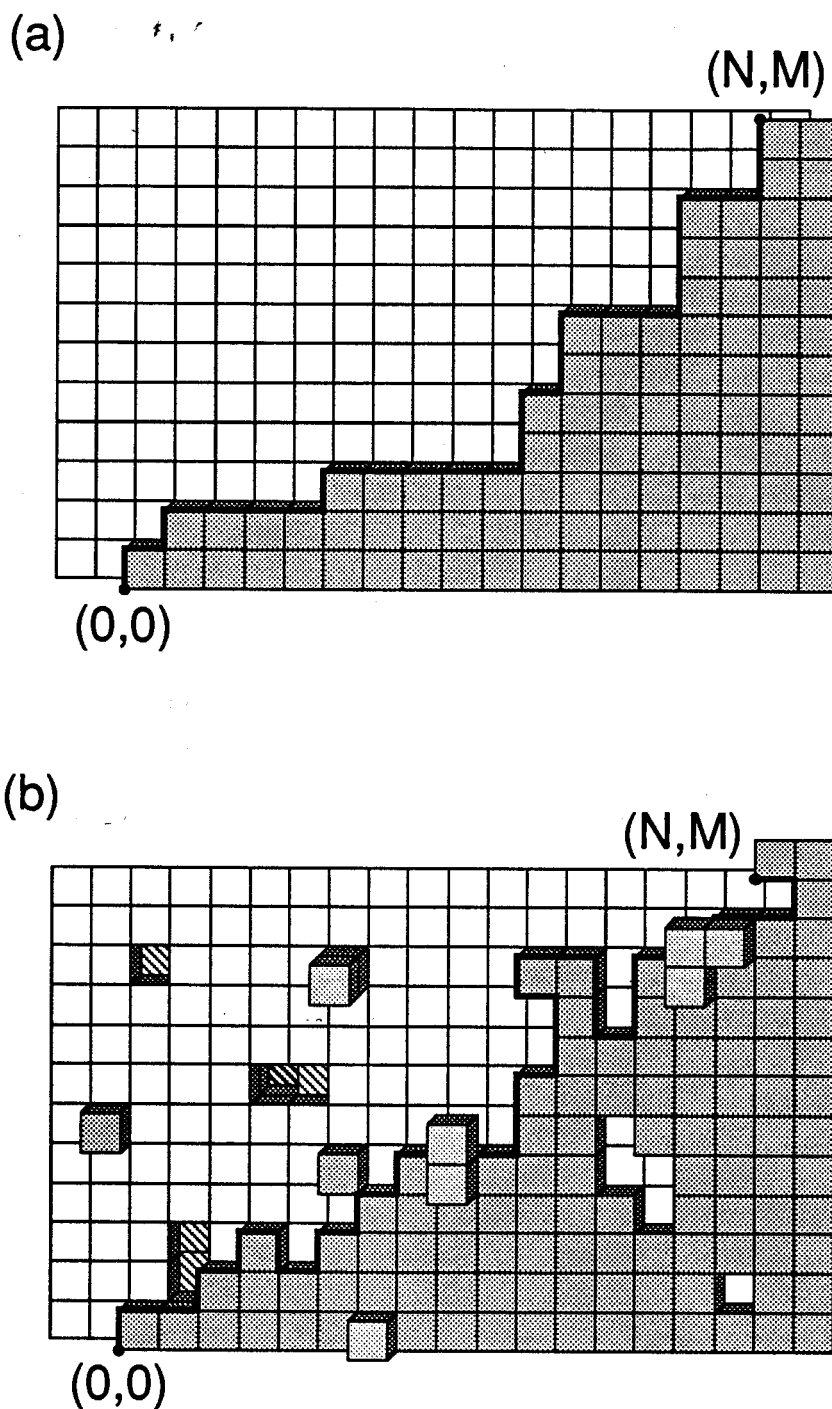


FIG. 3.7: Typical step configurations of the simple cubic Ising (100) interface: a.)  $T=0$  b.)  $T>0$ . The "bare" step is, by our convention, a non-self-intersecting line lying in the plane as indicated by the bold line.

In the canonical ensemble, the macroscopic orientation of the step is fixed by fixing  $N$  and  $M$ . As a consequence, plaquettes can only be excited in pairs, so that  $\mathcal{H}$  has eigenvalues  $E_n = 4n$ , where  $n$  is one half the number of plaquettes. The lowest excited state corresponds to adding two plaquettes to the step. The canonical low-T expansion variable is, therefore,  $v \equiv e^{-4\beta}$ , and the expansion of the canonical partition functions becomes

$$\text{Tr} e^{-\beta \mathcal{H}_{z,\theta}} = d_0 e^{-2\beta(A+K)} \left( 1 + \sum_{n=1}^{\infty} g_n(N, M; A; V) v^n \right), \quad (3.14)$$

where  $d_0 g_n$  is the degeneracy of the  $n$ th excited state.

In the grand canonical ensemble, step orientations are summed over by summing over  $M$  at fixed  $N$ . The ground state is then nondegenerate and corresponds to a straight step of  $N$  plaquettes from  $(0,0)$  to  $(N, M=0)$ . Because  $M$  is free, plaquettes can be excited one at a time with the lowest excited state corresponding to the two steps of  $N+1$  plaquettes from  $(0,0)$  to  $(N, M=\pm 1)$ . The expansion variable is now  $w \equiv e^{-2\beta} = \sqrt{v}$ . At order  $w^n$  the step can terminate at the  $n+1$  positions  $[N, M(n, m)]$ , where  $M(n, m) = n - 2m$  with  $m \in \{0, 1, 2, \dots, n\}$ . For a step terminating at  $M$ , the field contribution to the Hamiltonian is

$x \hat{x} \cdot \int_{\mathcal{L}} d\mathcal{L} \hat{n} = -xM$  and the grand partition function becomes

$$\sum_{\theta} \text{Tr} e^{-\beta[\mathcal{H}_{z,\theta} - x \int_{L_x} dx' s(x')]} = e^{-2\beta(A+N)} \left( 1 + \sum_{n=1}^{\infty} \tilde{g}_n(x) w^n \right), \quad (3.15)$$

with

$$\tilde{g}_n(x) = \sum_{M=n \bmod 2}^n \binom{K}{M} g_{(n-M)/2}(N, M; A; V) [2 \cosh(\beta x M) - \delta_{M,0}]. \quad (3.16)$$

The prime indicates that the sum is over even (odd)  $M$  if  $n$  is even (odd), and we have taken advantage of the symmetry,  $g_n(N, M) = g_n(N, -M)$ . Low- $T$  expansions for  $\Gamma(\hat{z})$  and  $f_b$  take the form,<sup>†</sup>

$$\Gamma(\hat{z}) = 2 - T \sum_{j=2}^{\infty} \Gamma_j v^j \quad (3.17)$$

and

$$f_b = -T \sum_{j=3}^{\infty} f_{b,j} v^j. \quad (3.18)$$

Low  $T$  expansions of  $\gamma(\theta)$  and  $y(x)$  are obtained by substituting (3.14) and (3.15) [and also (3.17) and (3.18)] into (3.6b) and (3.7), respectively, to obtain

$$\begin{aligned} \gamma(\theta) = & 2(c+s) - T [(c+s)\ln(c+s) - c \ln c - s \ln s] \\ & - T \lim_{L \rightarrow \infty} \frac{1}{L} \sum_{j=1}^{\infty} (\gamma_j - A\Gamma_j - Vf_{b,j}) v^j \end{aligned} \quad (3.19)$$

and

$$y(x) = 2 - T \lim_{N \rightarrow \infty} \frac{1}{N} \left[ \sum_{j=1}^{\infty} y_j w^j - \sum_{i=2}^{\infty} (A\Gamma_i + Vf_{b,i}) w^{2i} \right], \quad (3.20)$$

where  $c \equiv |\cos\theta|$  and  $s \equiv |\sin\theta|$ .  $\sum_{j=1}^{\infty} \gamma_j v^j$  and  $\sum_{j=1}^{\infty} y_j w^j$  are the series expansions of

$\ln(1 + \sum_{n=1}^{\infty} g_n v^n)$  and  $\ln(1 + \sum_{n=1}^{\infty} \tilde{g}_n w^n)$ , respectively. Note that, if the limit of Eq.

<sup>†</sup> The expansion for the (100) surface tension of the simple cubic Ising model was calculated by J. Weeks, G. H. Gilmer and H. J. Leamy in 1973. The series was not published in the original literature and was only recently quoted by Shaw and Fisher in 1989 as:

$$\Gamma(\hat{z})(\text{Ising}) = 2 - T \left( 2v^2 + 2v^3 + 10v^4 + 16v^5 + \frac{242}{3}v^6 + 150v^7 + 734v^8 + \frac{4334}{3}v^9 + \dots \right).$$

For completeness we also quote their SOS result, which was published by Leamy in 1975:

$$\Gamma(\hat{z})(\text{SOS}) = 2 - T \left( 2v^2 + 4v^3 + 10v^4 + 24v^5 + \frac{194}{3}v^6 + 172v^7 + 452v^8 + \frac{3185}{3}v^9 + \dots \right).$$

(3.20) is to exist, then  $y_{\text{odd}}$  cannot contain any A- or V-dependent terms. Eq. (3.19) shows that, at  $T=0$ ,  $\gamma(\theta)$  has cusps at  $\theta=0$  and symmetry equivalent angles. Since we are expanding about  $T=0$ , we anticipate convergence problems in the vicinity of these singularities. (In fact we will see below that the canonical expansion is divergent at the cusps.) Also, note that it follows from the symmetry of the lattice that, at finite temperature,  $\partial\gamma(\theta)/\partial\theta=0$  at  $\theta=\frac{\pi}{4}$  and  $\theta=0$ . Since all step orientations are stable, Eq. (1.12) then implies that, conveniently,  $\gamma(0)=y(0)$  and  $\gamma(\frac{\pi}{4})=\sqrt{2}y(x=y)$ .

To calculate the degeneracies  $g_n$ , it is most useful to develop a diagrammatic notation. To this end, we distinguish three classes of excitations (see Fig. 3.7b). These are 1.) single-layer ad- and desorptions on the upper and lower terraces but not overhanging the step, 2.) multilayer excitations and overhangs, and 3.) bulk excitations (bubbles), i.e., excitations not topologically connected to the main sheet of plaquettes. Class 2 may be further subdivided into SOS and non-SOS configurations. If we include only class 1 and class 2 SOS configurations, we obtain the expansion for the corresponding SOS model. For combinatorial convenience, it is our convention here to take the step itself (the "bare" step) to be a single, non-self-intersecting line lying in the plane. Since this line cannot generally be chosen without ambiguity in the presence of additional excitations (see Fig. 3.8), summing over all possible distinct lines (of some given length) in accordance with this convention leads to an overcounting which must be compensated. The method described below turns out to handle this problem automatically, at least to the orders calculated. We shall comment further on this point at the end of this Sub-section. For class 1 configurations, we adopt the diagrammatic notation shown in Table 3.I. Class 2 and 3 excitations will be denoted by self-explanatory pictures (Table 3.II).

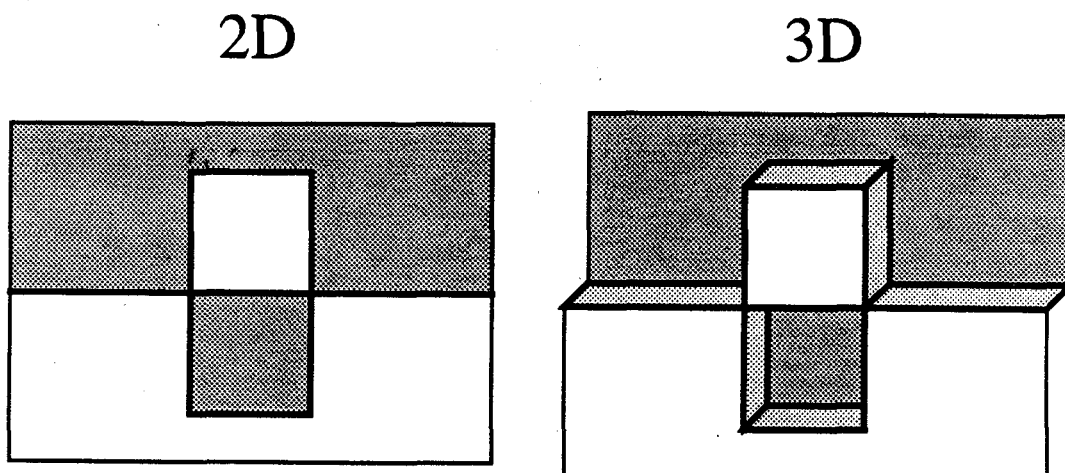


FIG. 3.8: This figure illustrates that the step cannot be chosen as a single non-self-intersecting line without ambiguity. For the configuration shown, that ambiguity arises in the same way for the 2D and 3D Ising models. If we let white be "up" and shaded be "down", this configuration could be considered to be either a step with a downward indentation and a white disconnected excitation or a step with an upward indentation and a shaded disconnected excitation. At each order considered in this work, the number of ambiguous 2D configurations equaled the number of ambiguous 3D configurations.

Each diagram contains the "bare" step plus a number (possibly zero) of disconnected parts denoting additional excitations. These disconnected parts contain contributions to facet and bulk free energies in addition to the step free energy. The contribution to the step free energy results from the fact that the presence of the step reduces the number of configurations available to the disconnected excitations. Since a given state of  $\mathcal{H}$  corresponds to a fixed number of plaquettes, we can describe this interaction as being due to two mechanisms: First, disconnected diagrams abutting the step are not allowed because this would annihilate plaquettes and, secondly, disconnected diagrams straddling the step are not allowed as this would create plaquettes. We may, therefore, write for the class 1 diagram  $S-D$


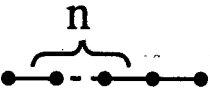
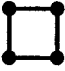
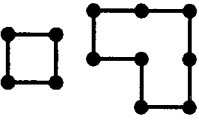
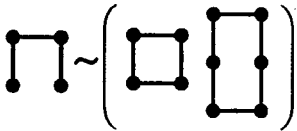
$$S \sim \mathcal{D} = S \times \mathcal{D} - (S \sim \mathcal{D})_d, \quad (3.21)$$

where  $(S \sim \mathcal{D})_d$  denotes the number of  $\mathcal{D}$  configurations disallowed in the presence of the step  $S$ . For singly disconnected diagrams we have

$$(S \sim \mathcal{D}^1)_d = (S \sim \mathcal{D}^1)_A + (S \sim \mathcal{D}^1)_S, \quad (3.22)$$

where  $(S \sim \mathcal{D})_A$  denotes the number of abutting and  $(S \sim \mathcal{D})_S$  the number of straddling configurations. Multiply disconnected diagrams are more complicated but the same general principles apply.

**Table 3.I**  
Definitions for Class 1 Diagrams

generic symbol	diagram	definition
$S_0$		$\frac{1}{d_0} \times$ [number of configurations of a step of $ M + N +n$ plaquettes whose ends are fixed at $(0,0)$ and $(N,M)$ ]; $d_0 \equiv \binom{ M + N }{ M }$
$S_n$		
$\mathcal{D}^1$		number of configurations available to ad/desorptions of the shape indicated
$\mathcal{D}^2$		
$S \sim \mathcal{D}$		$\frac{1}{d_0} \times$ (number of disconnected configurations possible in the presence of the step indicated)



If we were to allow only desorptions on the upper terrace level and adsorptions on the lower, interface configurations would be isomorphic to those of the 2D square Ising model with an interface between “up” and “down” phases in lieu of the step. Although the symmetry of  $\mathcal{H}$  between ad- and desorptions destroys this isomorphism, we can still take advantage of the exact 2D solution for the interfacial free energy,  $\Gamma_{2D}(\theta)$ , and for the ECS,  $y_{2D}(x)$ , to simplify the full 3D combinatorics. Note that class 1 diagrams can equally well be used in the expansion of  $\Gamma_{2D}(\theta)$  and  $y_{2D}(x)$ , if we ignore the fact that they are to represent both ad- and desorptions. In 2D, the nature of the “interaction” between disconnected parts and the step remains unchanged from 3D (dual-lattice bonds replacing dual-lattice plaquettes), so Eqs. (3.21) and (3.22) hold also for the 2D interpretation of the diagrams. For singly disconnected diagrams  $(S\sim\mathcal{D}^1)_{3DS} = 2(S\sim\mathcal{D}^1)_{2DS}$ , as both ad- and desorptions can straddle the step. However,  $S$  and  $(S\sim\mathcal{D}^1)_A$  have the same value, whether interpreted as 2D or 3D configurations, because adsorptions (desorptions) are allowed to abut the step on the upper (lower) terrace. This allows us to shift the necessity for doing the explicit combinatorics of many 2D configurations up by several orders from where they first occur by writing

$$\gamma(\theta) = \Gamma_{2D}(\theta) - T \lim_{L \rightarrow \infty} \frac{1}{L} \sum_{j=1}^{\infty} \left\{ (\gamma_j - \gamma_{2Dj}) - A(\Gamma_j - f_{2Db_j}) - V f_b \right\} v^j \quad (3.23)$$

$$\equiv \Gamma_{2D}(\theta) - T \sum_{j=1}^{\infty} \left( \lim_{L \rightarrow \infty} \frac{\Delta \gamma_j}{L} \right) v^j \equiv \Gamma_{2D}(\theta) - T \sum_{j=1}^{\infty} b_j v^j \quad (3.24)$$

and

$$y(x) = y_{2D}(x) - T \lim_{L \rightarrow \infty} \frac{1}{L} \left\{ \sum_{j=1}^{\infty} (y_j - y_{2Dj}) w^j - \sum_{i=2}^{\infty} \left[ A(\Gamma_i - f_{2Db_i}) + V f_{b_i} \right] w^{2i} \right\} \quad (3.25)$$

$$\equiv y_{2D}(\theta) - T \sum_{j=1}^{\infty} \left( \lim_{L \rightarrow \infty} \frac{\Delta y_j}{L} \right) w^j \equiv y_{2D}(\theta) - T \sum_{j=1}^{\infty} b_j w^j \quad (3.26)$$

In these equations  $\gamma_{2D_i}$  and  $y_{2D_i}$  are the 2D versions of  $\gamma_i$  and  $y_i$ , respectively, i.e., they are the terms in Eqs. (3.19) and (3.20) arising from the 2D interpretation of class 1 diagrams.  $f_{2D_b}$  is the 2D bulk free energy for the 2D Ising model. The effect of this rearrangement is that many terms cancel in the curly brackets of (3.23) and (3.25), so that the number of diagrammatic terms corresponding to  $\Delta\gamma_i$  and  $\Delta y_i$ , which remain to be evaluated is significantly reduced (at least at low orders). This is a tremendous simplification, as the order-by-order calculation of  $S$  and  $(S\sim\mathcal{D})_A$  diagrams is exceedingly tedious. Also, all terms involving  $A$  and  $V$  vanish, as is necessary if the thermodynamic limit  $L\rightarrow\infty$  is to exist. Because these terms cancel, the  $\Delta\gamma_i$  and  $\Delta y_i$  can be expressed entirely in terms of the  $A$ - and  $V$ -independent parts of  $g_i$  and  $g_{2D_i}$ . If  $a_i$ ,  $\Delta g_i$ ,  $\tilde{a}_i$ , and  $\Delta\tilde{g}_i$  denote the  $A$ - and  $V$ -independent parts of  $g_{2D_i}$ ,  $(g_i - g_{2D_i})$ ,  $\tilde{g}_{2D_i}$  and  $(\tilde{g}_i - \tilde{g}_{2D_i})$ , respectively, we can, therefore, simply write

$$\sum_{j=1}^{\infty} \Delta\gamma_j v^j = \ln \left[ 1 + \sum_{i=1}^{\infty} (a_i + \Delta g_i) v^i \right] - \ln \left( 1 + \sum_{i=1}^{\infty} a_i v^i \right) \quad (3.27)$$

and

$$\sum_{j=1}^{\infty} \Delta y_j w^j = \ln \left[ 1 + \sum_{i=1}^{\infty} (\tilde{a}_i + \Delta\tilde{g}_i) w^i \right] - \ln \left( 1 + \sum_{i=1}^{\infty} \tilde{a}_i w^i \right). \quad (3.28)$$

It is crucial here that  $a_i$ ,  $\Delta g_i$ ,  $\tilde{a}_i$ , and  $\Delta\tilde{g}_i$  contain not only the terms of order  $L^1$ , but also those of order  $L^0$ , since the latter get multiplied by order  $L^1$  terms at higher order in the expansion of the logarithms. The nonvanishing  $a$ 's and  $\Delta g$ 's needed in (3.27) for the calculation of the  $\Delta\gamma_i$  to order 5, inclusively, have the diagrammatic expansions,

$$\begin{aligned}
a_1 &= \text{(I)} \\
a_2 &= \text{(III)} - \text{(II)} \\
\Delta g_3 &= \text{(1)} \\
\Delta g_4 &= \text{(2)} + \text{(3)} + \text{(4)} + \text{(5)} + \text{(6)} + \text{(7)} + \text{(8)} \\
\Delta g_5 &= \sum_{D=9}^{29} \text{(D)} ,
\end{aligned} \tag{3.29}$$

where the numbers in brackets label diagrams listed (with their numerical equivalents) in Table 3.II (some combinatorial details are given in Appendix E). The corrections  $\Delta y_i$  can now be evaluated to 11th order *without* calculating additional diagrams. The expansions of the necessary nonvanishing  $\tilde{a}_i$  and  $\Delta \tilde{g}_i$  are simply obtained by appropriate substitution into Eq. (3.16) (put  $g=a$  to evaluate  $\tilde{a}$  and  $g=\Delta g$  to evaluate  $\Delta \tilde{g}$ ).<sup>†</sup>

To the orders calculated here, the method of expansion described above solves the problems associated with the ambiguity of defining the step as a single, non-self-intersecting line (Fig. 3.8). We find that, with consistent use of that definition, diagrams conspire such that the number of overcounted configurations is the same for the 2D model as it is for the 3D model, so that they cancel in the calculation of the  $\Delta g_i$ . This cancellation is transparent for simple diagrams such as shown in Fig. 3.8. It can be checked to occur at the orders considered in this work; whether it persists to all orders is unclear.

---

<sup>†</sup> The calculation of the diagrams appearing in the grand canonical expansion is easier (at least at low orders) than the calculation of the canonical diagrams, in the sense that the former, unlike the latter, need not be calculated for general  $M$ . This fact may be useful to push our calculation to higher order to get more information in the critical region. Since the facet is essentially isotropic there, the fact that the grand canonical series converges best in only one symmetry direction ( $\theta=0$ ) is not a serious limitation.

*And thick and fast  
They came at last,  
And more and more and more.*

L. CARROLL

Table 3.II  
Diagrams and their Numerical Equivalents

#	DIAGRAM	WEIGHT
I		$\frac{ N ( N+1) }{ M+1 } + \frac{ M ( M+1) }{ N+1 }$
II	$\left( \text{---} \sim \text{---} \right)_A$ 	$2\left(K - \frac{ NM }{K}\right)$
III		$\left\{ \frac{1}{2} \left[ \frac{ N ( N+1) }{( M+1 )( M+2 )} (K+ M +N^2+2) +  NM  \right] \right.$ $\left. + 2 \frac{K+1}{ M+1 } + K - \frac{ NM }{K} - 2 \right\} + \{N \leftrightarrow M\}$
IV	$\left( \text{---} \sim \text{---} \right)_A$ 	$\left\{ \frac{2 N (N^2+ N+1 )}{ M+1 } + K +  NM  \right\} + \{N \leftrightarrow M\}$
V	$\left( \text{---} \sim \text{---} \right)_A$ 	$4K - \frac{4 NM }{K} + 2$

$\Delta g_3$ :  
CLASS 1

#	DIAGRAM	WEIGHT
1	$-\left( \text{---} \sim \text{---} \right)_{2DS}$ 	$-K$

$\Delta g_4$ :  
CLASS 1

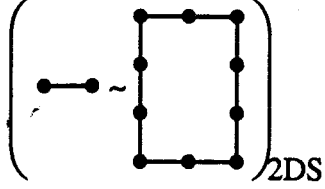
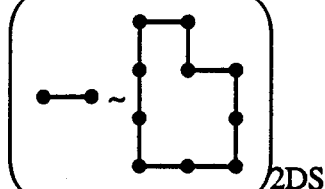
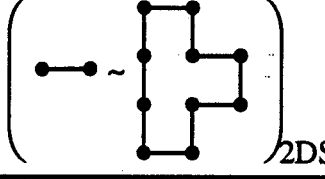
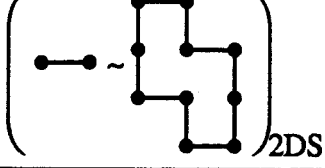
#	DIAGRAM	WEIGHT
2	$-\left( \begin{array}{c} \text{---} \\ \text{---} \\ \text{---} \end{array} \sim \begin{array}{c} \text{---} \\ \text{---} \\ \text{---} \\ \text{---} \\ \text{---} \end{array} \right)_{2DS}$	$-(K+2) \times (I)$
3	$-\left( \text{---} \sim \begin{array}{c} \text{---} \\ \text{---} \\ \text{---} \\ \text{---} \\ \text{---} \end{array} \right)_{2DS}$	$-(K+1)$
4	$-\left( \text{---} \sim \begin{array}{c} \text{---} \\ \text{---} \\ \text{---} \\ \text{---} \end{array} \right)_{2DS}$	$-2K$
5	$-\left( \text{---} \sim \begin{array}{c} \text{---} \\ \text{---} \\ \text{---} \\ \text{---} \\ \text{---} \end{array} \right)_{2DS}$	$-2K - (II)$
6	$\Delta \left[ \text{---} \sim \left( \begin{array}{c} \text{---} \\ \text{---} \\ \text{---} \\ \text{---} \end{array} \right) \right]$	$(II) + K$

CLASS 2

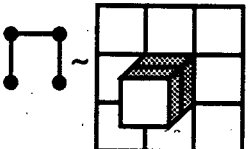
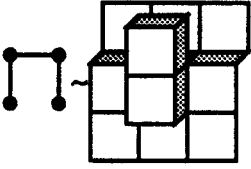
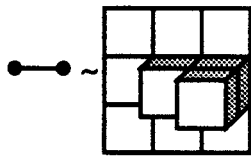
#	DIAGRAM	WEIGHT
7		$-(II)$
8		$2K$

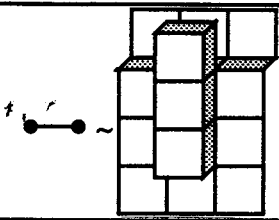
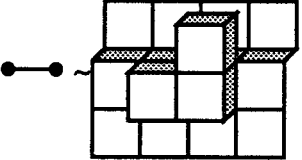
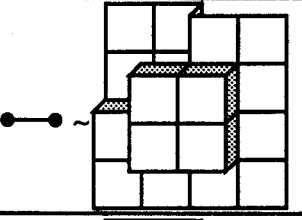
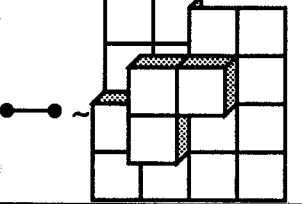
$\Delta g_5$ : CLASS 1

#	DIAGRAM	WEIGHT
9	$f_1 - \left( \begin{array}{c} \text{Diagram 9} \\ \text{2DS} \end{array} \right)$	$-(K+4) \times (\text{III})$
10	$- \left( \begin{array}{c} \text{Diagram 10} \\ \text{2DS} \end{array} \right)$	$-(K+3) \times (\text{I})$
11	$- \left( \begin{array}{c} \text{Diagram 11} \\ \text{2DS} \end{array} \right)$	$-2(K+2) \times (\text{I}) + 2 \frac{N^2+M^2}{K}$
12	$- \left( \begin{array}{c} \text{Diagram 12} \\ \text{2DS} \end{array} \right)$	$-2(K+2) \times (\text{I}) - (\text{IV})$
13	$\Delta \left[ \begin{array}{c} \text{Diagram 13} \end{array} \right]$	$(\text{IV}) + (K+2) \times (\text{I})$
14	$\Delta \left[ \begin{array}{c} \text{Diagram 14} \end{array} \right]$	$2K - 10 \times (\text{I}) + 2 \times (\text{V})$ $+(K+6) \times (\text{II})$
15	$- \left( \begin{array}{c} \text{Diagram 15} \\ \text{2DS} \end{array} \right)$	$-3K$
16	$- \left( \begin{array}{c} \text{Diagram 16} \\ \text{2DS} \end{array} \right)$	$-12K + 2 NM  \frac{3K-4}{K(K-1)}$

17		$-3K - 4$
18		$-8(K+1) - 2 \times (\text{II})$
19		$-2K - 2 \times (\text{II})$
20		$-2K - 2 \times (\text{II})$

CLASS 2

#	DIAGRAM	WEIGHT
21		$- (\text{IV})$
22		$2(K+2) \times (\text{I})$
23		$8 \frac{ \text{NMI} }{K} - 12K - 4$

24		$2K$
25		$2 \times (\text{II})$
26		$2 \frac{ NM }{K}$
27		$2 \frac{ NM }{K}$

## CLASS 3

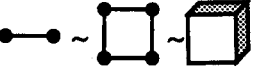
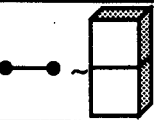
#	DIAGRAM	WEIGHT
28		$-2K$
29		$-K$

Table 3.II: A list of the diagrams which had to be evaluated explicitly to obtain the correction terms to the 2D Ising model at the orders indicated (some combinatorial details are given in Appendix E). Each of the class 2 and 3 diagrams shown has another version in which gas and solid sites are symmetrically interchanged. All these configurations are of course included in the weights given. Only V- and A-independent terms are given; as in the text,  $K=|M|+|N|$ . The subscript A indicates that the number of forbidden *abutting* configurations is to be counted. The subscript 2DS means that the number of forbidden *straddling* configurations of the diagram,



*interpreted as a 2D diagram*, is to be calculated.  $\Delta(\text{diagram})$  denotes the difference between the 3D and 2D interpretations of the diagram. The notation  $+ \{N \leftrightarrow M\}$  means that the previous term with  $N$  and  $M$  interchanged is to be added.

### 3.4 Results and Discussion

The results of our expansions are summarized in Tables 3.III and 3.IV. The series for  $\Gamma_{2D}(\theta)$  and  $y(x)_{2D}$  are given in Appendix C. Let  $\gamma(\theta, N)$  and  $y(x, N)$  denote the series for  $\gamma(\theta)$  and  $y(x)$  summed to order  $N$ , inclusively. Fig. 3.9 shows the behaviour of the canonical expansion as a function of  $\theta$ .  $\gamma(\theta, N)$  diverges about its  $T=0$  cusps at  $\theta=0$  and converges best at  $\theta=\frac{\pi}{4}$  (and their symmetry equivalent angles). Interestingly, the angular radius of convergence decreases with increasing  $T$  and presumably vanishes at  $T_R$ , reflecting the Kosterlitz-Thouless singularity of  $\gamma(\theta)$  at  $T_R$  [cf. Eq. (3.1)]. On the other hand,  $y(x, N)$  converges best at  $x=0$  ( $\theta=0$ ), with a radius of convergence in  $x$  which also appears to vanish as  $T \rightarrow T_R$ . Fig. 3.10 shows  $y(x, 11)$  as a function of  $x$  and the Legendre transform of  $\gamma(\theta, 5)$ , both normalized to the crystal diameter [cf., Eq. (3.12)]. At low temperatures the grand canonical series nicely fills in the part of the facet shape not obtainable from the canonical series. Fig. 3.11 shows a plot of  $\gamma(\theta, N)$  versus  $T$  in the symmetry directions  $\theta=\frac{\pi}{4}$  and  $\theta=0$ . These series appear to converge to the asymptotic form (3.1) (see also Fig. 3.13) by developing minima which move with increasing order toward the  $T$  axis from below. This behaviour of the series is consistent with that of the BCRSOS model (van Beijeren, 1977; Jayaprakash et al., 1983) which, for  $\theta=\frac{\pi}{4}$ , is given to order  $v^{40}$  in Appendix D.

**Table 3.III**  
 Summary of the Low-T Expansion of the  
 Step Free Energy  $\gamma(\theta)$

$\gamma(\theta) = \Gamma_{2D}(\theta) - T \sum_{n=3}^{\infty} b_n e^{-4\beta n}$				
$c \equiv  \cos\theta $ ; $s \equiv  \sin\theta $				
	3D Ising		SOS	
n	$b_n$	$\theta = \frac{\pi}{4}$	$b_n$	$\theta = \frac{\pi}{4}$
3	$-(c+s)$	$-\sqrt{2}$	$-(c+s)$	$-\sqrt{2}$
4	$2\frac{cs}{c+s} - 4(c+s) - 2\left(\frac{c^2}{s} + \frac{s^2}{c}\right)$	$-\frac{11}{2}\sqrt{2}$	$2\frac{cs}{c+s} - 6(c+s) - 2\left(\frac{c^2}{s} + \frac{s^2}{c}\right)$	$-\frac{15}{2}\sqrt{2}$
5	$2\left(\frac{c^4}{s^3} + \frac{s^4}{c^3}\right) + \frac{2}{c+s}(7cs-1)$ $- 27(c+s) - 8\left(\frac{c^2}{s} + \frac{s^2}{c}\right)$	$-\frac{61}{2}\sqrt{2}$	$2\left(\frac{c^4}{s^3} + \frac{s^4}{c^3}\right) + \frac{2}{c+s}(7cs-1)$ $- 30(c+s) - 12\left(\frac{c^2}{s} + \frac{s^2}{c}\right)$	$-\frac{75}{2}\sqrt{2}$

**Table 3.IV**  
 Summary of the Low-T Expansion of the  
 Equilibrium Facet Shape  $y(x)$

$y(x) = y_{2D}(x) - T \sum_{n=6}^{\infty} \bar{b}_n(x) e^{-2\beta n}$				
$\chi \equiv \cosh(\beta x)$				
	3D Ising		SOS	
n	$\bar{b}_n(x)$	x=0	$\bar{b}_n(x)$	x=0
6	-1	-1	-1	-1
7	$-2\chi$	-2	$-2\chi$	-2
8	$-4\chi^2$	-4	$-4\chi^2 - 2$	-6
9	$-8\chi^3 + 2\chi$	-6	$-8\chi^3 - 2\chi$	-10
10	$-16\chi^4 - 16\chi^2 + 3$	-29	$-16\chi^4 - 24\chi^2 + 8$	-32
11	$-32\chi^5 - 72\chi^3 + 68\chi$	-36	$-32\chi^5 - 88\chi^3 + 74\chi$	-46

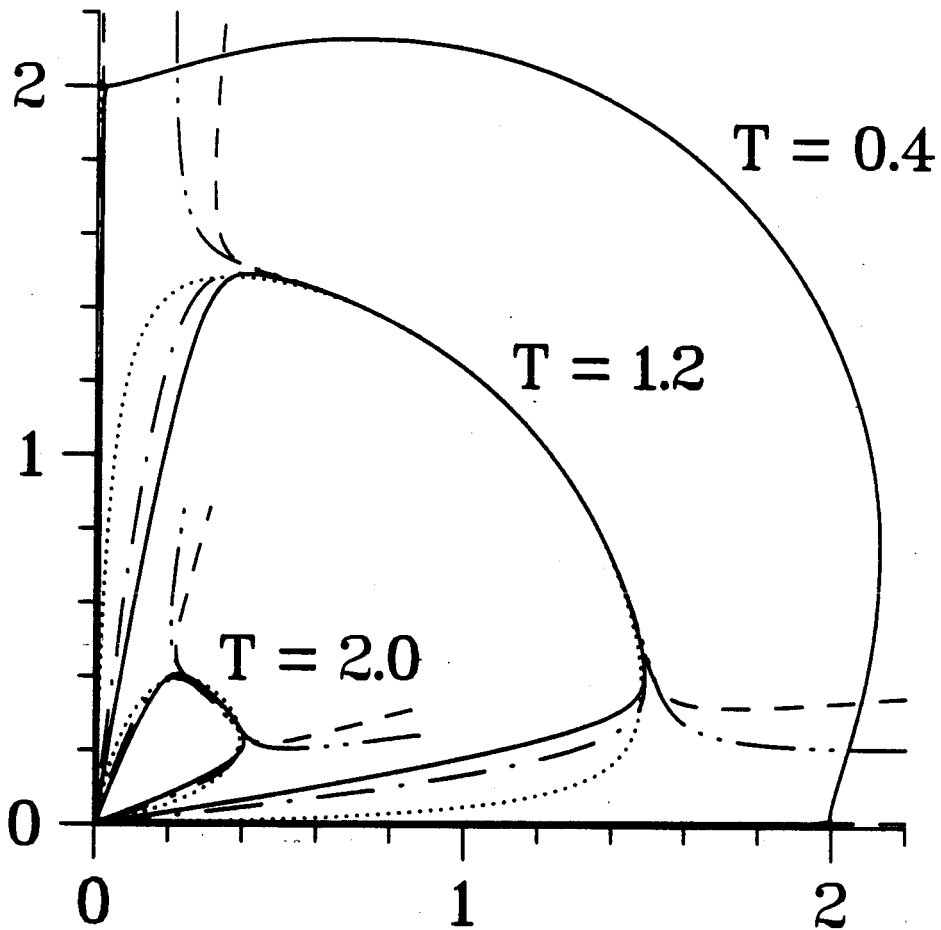


FIG. 3.9: Polar plots of the low-temperature series of  $\gamma(\theta)$  at the temperatures indicated. The different line styles indicate the order to which the series was summed:  $\cdots\cdots$  = 1st,  $-\cdot-\cdot-$  = 2nd,  $-\cdot-\cdot-\cdot-$  = 3rd,  $-\cdot-\cdot-\cdot-\cdot-$  = 4th, and  $—$  = 5th order. At  $T=0.4$  the divergent region about  $\theta=0$  and  $\frac{\pi}{2}$  is still very narrow and barely resolved in the figure.

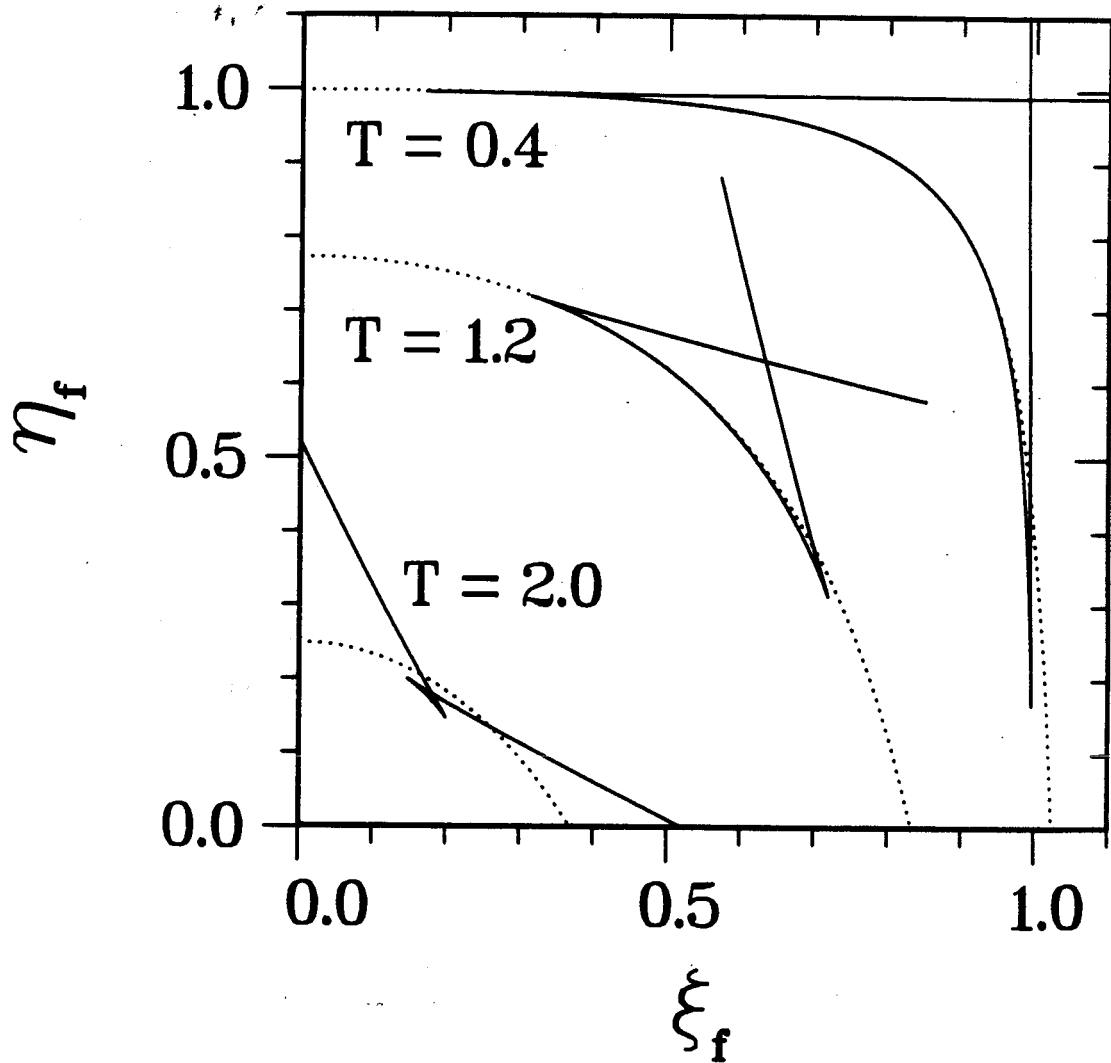


FIG. 3.10: The facet shape at different temperatures, normalized to the centre-of-crystal to centre-of-facet distance as obtained from the 11th order series for  $\gamma(x)$  (dotted curve) and the Legendre transform of the 5th order series for  $\gamma(\theta)$  (solid curve). The non-physical parts of the Legendre transform are the result of the divergences of the series for  $\gamma(\theta)$  (see Fig. 3.9). Note that the dotted curve is not symmetric under reflection about  $x=y$ . This effect is a consequence of distinguishing the  $x$  and  $y$  axes in the grand canonical expansion and disappears at infinite order. Because of the convergence properties of the series, the best numerical estimates of the facet shape at finite order are obtained for  $\theta \in [\frac{\pi}{4}, \frac{\pi}{2}]$ .

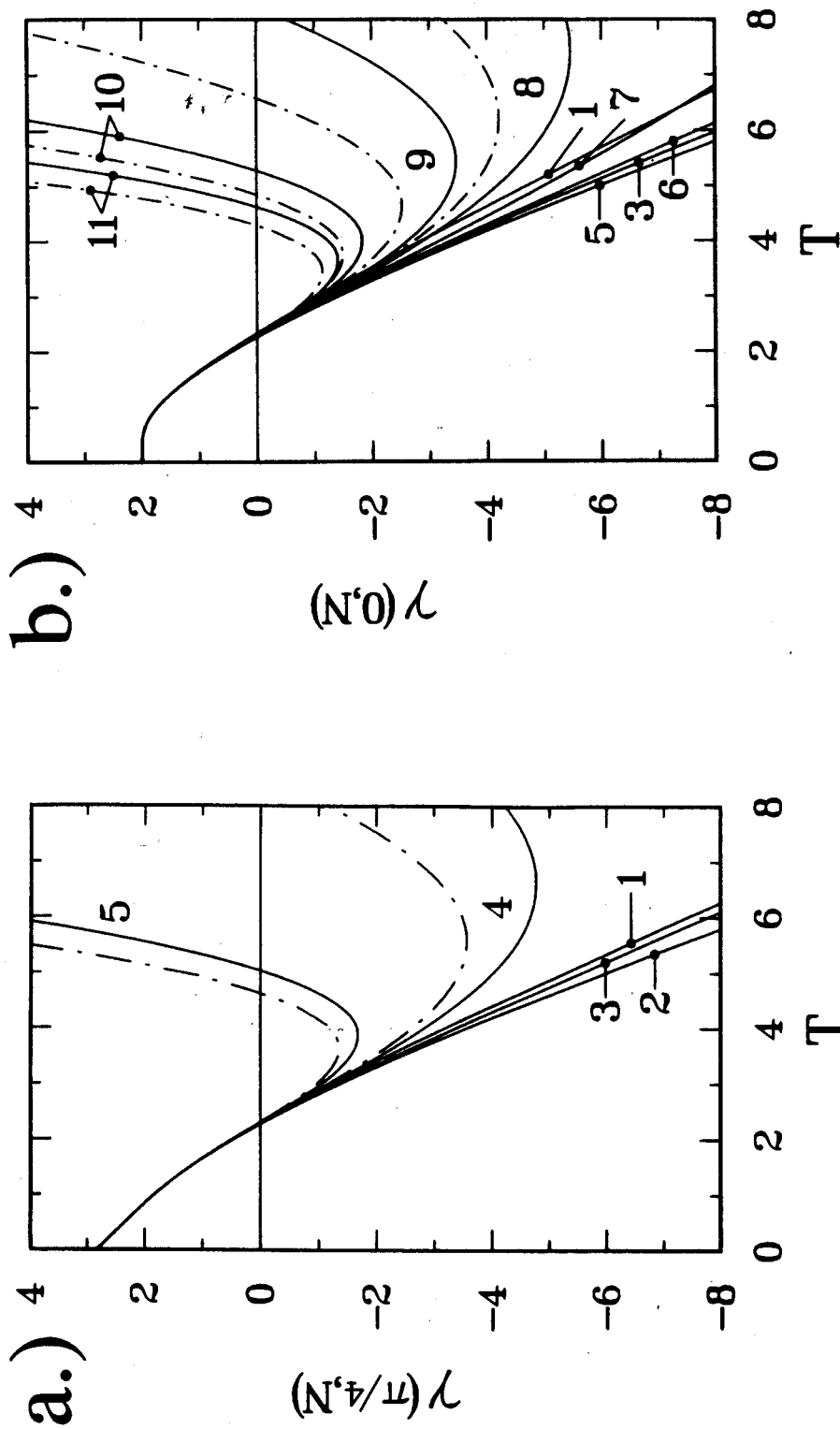


FIG. 3.11: a.) The canonical series  $\gamma(\frac{\pi}{4}, N)$  for the step free energy and b.) the grand canonical series  $\gamma(0, N)$  for the facet shape, summed to the orders  $N$  indicated, as a function of temperature. Conveniently,  $\sqrt{2}\gamma(x=y)=\gamma(\frac{\pi}{4})$  and  $\gamma(0)=\gamma(0)$  as discussed after Eq. (3.20). The solid curves are the Ising result; the broken curves, the SOS result.

To investigate the asymptotic properties of our series, standard Padé and ratio methods (e.g., Gaunt and Guttmann, 1974) cannot be used directly because the singularity of Eq. (3.1) is an essential singularity. Since there is no obvious way of circumventing this problem, we use alternate methods, motivated mainly from a study of the exact solution of the BCRSOS model. The low-T series for  $\gamma(\frac{\pi}{4})$  of the BCRSOS model (see Appendix D) is an alternating series: Order  $v$  is negative, orders  $v^2$  to  $v^{10}$  are positive, orders  $v^{11}$  to  $v^{35}$  are negative, and so on. The number of consecutive terms of like sign presumably increases with increasing order. For  $T \leq 0.85T_R$ , the convergence of this series is dominated by the first sequence of positive terms, i.e., the terms of order  $v^n$  with  $n \in \{k, \dots, l\}$ , where  $k=2$  and  $l=10$  here. Let  $a_n$  denote the coefficient of  $v^n$ . It turns out that the ratio  $r_n \equiv a_n/a_{n-1}$ , decreases with  $n$  for  $n \in \{k+1, \dots, l\} \equiv \mathcal{P}$ . Hence, if  $T$  is sufficiently low such that  $v r_m < 1$ , it follows that  $v r_n < 1$  for  $n \geq m$  ( $n, m \in \mathcal{P}$ ) and, therefore, the series  $\sum_{n=m+1}^l a_n v^n$  is bounded by the geometric series  $x a_m v^m \sum_{j=0}^{l-m-1} x^j \equiv x a_m v^m S(l, m)$ , where  $x \equiv v r_m$ . Thus, if  $m \ll l$ , a reasonable estimate for  $\sum_{n=m+1}^{\infty} a_n v^n$  is  $a_m v^m x S(\infty, m) = a_m v^m x / (1-x)$ .

We shall assume that the generic form of the complete series for the SFE of the sc Ising model is similar to that of the corresponding series of the BCRSOS model. In order to estimate the error made in truncating the series after order  $N$ , let us assume further that the grand canonical series cannot converge significantly better than the canonical series, so that we can restrict our analysis to  $\theta = \frac{\pi}{4}$ . For the Ising and SOS models, the forgoing paragraph then implies that it is reasonable to expect the series for the error  $\Delta_N \equiv \gamma(\frac{\pi}{4}) - \gamma(\frac{\pi}{4}, N)$ , for  $N \geq 4$ , to be bounded by a geometric series, so that  $\Delta_N \leq \bar{\Delta}_N \equiv -T v^N (b_N + \frac{\sqrt{2}}{N}) x / (1-x)$ , provided  $0 < x < 1$ , where  $x = v (b_N + \frac{\sqrt{2}}{N}) / (b_{N-1} + \frac{\sqrt{2}}{N-1})$  is the ratio of the  $N$ th to the  $(N-1)$ st term of  $\gamma(\frac{\pi}{4}, N)$ . While it is only clear that this must be

so at sufficiently low  $T$ , we shall assume that  $\bar{\Delta}_N$  gives a reasonable error estimate for fractional errors  $\bar{\Delta}_5/[\gamma(\frac{\pi}{4},5)+\bar{\Delta}_5]$  as high as  $\sim 10\%$ . For  $N=5$  we find that the fractional error is less than (0.1%,1%,5%,10%) for  $T \leq (1.72,1.92,2.04,2.09)$ ; for  $N=4$  these temperatures are (1.61,1.78,1.87,1.90). For the SOS model the corresponding estimates are for  $N=5$ ,  $T \leq (1.73,1.93,2.07,2.12)$  and for  $N=4$ ,  $T \leq (1.51,1.62,1.66,1.67)$ .

If we take the fractional error in approximating  $\gamma(\theta)$  by  $\Gamma_{2D}(\theta)$  to be  $1-\Gamma_{2D}(\theta)/[\gamma(\frac{\pi}{4},5)+\bar{\Delta}_5]$ , we find it to be less than 1% for  $T < 1.79$  (less than 0.1% for  $T < 1.51$ ). Below  $T=1.79$  the order  $v^4$  and  $v^5$  non-SOS contributions are less than 0.08% and 0.03% respectively so that bubbles and overhangs are unimportant in this temperature range. Above  $T=1.79$ , the facet-shape anisotropy, as approximated by  $[\gamma(\frac{\pi}{4},5)-\gamma(0,11)]/\gamma(0,11)$ , is less than  $4 \times 10^{-3}$  for both the Ising and SOS models. At  $T=1.79$ , the normalized facet radius  $\rho_f = 0.4$ . It follows that, *in the region of temperature where the facet has experimentally significant anisotropy (i.e., for  $T \lesssim 1.8$ ), the facet shape is essentially given by the 2D Ising ECS with the convergent corrections calculated in Subsection 3.3.*

In the temperature range  $1.8 \lesssim T \lesssim 2.1$ ,  $T$  is high enough for the the series to differ significantly from the 2D Ising series but low enough for us still to have some confidence that the series have converged. Assuming that in this region  $\gamma(\frac{\pi}{4},5)$  and  $\gamma(0,11)$  are already well approximated by their asymptotic form (3.1), one may hope to extract the critical parameters  $B$ ,  $C$ , and  $T_R$ . Indeed, plots of  $C(T) \equiv -2(T_R - T)^{3/2} \partial \ln \gamma(\theta, N) / \partial T$  and  $B(T) \equiv \gamma(\theta, N) \exp[C(T) / \sqrt{T_R - T}]$  versus  $T$  for various values of  $T_R$ , at  $\theta = \frac{\pi}{4}$  and 0, show a plateau for  $T_R = T_{P(\text{plateau})} \approx 2.46$  over the temperature range  $1.8 \lesssim T \lesssim 2.0$  (see Fig. 3.12). The failure of the plateau to extend beyond  $T=2.0$  is consistent with the convergence estimates above. The functions  $B(T)$  and  $C(T)$  [which would be constants if the series were exactly equal to (33)] have qualitatively the same shape (Fig. 3.12): For  $T_R > T_p$ , they increase

monotonically over the temperature range of interest; for  $T_R < T_P$ , the plateau deepens into a minimum which becomes deeper and more narrow with decreasing  $T_R$ . Guided again by the BCRSOS model and the fact that we observe no significant change in the plateau parameters from order  $N=4$  to  $N=5$ , we take the plateau parameters to be the critical parameters (this works well for the BCRSOS model). To extract these parameters numerically, we performed a least squares fit of the functional form (3.1) to  $[\gamma(\frac{\pi}{4}, 5) + y(0, 11)]/2$  over a temperature interval of width 0.2 centred at  $T^*$  with fitting parameters  $B, C, T_R$ , and  $T^*$ . For both the SOS and Ising models we obtain  $T^* = 1.9$ . As shown in Table 3.V, the fits for the roughening temperatures  $T_R(\text{SOS})$  and  $T_R(\text{3D Ising})$  are consistent with those obtained by Adler. For the 3D Ising model, the fits for all the critical parameters are consistent with those obtained from Monte Carlo data by Mon et al..

**Table 3.V**  
Summary of Critical Parameters

	SOS	3D Ising	
B	10.3 ± 1.5	9.7 ± 1.0	this work
	—	9.84 ± 2.0	Mon et al.
C	2.13 ± 0.15	2.05 ± 0.15	this work
	—	2.12 ± 0.13	Mon et al.
$T_R$	2.48 ± 0.03	2.46 ± 0.02	this work
	—	2.44 ± 0.09	Mon et al.
	2.54 ± 0.07	2.475 ± 0.075	Adler

Table 3.V. Comparison of the critical parameters  $B$ ,  $C$ , and  $T_R$  as obtained by different methods. The uncertainties quoted for the rows “this work” are associated with the fit and do not necessarily represent an estimate of how close these numbers might be to the true critical values.



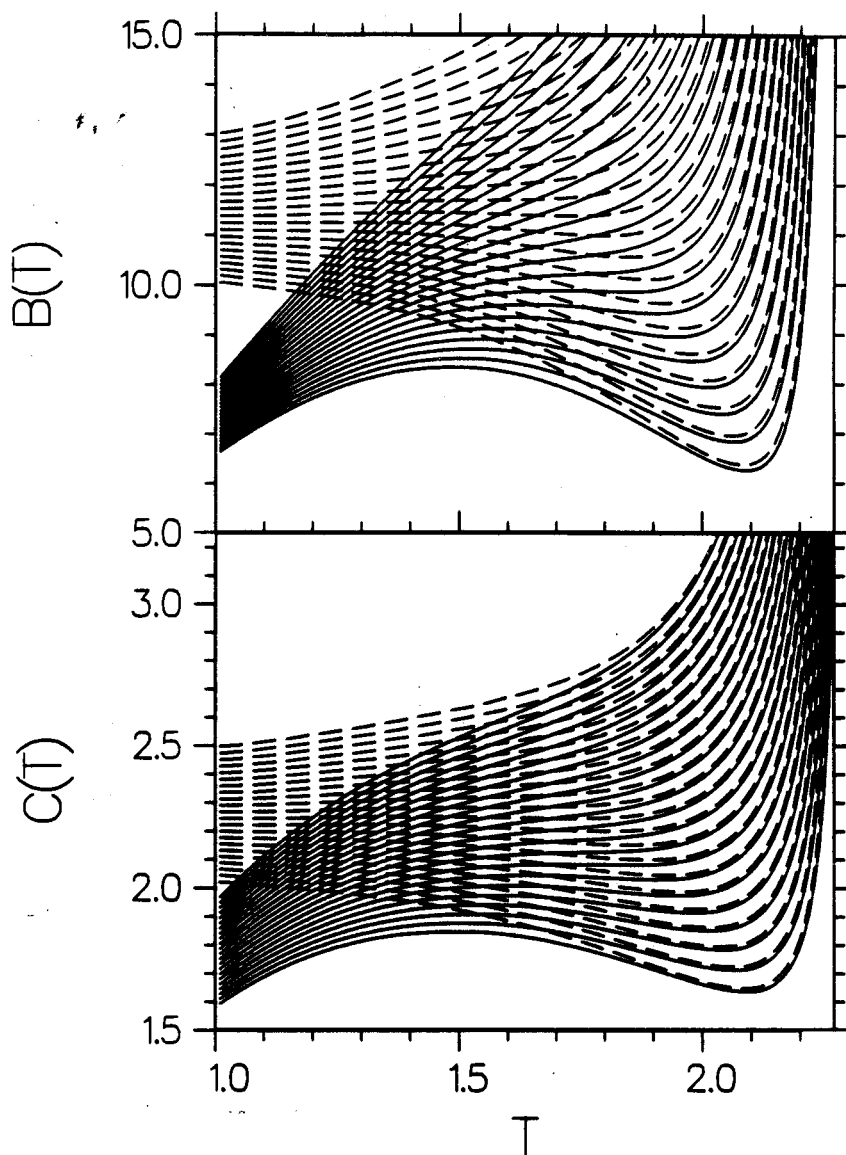


FIG. 3.12. Plots for the 3D Ising model of  $B(T) = \gamma(\theta, N) \exp[C(T)/\sqrt{T_R - T}]$ , with  $C(T) = -2(T_R - T)^{3/2} \partial \ln \gamma(\theta, N) / \partial T$ , and of  $C(T)$  versus temperature  $T$  for various values of  $T_R$ . The dashed lines correspond to  $\gamma(\frac{\pi}{4}, 5)$ , i.e., to the canonical series summed to 5th order. The solid lines correspond to  $\gamma(\theta, N) = \gamma(0, 11)$ , i.e., to the grand canonical series summed to 11th order. In each "bundle" of lines the lowest curve corresponds to  $T_R = 2.40$ . With successively higher lines,  $T_R$  is incremented in steps of 0.01 to  $T_R = 2.61$ . If  $\gamma(\theta)$  satisfied the Kosterlitz-Thouless form (3.1) everywhere,  $B(T)$  and  $C(T)$  would be constants. For a value of  $T_R \sim 2.46$  the curves show a plateau centred about  $T^* = 1.9$ . The corresponding values of  $B$  and  $C$  at the plateau were taken to be the critical parameters and guided more accurate least-square fits of our series to the Kosterlitz-Thouless form (3.1) as described in the text.

Fig. 3.13 shows the  $T$  dependence of the normalized facet diameter of the Ising model, extrapolated all the way to  $T_R$  using our fit to Eq. (3.1). The lower (upper) limit of the error bars shown there correspond to fits obtained over the interval  $1.905 \leq T \leq 1.955$  with  $T_R$  constrained to be the lower (upper) limit of Adler's estimates for  $T_R$ . It is to be emphasized, that the methods of Sub-section 3.3 are not recommended if one is interested in  $T_R$  only (and not, for example, in the amplitudes  $B$  and  $C$  also). In such cases, the series methods of Weeks et al., with their well understood asymptotic analysis by Adler, are probably more efficient. The calculation presented here, on the other hand, is the only one so far to address the anisotropic step free energy and the shape and size of facets.

It is interesting to examine the assumption that the series are already in the asymptotic regime over the temperature range  $1.8 \lesssim T \lesssim 2.1$  in the context of the Monte Carlo simulations of Mon. et al.. While their data, extrapolated to infinite system size, shows (3.1) to hold over the entire temperature range  $1.8 < T < T_R$ , they fall below the 2D Ising value by about 10% at  $T=1.8$ , where our expansion implies that the 2D Ising result is a lower bound. In principle, this discrepancy could be due to large negative coefficients at higher orders of our expansion; however, in light of the discussion above, this is unlikely. A more likely source of error, as pointed by Mon et al., is the finite-size-scaling analysis of the Monte Carlo data, performed with only three data points at each value of  $T$ . The fact that our critical parameters agree with those of Mon et al. in spite of these problems is probably attributable to the sensitive dependence of  $\gamma(\theta)$  on the precise numerical values of the critical parameters.

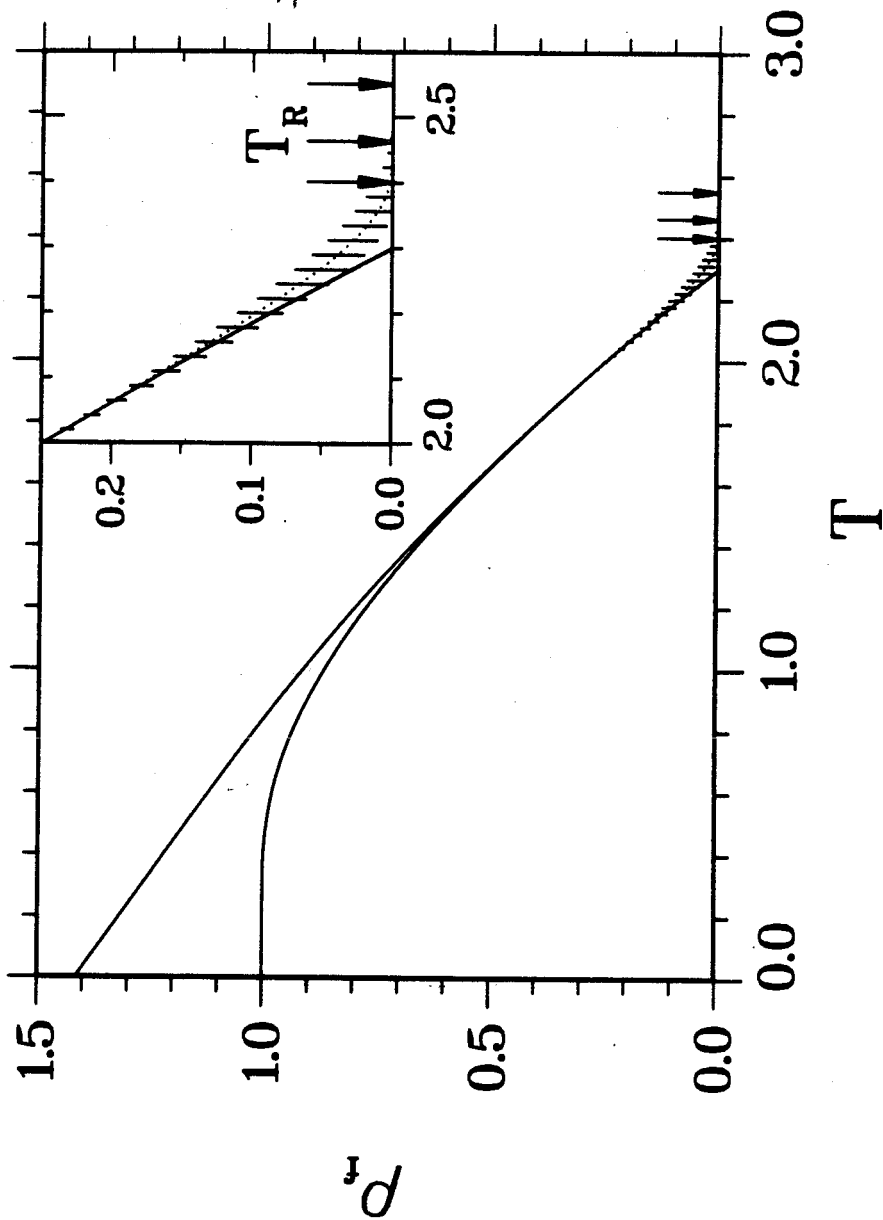


FIG. 3.13: The normalized facet radius  $\rho_f$  in the symmetry directions as a function of temperature. The lower (upper) solid curve is calculated from the canonical (grand canonical) series summed to  $5/h$  ( $11/h$ ) order at  $\theta=0$  ( $\theta=\frac{\pi}{4}$ ). The dotted curve is an extrapolation into the critical region, as described in the text. The error bars indicate the uncertainty associated with that extrapolation. The middle arrow indicates the  $T_R$  associated with the dotted curve. The arrow on the left (right) indicates the lower (upper) limit of  $T_R$ , as estimated by Adler in 1987, and corresponds to the lower (upper) limits of the error bars shown.

## 3.5 Conclusions

We have shown how to calculate step free energies and the corresponding equilibrium facet shapes in low-temperature expansion. The combinatorics involved is significantly reduced by structuring these expansions as perturbation series about the interfacial properties of the 2D Ising model. The two expansions are related by a Legendre transform and can be thought of as canonical and grand canonical representations of the same physics. The grand canonical form of the expansion gives the facet shape where it is not accessible from the canonical expansion of the step free energy.

At temperatures where the facet has experimentally significant anisotropy, the facet shape is essentially given by the 2D Ising ECS normalized to the facet's surface free energy, with convergent corrections displayed in Tables 3.III and 3.IV. Corrections to the 2D Ising result due to additional (non-2D) SOS, overhanging, and bubble configurations enter at orders  $e^{-12\beta J}$ ,  $e^{-16\beta J}$ , and  $e^{-20\beta J}$ , respectively. These corrections are less than 1% for  $0 < T < 1.79 \approx 0.72T_R$  and less than 0.1% for  $0 < T < 1.51 \approx 0.61T_R$ . In this temperature range, overhangs and bubbles are unimportant. At higher temperatures the facet shape is nearly circular, with a normalized facet radius of less than 0.4 and anisotropies of less than 0.1%. Numerical extrapolations into the asymptotic critical temperature region of the step free energy yield roughening amplitudes consistent with the Monte Carlo data of Mon et al.. The effect of non-2D-Ising configurations is to raise the roughening temperature from  $T_c(2D \text{ Ising})$  to the true  $T_R$  (an increase of  $\sim 9\%$ ) and to build in the proper Kosterlitz-Thouless roughening singularity.

The facet-shape information provided by Figs. 3.10 and 3.13 is potentially useful in analyzing experimental data from any real crystals which may be modeled by the nearest-neighbour sc Ising model, but for which the effective nearest neighbour coupling is

unknown. For example,  $T_R$  is often difficult to measure by direct observation of the vanishing of the facet, either because the facet edge cannot be located precisely (e.g., F. Gallet et al., 1986) [and/or is very sensitive to dynamical effects (e.g., Keshishev, 1981)] or because the roughening transition is preempted by bulk melting. In such situations, it may be feasible to measure the facet diameter in one of the symmetry directions at a lower temperature  $T_{\text{exp}}$ . The corresponding reduced temperature  $T$  can be read off Fig. 3.13, from which the effective nearest neighbour coupling is determined as  $J = k_B T_{\text{exp}}/T$ . The roughening temperature is then given by (from Adler, 1987)  $T_{R_{\text{exp}}} = (T_{\text{exp}}/T) \times (2.475 \pm 0.075)$ .

In nature most crystals are unfortunately not simple cubic and next-nearest-neighbour interactions cannot always be neglected. As long as interactions remain nearest neighbour, generalization is straightforward. If next-nearest-neighbour forces must be accounted for, the nature of the problem changes drastically. The energy of a configuration will now depend not only on the number of plaquettes but also on the number of corners. This makes the combinatorics very difficult and completely different in character from what we have had to deal with here. It is clear that, in any case, it will be useful to expand about a 2D model describing the central layer containing the step. An interesting open question is whether the step free energy is rigorously bounded from below by the interfacial free energy of that 2D model and, if so, under what conditions.

# Appendix A: Analytic structure of the Feynman-Vdovichenko matrix - two examples

In this Appendix we explore the analytic structure of the FV matrix for two explicit examples: The ferromagnetic Ising model defined on the square and honeycomb lattices. Specifically, we will look at the  $X$ -dependence of 1.) the location of the zeros of  $\text{Det}[1-\Lambda(k_x, -i\beta\lambda X)]$  and 2.) the location of the regions in the  $k_x$ -plane where at least one eigenvalue of  $\Lambda(k_x, -i\beta\lambda X)$  is greater or equal to unity in modulus (regions of nonconvergence). To illustrate the generic behaviour of these matrices it will suffice to consider the case of all interactions being equal. We choose units such that  $J=k_B=\lambda=1$ . To obtain a  $[-\pi, \pi] \times [-\pi, \pi]$  Brillouin zone (BZ), we choose the basis vectors of the lattices to be  $\mathbf{a}=\hat{\mathbf{x}}$  and  $\mathbf{b}=\hat{\mathbf{y}}$  (for a definition of the basis vectors see Fig. 2.5).

Consider first the square lattice. The FV walk takes place on the dual square lattice with the following set of available steps

$$\{\mathbf{d}_1, \mathbf{d}_2, \mathbf{d}_3, \mathbf{d}_4\} = \{\hat{\mathbf{y}}, -\hat{\mathbf{y}}, \hat{\mathbf{x}}, -\hat{\mathbf{x}}\}. \quad (\text{A1})$$

The corresponding FV matrix is then given by

$$\Lambda = e^{-2\beta} \mathbf{A} \mathbf{M}, \quad (\text{A2})$$

with

$$\mathbf{M} = \begin{pmatrix} 1 & 0 & \alpha & \alpha^* \\ 0 & 1 & \alpha^* & \alpha \\ \alpha^* & \alpha & 1 & 0 \\ \alpha & \alpha^* & 0 & 1 \end{pmatrix} \quad (\text{A3})$$

and

$$\mathbf{A} = \text{diag}(e^{-ik_y}, e^{ik_y}, e^{-ik_x}, e^{ik_x}), \quad (\text{A4})$$

where  $\alpha \equiv e^{i\pi/4}$ . The condition that  $\text{Det}(\mathbf{1}-\mathbf{A})$  be zero is obtained as

$$c^2 - s [\cos(k_x) + \cos(k_y)] = 0, \quad (\text{A5})$$

where  $c = \cosh(2\beta)$  and  $s = \sinh(2\beta)$ . Thus, with the notation  $f(X) = c^2/s - \cosh(\beta X)$ , the zeros of  $\text{Det}[\mathbf{1}-\mathbf{A}(k_x, -i\beta X)]$  are given by

$$k_x = \begin{cases} \pm \arccos[f(X)] & \text{if } |f(X)| \leq 1 \\ \mp i \text{arccosh}[f(X)] & \text{if } f(X) \geq 1 \\ \pm i \text{arccosh}|f(X)| \pm \pi & \text{if } f(X) \leq -1 \end{cases}, \quad (\text{A6})$$

where the inverse functions are to be evaluated as the principle value. Since for  $T < T_c$ ,  $c^2/s > 2$ , there is always a non-empty region  $X \in [X_{\min}, X_{\max}]$  (corresponding to the ECS) for which  $f(X) \geq 1$ . The condition  $f(X) \leq -1$  defines the region  $[-\infty, X_L] \cup [X_R, +\infty]$  (here,  $X_L = -X_R$ ).

The trajectories of the zeros (A6), as  $X$  ranges from  $-\infty$  to  $+\infty$ , are sketched in the  $k_x$ -plane in Fig. A.1 and in the  $z$ -plane in Fig. A.2, where  $z = \exp(ik_x)$ . Figure A.3 shows the two zeros of  $\text{Det}[\mathbf{1}-\mathbf{A}(k_x, -i\beta X)]$  in the  $z$ -plane,  $z_1$  and  $z_2$ , as a function of  $X$  for those  $X$  for which  $z_1$  and  $z_2$  are purely real. In the  $z$ -plane, one and only one real zero is inside the unit circle  $|z|=1$ , and the integration of Eq. (2.15) picks up the correct pole [depending on the sign of  $N$ ; see the discussion following Eq. (2.15)]. Since  $\mathbf{A}$  is a  $4 \times 4$  matrix, the eigenvalues can be found analytically. However, since we will soon be interested in a case where this is generally not possible, anyway, we contend ourselves with a numerical investigation. One finds that for  $X \in [X_{\min}, X_{\max}]$  the modulus of all eigenvalues of  $\mathbf{A}(k_x, -i\beta X)$  remain less than unity along the unit circle  $|z|=1$  so that the contour need not be deformed. As  $X$  is increased beyond  $X_{\max}$  (decreased beyond  $X_{\min}$ ), the path in the  $k_x$ -plane from  $-\pi$  to  $\pi$  is pinched off, as the two regions of nonconvergence join at  $k_x=0$ .

With further increasing (decreasing)  $X$ , the “barrier” blocking convergent passage from  $-\pi$  to  $\pi$  continues to grow. Beyond  $X_R$  ( $X_L$ ) the matrix  $\Lambda(k_x, -i\beta\lambda X)$  is divergent for all real  $k_x$ . In Fig. A.4 the regions of nonconvergence of  $\Lambda(k_x, -i\beta\lambda X)$  are mapped out in the  $k_x$ -plane and in Fig. A.5, in the (real) BZ.<sup>†</sup>

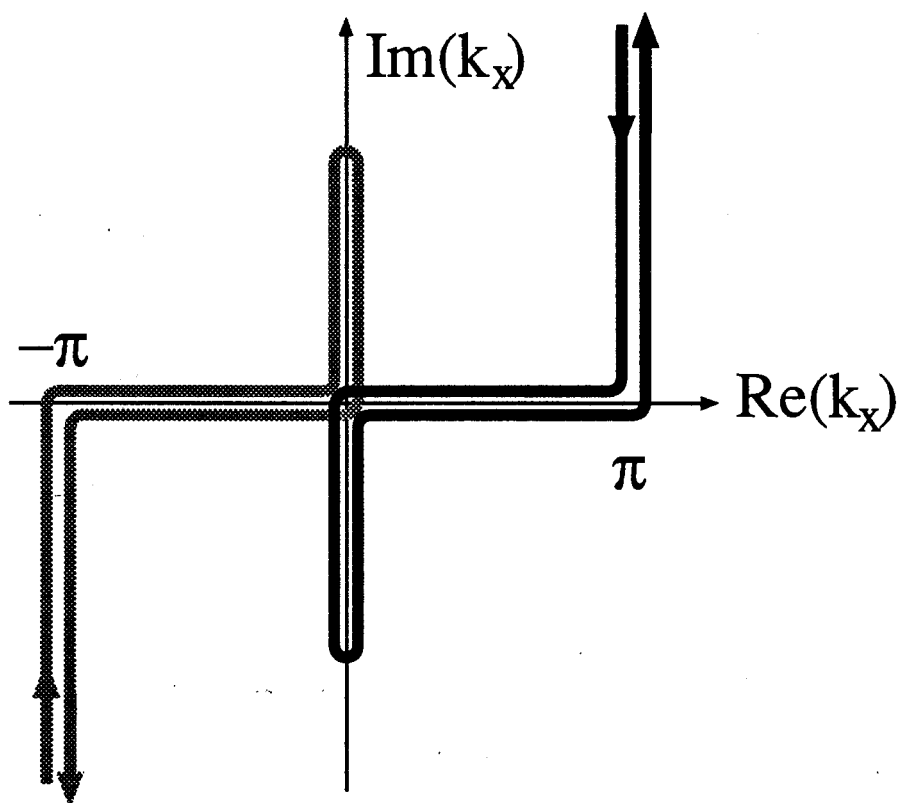


Fig. A.1: Trajectories of the two zeros of  $\text{Det}[1 - \Lambda(k_x, -i\beta\lambda X)]$  in the  $k_x$ -plane for the square lattice [cf. Eq. (A.6)] as  $X$  ranges from  $-\infty$  to  $\infty$ .

<sup>†</sup> The matrix  $\Lambda(k_x, -i\beta X)$  was diagonalized numerically at each point of a  $31 \times 31$  grid over the region of interest.



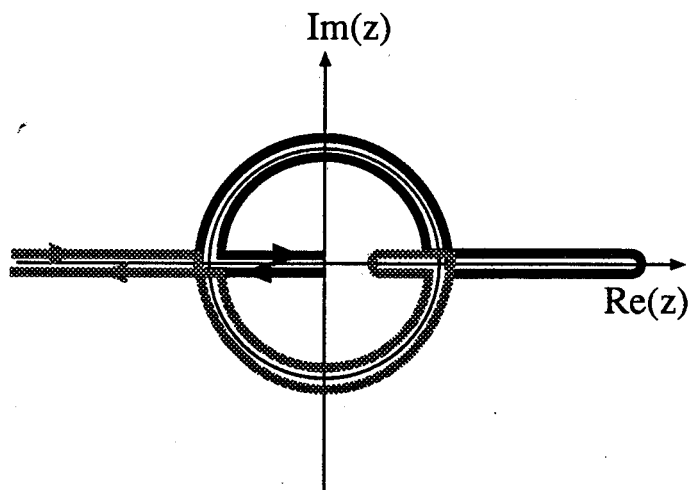


Fig. A.2: Trajectories of the two zeros of  $\text{Det}[1-\Lambda(k_x, -i\beta\lambda X)]$  in the  $z$ -plane for the square lattice [cf. Eq. (A.6)] as  $X$  ranges from  $-\infty$  to  $\infty$ .

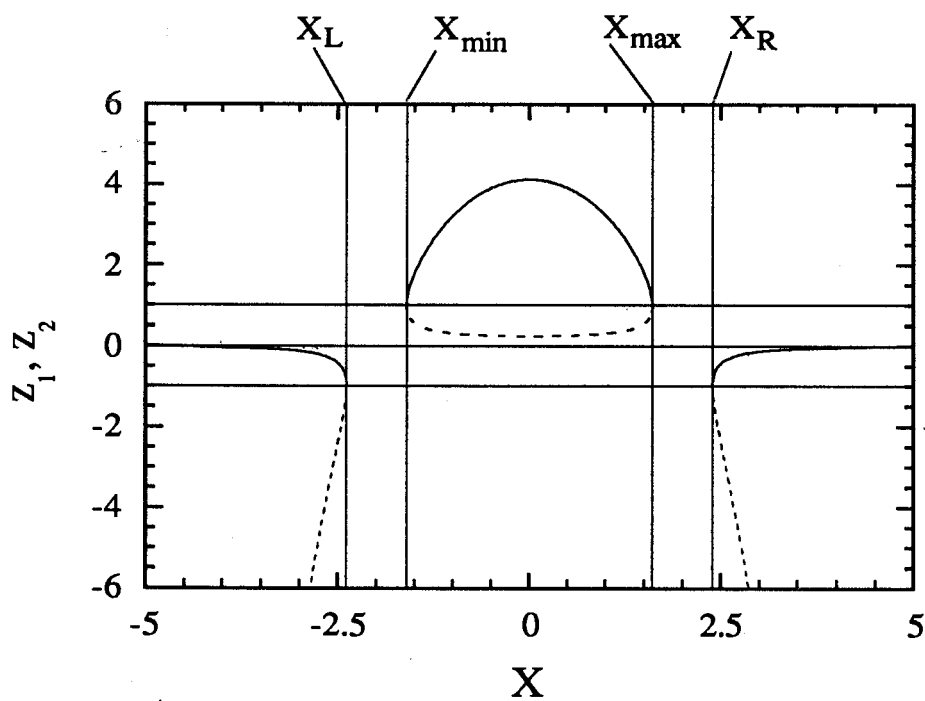


Fig. A.3: The real zeros of  $\text{Det}[1-\Lambda(k_x, -i\beta\lambda X)]$  for the square lattice in the  $z$ -plane as a function of  $X$ . For  $X \in [X_{\min}, X_{\max}]$ ,  $0 < z_1 \leq 1$  and  $z_2 \geq 1$ .

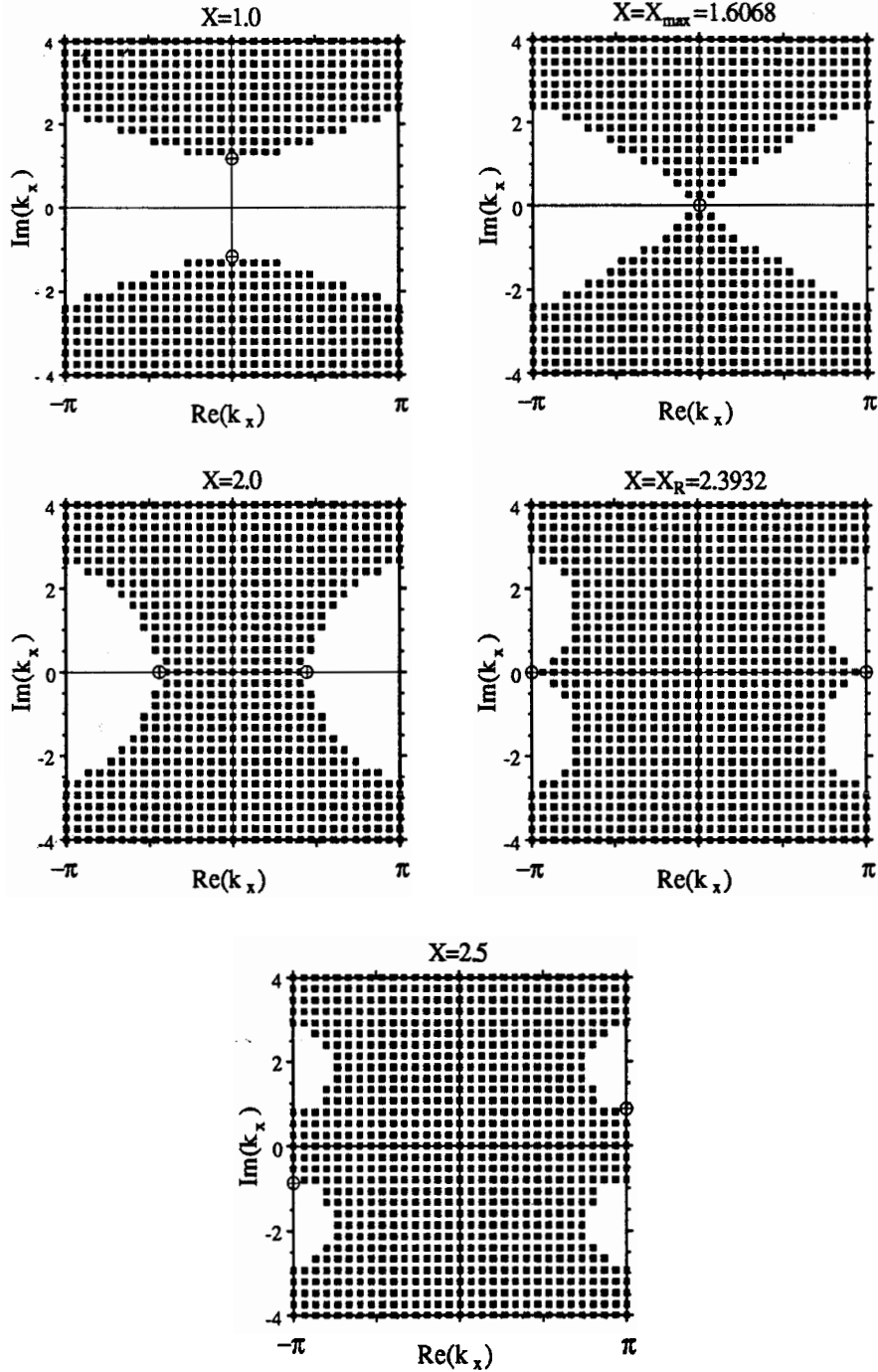


Fig. A.4: Regions of nonconvergence (black squares) of  $\Lambda(k_x, -i\beta\lambda X)$  in the  $k_x$ -plane for the square lattice at  $T=T_c/2$  for the values of  $X$  indicated. A path from  $-\pi$  to  $\pi$  is possible along the real  $k_x$ -axis for  $X \in [X_{\min}, X_{\max}]$ . At  $X=X_{\max}$  the two regions of nonconvergence join at  $k_x=0$ . The zeros of  $\text{Det}[1-\Lambda(k_x, -i\beta\lambda X)]$  are indicated by the symbol  $\oplus$ .

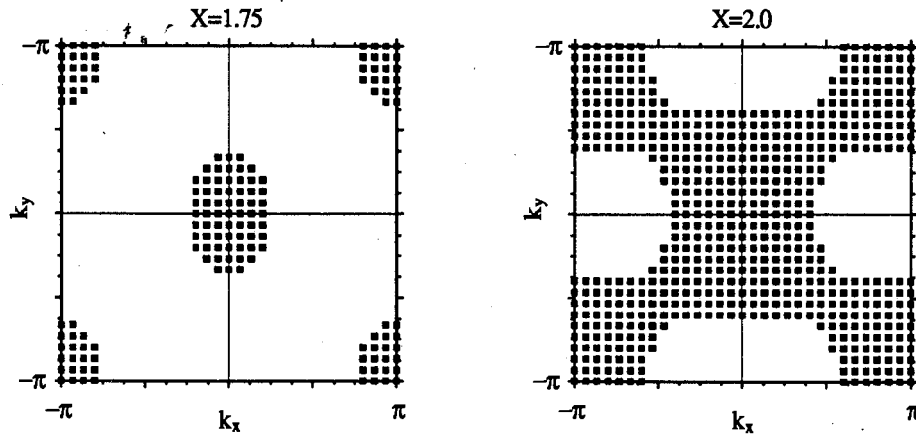


Fig. A.5: Regions of nonconvergence (black squares) of  $\Lambda(k_x, -i\beta\lambda X)$  in the Brillouin zone for the square lattice at  $T_c/2$  for the values of  $X$  indicated.

Let us now look at the hexagonal lattice. Note that with the chosen unit vectors this lattice is less symmetric than the square lattice. The dual lattice is triangular and the FV walker has available the following steps

$$\{\mathbf{d}_1, \mathbf{d}_2, \mathbf{d}_3, \mathbf{d}_4, \mathbf{d}_5, \mathbf{d}_6\} = \{\hat{y}, \hat{x} + \hat{y}, \hat{x}, -\hat{y}, -\hat{x} - \hat{y}, -\hat{x}\}. \quad (\text{A7})$$

The corresponding FV matrix is given by Eq. (A2) with<sup>†</sup>

---

<sup>†</sup> For the phase factors, we have not used the actual angles of turn for the steps (A.7) (which would be multiples of  $\pi/4$ ). To obtain a more aesthetic form of  $\mathbf{M}$ , we have used, instead, the angles of turn for walker on a lattice of equilateral triangles. Since the phase only keeps track of the topology (self-intersections) of the lattice paths, this is equivalent to using phase factors derived from the actual angles of turn.

$$\mathbf{M} = \begin{pmatrix} 1 & \alpha & \alpha^2 & 0 & \alpha^{*2} & \alpha^* \\ \alpha^* & 1 & \alpha & \alpha^2 & 0 & \alpha^{*2} \\ \alpha^{*2} & \alpha^* & 1 & \alpha & \alpha^2 & 0 \\ 0 & \alpha^{*2} & \alpha^* & 1 & \alpha & \alpha^2 \\ \alpha^2 & 0 & \alpha^{*2} & \alpha^* & 1 & \alpha \\ \alpha & \alpha^2 & 0 & \alpha^{*2} & \alpha^* & 1 \end{pmatrix} \quad (\text{A8})$$

and

$$\mathbf{A} = \text{diag} (e^{-ik_y}, e^{-i(k_y+k_x)}, e^{-ik_x}, e^{ik_y}, e^{i(k_y+k_x)}, ik_x), \quad (\text{A9})$$

where  $\alpha = e^{i\pi/6}$ . The condition for  $\text{Det}(\mathbf{1} - \mathbf{A}) = 0$  is obtained as

$$\frac{c^3+1}{s^2} - [\cos(k_x) + \cos(k_y) + \cos(k_x+k_y)] = 0. \quad (\text{A10})$$

Because of the  $\cos(k_x+k_y)$  term in Eq. (A.10), the analogue of the function  $f(X)$  of Eq. (A6) is the solution of a quadratic equation and can itself be complex. The resulting flow of the zeros of  $\text{Det}[\mathbf{1} - \mathbf{A}(k_x, -i\beta\lambda X)]$  with  $X$  is, therefore, slightly more complicated (Fig. A.6 and A.7). Figure A.8 shows the two zeros in the  $z$ -plane,  $z_1$  and  $z_2$ , as a function of  $X$  for those  $X$  for which  $z_1$  and  $z_2$  are purely real. Since for  $T < T_c$ ,  $(c^3+1)/s^2 > 3$ , there will again always be a non-empty region  $X \in [X_{\min}, X_{\max}]$  corresponding to the ECS, for which  $z_1$  and  $z_2$  are purely real and positive. The asymmetry of the lattice (in the general case additional asymmetry is introduced by unequal coupling constants) manifests itself in the fact that now there is a region  $[X_{\min}, X_A]$  for which both real, positive zeros are outside the unit circle  $|z|=1$  and a region  $[X_B, X_{\max}]$  for which both real, positive zeros are inside the unit circle  $|z|=1$ . Figures A.9 and A.10 show the regions of nonconvergence in the  $k_x$ -plane and in the BZ, respectively for various values of  $X$ . As  $X$  is increased beyond  $X_B$  (decreased beyond  $X_A$ ), the region of

nonconvergence begins to cross the real  $k_x$ -axis at  $k_x=0$ . However, for  $X \in [X_B, X_{\max}]$  (for  $X \in [X_{\min}, X_A]$ ) the path from  $-\pi$  to  $\pi$  may be deformed from the real  $k_x$ -axis so as to pass through a bottleneck of the convergent region between two regions of nonconvergence. Note that this automatically causes the relevant pole of the integral (2.15) to be included in the integration contour. When  $X$  is increased beyond  $X_B$  (decreased beyond  $X_A$ ) the bottleneck pinches off at  $\text{Re}(k_x)=0$ . Aside from the fact that the pinch occurs off the real  $k_x$ -axis, the regions of nonconvergence behave very much as they do in the case of the square Ising model.

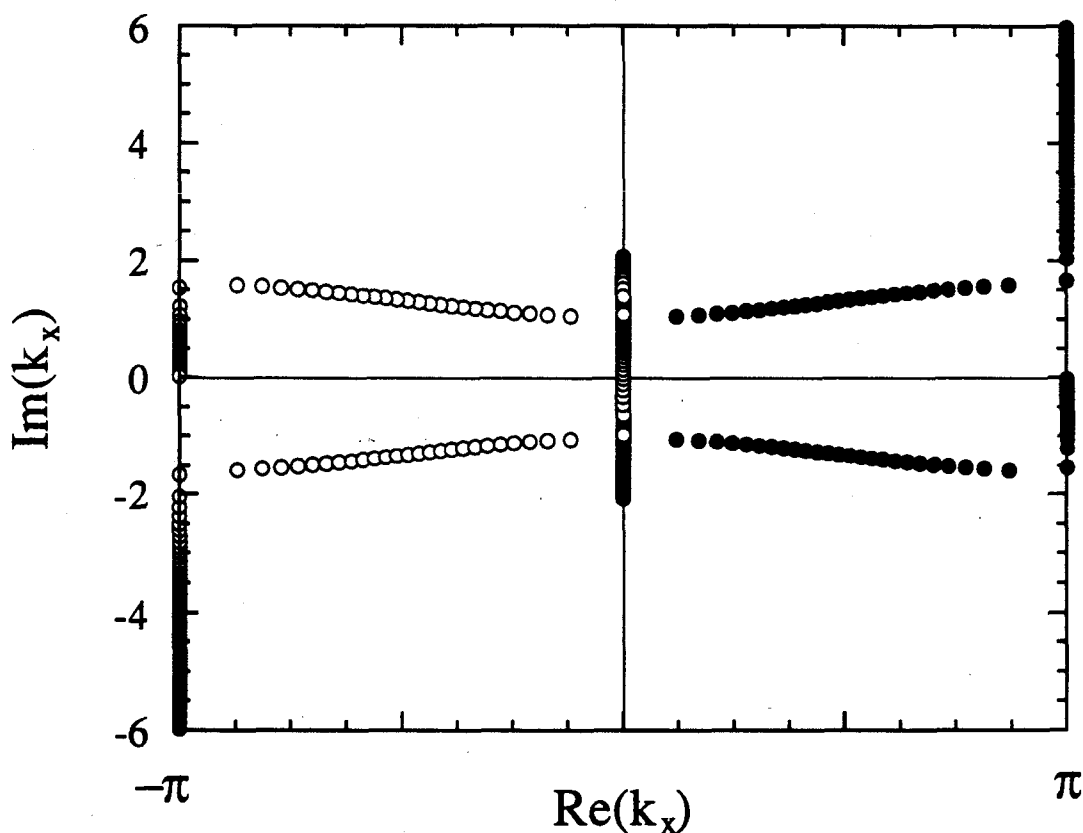


Fig. A.6: Trajectories of the two zeros of  $\text{Det} [1 - \Lambda(k_x, -i\beta\lambda X)]$  in the  $k_x$ -plane for the hexagonal lattice [cf. Eq. (A.6)] as  $X$  ranges from  $-\infty$  to  $\infty$ .

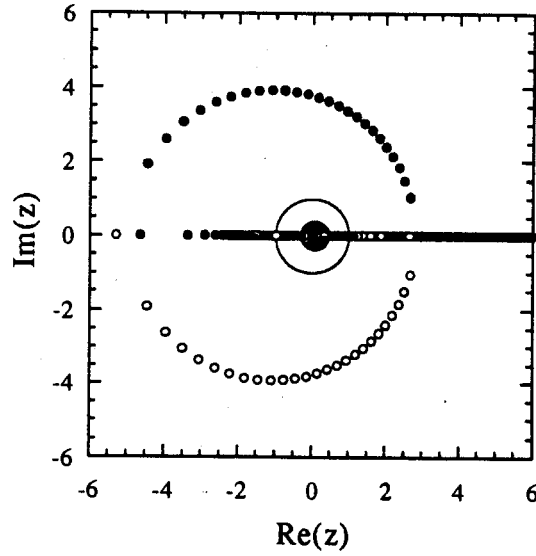


Fig. A.7: Trajectories of the two zeros of  $\text{Det}[1-\Lambda(k_x, -i\beta\lambda X)]$  in the  $z$ -plane for the hexagonal lattice [cf. Eq. (A.6)] as  $X$  ranges from  $-\infty$  to  $\infty$ . The circle shown (thin solid line) is the unit circle  $|z|=1$ . The trajectories off the real axis become increasingly heart-shaped as  $T \rightarrow T_c^-$ .

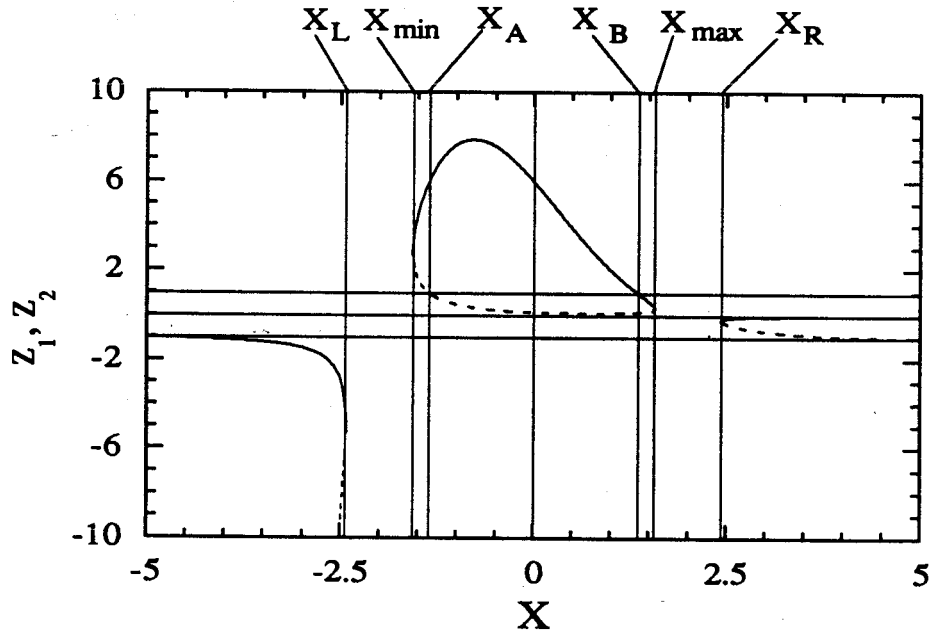


Fig. A.8: The real zeros of  $\text{Det}[1-\Lambda(k_x, -i\beta\lambda X)]$  in the  $z$ -plane for the hexagonal lattice as a function of  $X$ . For  $X \in [X_A, X_B]$ ,  $0 < z_1 \leq 1$  and  $z_2 \geq 1$ . For  $X \in [X_{\min}, X_A] \cup [X_B, X_{\max}]$ , either both or neither positive zeros are inside the unit circle  $|z|=1$ .

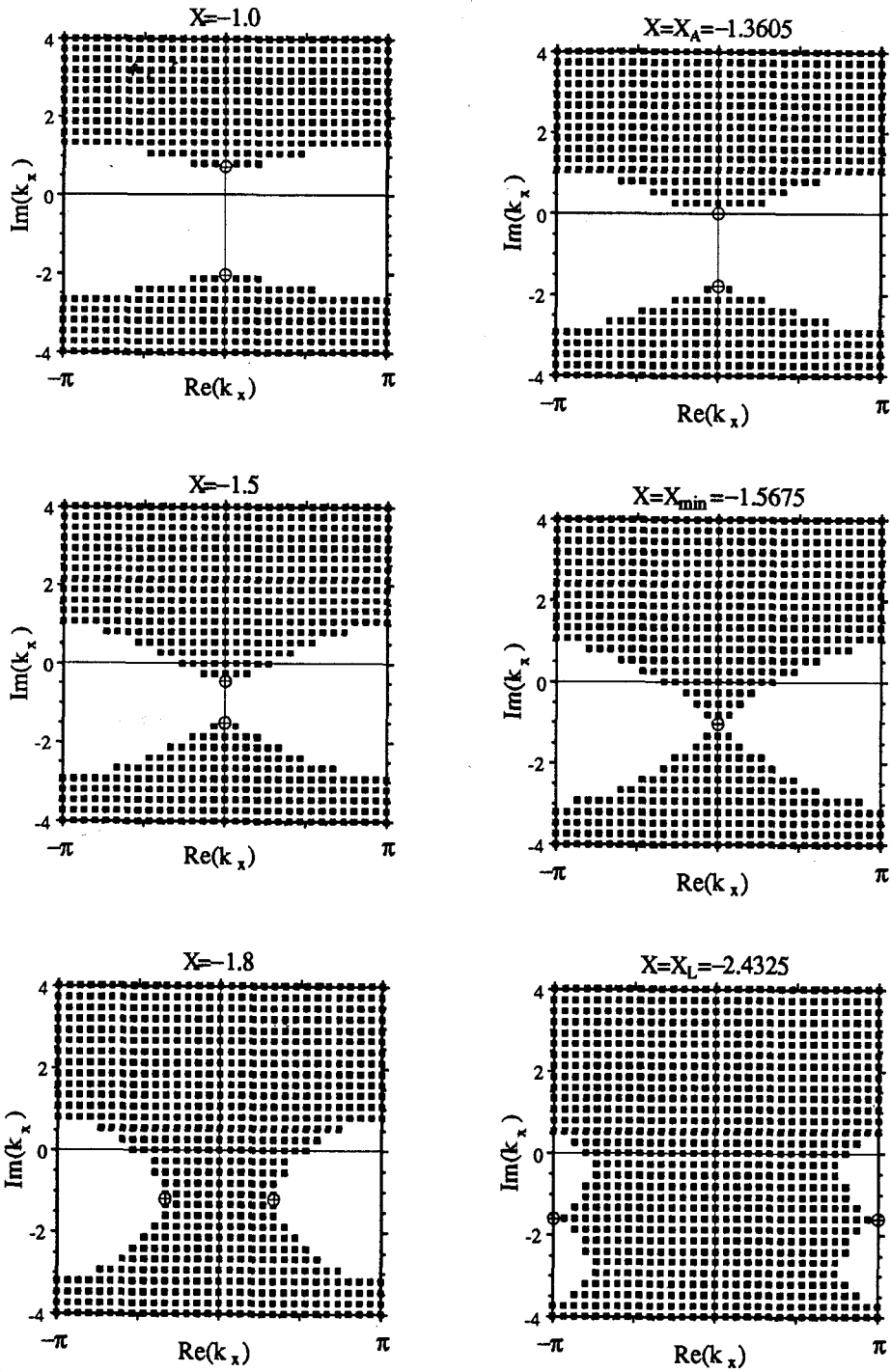


Fig. A.9: (continued on next page)

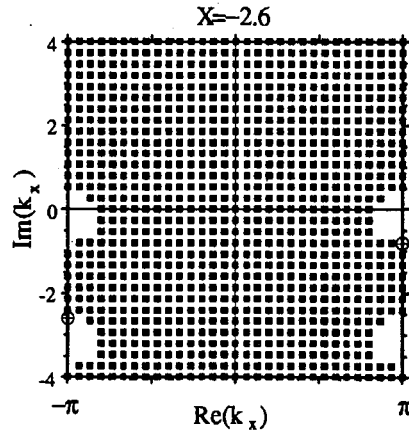


Fig. A.9: Regions of nonconvergence (black squares) of  $\Lambda(k_x, -i\beta\lambda X)$  in the  $k_x$ -plane for the hexagonal lattice at  $T=T_c/2$  for the values of  $X$  indicated. The corresponding pictures for positive  $X$  are simply obtained by changing  $\text{Im}(k_x)$  to  $-\text{Im}(k_x)$ . A path from  $-\pi$  to  $\pi$  is possible along the real  $k_x$ -axis for  $X \in [X_{\min}, X_{\max}]$ . For  $X \in [X_{\min}, X_B] \cup [X_A, X_{\max}]$ , a path from  $-\pi$  to  $\pi$  must be deformed from the real  $k_x$ -axis to avoid regions of nonconvergence. The zeros of  $\text{Det}[1 - \Lambda(k_x, -i\beta\lambda X)]$  are indicated by the symbol  $\oplus$ .

Investigations into the analytic structure of the FV matrix describing an interface between antiferromagnetic  $2 \times 1$  phases on a triangular lattice (see Section 2.3) show the same generic behaviour. Over the range of  $X$  for which the solutions to  $\text{Det}[1 - \Lambda(i\beta\lambda Y, -i\beta\lambda X)] = 0$  describe a convex shape, it is always possible to find a path from  $-\pi$  to  $\pi$  in the  $k_x$ -plane which avoids regions of nonconvergence and includes the correct pole. For other  $X$ , no such path exists.

For finite short-ranged interactions, at least, the behaviour exhibited by the two examples shown here presumably must be generic for any system for which the ECS is well defined. If this were not the case and the analytical continuation could not be performed such that regions of nonconvergence are avoided, then the entire formulation of the problem would be ill founded contrary to all evidence.



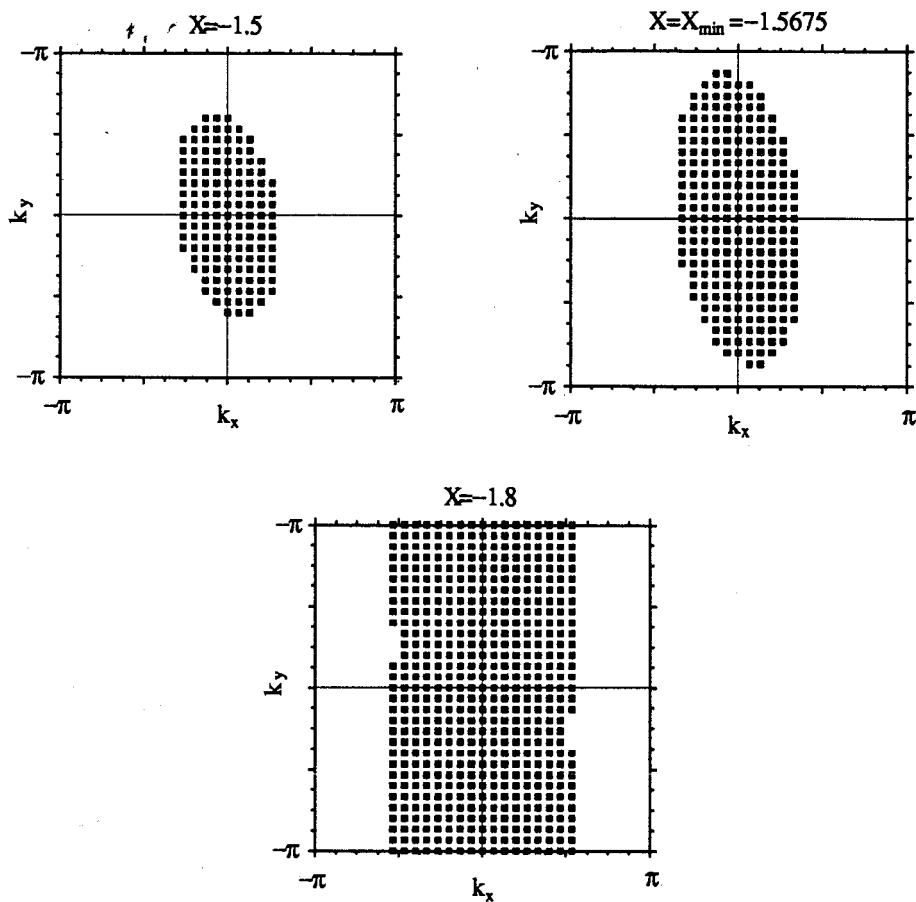


Fig. A.10: Regions of nonconvergence (black squares) of  $\Lambda(k_x, -i\beta\lambda X)$  in the Brillouin zone for the hexagonal lattice at  $T=T_c/2$  for the values of  $X$  indicated.

## Appendix B: Inversion of the ECS of the 2D rectangular Ising model

From Table 2.I, with  $\mathbf{a}=\hat{\mathbf{x}}$  and  $\mathbf{b}=\hat{\mathbf{y}}$  (see also Fig. 2.5), the ECS,  $y(x)$ , of the rectangular Ising model is given by

$$c_1 c_2 - s_1 \cosh(\beta \lambda y) - s_2 \cosh(\beta \lambda x) = 0 \quad . \quad (\text{B1})$$

Differentiating with respect to  $x$  and substituting  $\partial y / \partial x = -\tan \theta$  [cf. Eq. (2.20)], we obtain

$$\tan \theta = \frac{s_2 \sinh(\beta \lambda x)}{s_1 \sinh(\beta \lambda y)} \quad . \quad (\text{B2})$$

We now need to solve for  $x$  and  $y$  as a function of  $\theta$ , so that we can get  $\Gamma(\theta)$  from the equation [cf. Eq (2.20)],

$$\Gamma_{2D}(\theta) = \lambda x \sin \theta + \lambda y \cos \theta \quad . \quad (\text{B3})$$

We make the definitions,

$$\begin{aligned} \cosh(\beta \lambda x) &\equiv \chi \\ \cosh(\beta \lambda y) &\equiv \eta \\ \tan \theta &\equiv \tau \end{aligned} \quad . \quad (\text{B4})$$

Eqs. (B1) and (B2) then become simple algebraic equations for  $\chi$  and  $\eta$

$$c_1 c_2 - s_1 \eta - s_2 \chi = 0 \quad (\text{B5})$$

and

$$\eta^2 \tau^2 s_1^2 - \chi^2 s_2^2 + s_2^2 - \tau^2 s_1^2 = 0 \quad . \quad (\text{B6})$$

Eqs. (B5) and (B6) can now easily be solved to find

$$\chi = \frac{-c_1 c_2 + \sqrt{\tau^{-4} s_2^2 + \tau^{-2} (s_1^2 s_2^2 + 1) + s_1^2}}{s_2 (\tau^{-2} - 1)} = \chi(\theta) \quad (\text{B7})$$

$$\eta = \frac{-c_1 c_2 + \sqrt{\tau^4 s_1^2 + \tau^2 (s_1^2 s_2^2 + 1) + s_2^2}}{s_1 (\tau^2 - 1)} = \eta(\theta) . \quad (\text{B8})$$

In Eqs. (B7) and (B8) the plus sign on the radical was chosen to ensure that  $\chi \geq 1$  and  $\eta \geq 1$  for  $\theta \in [0, 2\pi)$ . Thus, we get  $\Gamma_{2D}(\theta)$  explicitly as

$$\Gamma_{2D}(\theta) = |\sin\theta| \operatorname{arccosh}[\chi(\theta)] + |\cos\theta| \operatorname{arccosh}[\eta(\theta)] , \quad (\text{B9})$$

where we have put the  $\cos\theta$  and  $\sin\theta$  factors in absolute values so that  $\operatorname{arccosh}(\cdot)$  may simply be evaluated as its principle value for all  $\theta \in [0, 2\pi)$ . We note that the expression (B9) with (B7-8) is much simpler than (although, equivalent to) that originally given in the literature by Avron et al. in 1982.

For equal couplings ( $c_1 = c_2 = \cosh 2\beta J$ ;  $s_1 = s_2 = \sinh 2\beta J$ ), some further straightforward manipulations give the result for  $\Gamma_{2D}(\theta)$  as stated by Rottman and Wortis in 1981:

$$\beta \Gamma_{2D}(\theta) = |\cos\theta| \operatorname{arcsinh}(\alpha |\cos\theta|) + |\sin\theta| \operatorname{arcsinh}(\alpha |\sin\theta|) \quad (\text{B10})$$

with

$$\alpha \equiv \frac{1}{h} \sqrt{\frac{1 - 4h^2}{1 + \sqrt{\sin^2 2\theta + 4h^2 \cos^2 2\theta}}} \quad (\text{B11})$$

and

$$h \equiv \frac{\sinh 2\beta J}{\cosh^2 2\beta J} . \quad (\text{B12})$$

For equal couplings, the equation for the ECS, Eq. (B1), may be written ( $\lambda=1$ )

$$\beta |y_{2D}(x)| = \operatorname{arccosh}\left(\frac{1}{h} - \cosh(\beta x)\right) . \quad (\text{B13})$$

# Appendix C: Series expansions for the 2D square Ising model

In the dimensionless units of Section 3, expanding (C10) in powers of  $v \equiv e^{-4\beta}$  and (B13) in powers of  $w \equiv e^{-2\beta}$ , we obtain, with the aid of the algebraic manipulator REDUCE, the series displayed in Tables CI and CII. In the symmetry directions these expressions simplify to

$$\Gamma_{2D}(0) = y_{2D}(0) = 2 + T \ln (\tanh \beta) = 2 - 2T \sum_{n_{\text{odd}}=1}^{\infty} \frac{w^n}{n} \quad (\text{C1})$$

and

$$\frac{1}{\sqrt{2}} \Gamma_{2D}\left(\frac{\pi}{4}\right) = y_{2D}(x=y_{2D}) = T \ln (\sinh 2\beta) = 2 - T \left( \ln 2 + \sum_{n=1}^{\infty} \frac{v^n}{n} \right). \quad (\text{C2})$$

### Table CI

Coefficients of the low-T expansion of the 2D-Ising interfacial free energy  $\Gamma_{2D}(\theta)$ .

$\Gamma_{2D}(\theta) = 2 - T \sum_{n=0}^{\infty} b_{2Dn}(\theta) e^{-4\beta n}$		
n	$b_{2Dn}(\theta)$	$c \equiv  \cos\theta $ ; $s \equiv  \sin\theta $
0	$(c+s) \ln (c+s) - c \ln c - s \ln s$	
1	$(c^3+s^3)/(cs)$	
2	$[-3(c^7+s^7)+2(s^5+c^5)]/(2c^3s^3)$	
3	$[9(c^{11}+s^{11})-10(c^9+s^9)+3(c^7+s^7)]/(3c^5s^5)$	
4	$[-31(c^{15}+s^{15})+44(c^{13}+s^{13})-22(c^{11}+s^{11})+4(c^9+s^9)]/(4c^7s^7)$	
5	$[121(c^{19}+s^{19})-204(c^{17}+s^{17})+132(c^{15}+s^{15})-40(c^{13}+s^{13})+5(c^{11}+s^{11})]/(5c^9s^9)$	
6	$[-515(c^{23}+s^{23})+1006(c^{21}+s^{21})-786(c^{19}+s^{19})+312(c^{17}+s^{17})-65(c^{15}+s^{15})+6(c^{13}+s^{13})]/(6c^{11}s^{11})$	

Table CII

†, Coefficients of the low-T expansion of the 2D-Ising equilibrium crystal shape  $y_{2D}(\theta)$ .

$$y_{2D}(x) = 2 - T \sum_{n=1}^{\infty} b_{2D_n}(x) e^{-2\beta n}$$

n	$b_{2D_n}(x)$	$\chi \equiv \cosh(\beta x)$
1	$2\chi$	
2	$2\chi^2 - 2$	
3	$\frac{8}{3}\chi^3 - 2\chi$	
4	$4\chi^4 - 4$	
5	$\frac{32}{5}\chi^5 + 8\chi^3 - 14\chi$	
6	$\frac{32}{3}\chi^6 + 32\chi^4 - 46\chi^2 + \frac{10}{3}$	
7	$\frac{128}{7}\chi^7 + 96\chi^5 - 128\chi^3 + 14\chi$	
8	$32\chi^8 + 256\chi^6 - 304\chi^4 + 16$	
9	$\frac{512}{9}\chi^9 + 640\chi^7 - 608\chi^5 - \frac{704}{3}\chi^3 + 146\chi$	
10	$\frac{512}{5}\chi^{10} + 1536\chi^8 - 928\chi^6 - 1504\chi^4 + 818\chi^2 - \frac{122}{5}$	
11	$\frac{2048}{11}\chi^{11} + 3584\chi^9 - 512\chi^7 - 6560\chi^5 + 3448\chi^3 - 146\chi$	
12	$\frac{1024}{3}\chi^{12} + 8192\chi^{10} + 3584\chi^8 - 23552\chi^6 + 11556\chi^4 - \frac{364}{3}$	

## Appendix D: Series for $\gamma(\frac{\pi}{4})$ of the BCRSOS model

Jayaprakash et al. gave in 1983 the following expression for the Cartesian coordinates of the BCRSOS facet shape:

$$\beta A \lambda x = -\sqrt{2} Z(\omega + \phi), \quad \beta A \lambda y = -\sqrt{2} Z(\phi), \quad (D1)$$

where A is a constant,

$$\phi \in [-2\omega, 2\omega), \quad 2 \cosh \omega = e^{2\beta J} - 2, \quad (D2)$$

and

$$Z(\xi) \equiv \ln \frac{\cosh \frac{1}{2}(\omega + \xi)}{\cosh \frac{1}{2}(\omega - \xi)} - \frac{1}{2} \xi - \sum_{n=1}^{\infty} \frac{(-1)^n e^{-2n\omega} \sinh n\xi}{n \cosh n\omega}. \quad (D3)$$

These coordinates are rotated by  $\pi/4$  from those used for the facet shape in Section 3.  $\theta = \pi/4$  (in the coordinates of Section 3) corresponds to the parameter  $\phi = 0$ , when  $y = 0$ , and

$$\gamma\left(\frac{\pi}{4}\right)(\text{BCRSOS}) = x = -\frac{\sqrt{2}}{\beta A \lambda} Z(\omega). \quad (D4)$$

To make contact with the energy scale of Section 3, we take  $J \rightarrow 2J$ . To normalize the BCRSOS facet shape so that  $\gamma(\theta = \pi/4, T=0) = 2\sqrt{2}$ , we take  $A\lambda = 1$ . Thus, to get a low-T expansion of  $\gamma(\pi/4)$ , we must expand

$$Z(\omega) = \ln \cosh \omega - \frac{\omega}{2} - \sum_{n=1}^{\infty} \frac{(-1)^n}{n} e^{-2n\omega} \tanh n\omega, \quad (D5)$$

with

$$\cosh \omega = \frac{1}{2v} - 1, \quad (D6)$$

in powers of  $v = \exp(-4\beta J)$ . After some elementary manipulations, we obtain, aided by the algebraic manipulation program REDUCE, the following series (in the dimensionless units of Section 3):

$$\begin{aligned}
& \frac{1}{\sqrt{2}} \gamma\left(\frac{\pi}{4}\right) (\text{BCRSOS}) = \\
& = 2 + T \left( -\ln 2 - v + \frac{1}{2} v^2 + \frac{14}{3} v^3 + \frac{65}{4} v^4 + \frac{234}{5} v^5 + \frac{371}{3} v^6 + \frac{2148}{7} v^7 + \frac{5665}{8} v^8 + \frac{13010}{9} v^9 + \frac{10823}{5} v^{10} - \right. \\
& \frac{6172}{11} v^{11} - \frac{150053}{6} v^{12} - \frac{1993668}{13} v^{13} - \frac{5083256}{7} v^{14} - \frac{15445312}{5} v^{15} - \frac{198297247}{16} v^{16} - \\
& \frac{814643486}{17} v^{17} - \frac{1625206543}{9} v^{18} - \frac{12681689860}{19} v^{19} - \frac{4858460157}{2} v^{20} - 8726304516 v^{21} - \\
& \frac{340811734532}{11} v^{22} - \frac{2502599042576}{23} v^{23} - \frac{4536558436405}{12} v^{24} - \frac{32478199348916}{25} v^{25} - \\
& \frac{57358896324242}{13} v^{26} - \frac{399349718315896}{27} v^{27} - \frac{341863037952600}{7} v^{28} - \frac{4591877224341056}{29} v^{29} - \\
& \frac{7525021925258524}{15} v^{30} - \frac{47780502385670032}{31} v^{31} - \frac{145024421300144799}{32} v^{32} - \\
& \frac{410388042705413374}{33} v^{33} - \frac{510842904954910389}{17} v^{34} - \frac{1840425563886041612}{35} v^{35} + \\
& \frac{356819183917550041}{18} v^{36} + \frac{31642674797949425588}{37} v^{37} + \frac{11414142063730282438}{19} v^{38} + \\
& \left. \frac{422991335163343500056}{13} v^{39} + \frac{630708193372567078915}{4} v^{40} + \dots \right). \tag{D7}
\end{aligned}$$

## Appendix E: Combinatorial Details

*How do I love thee? Let me count the ways.*

*E. BROWNING*

In this Appendix we will go through the combinatorial methods which were employed to evaluate the diagrams of Table 3.II. Rather than evaluating all diagrams here, we will do the combinatorics for a few typical diagrams, each requiring a different technique. It is not claimed that the methods presented here necessarily maximize elegance or efficiency.

### The Basics:

The simple, basic ingredients needed in the sequel are:<sup>†</sup>

Theorem (proof is trivial):

*The number of ways of choosing a subset of  $m$  objects from a set of  $n$  distinguishable objects, without regard to order, is given by the binomial coefficient,*

$$\frac{n!}{m!(n-m)!} \equiv \binom{n}{m} = \binom{n}{n-m}. \quad (\text{E1})$$

The symbol  $\binom{n}{m}$  is read “ $n$  choose  $m$ ”. It is *very* useful to extend the definition of the binomial coefficient such that

---

<sup>†</sup> An excellent introduction to combinatorics is given in the book by Feller (Feller, 1957).



$$\binom{n}{m} = 0 \quad \text{if either } m > n \text{ or if } m < 0 . \quad (\text{E2})$$

These binomial coefficients obey many identities. For our purposes the most useful are:

$$\binom{n+1}{m} = \binom{n}{m} + \binom{n}{m-1} \quad (\text{E3})$$

$$\sum_{m=0}^n \binom{r}{m} \binom{s}{n-m} = \binom{r+s}{n} \quad , r, s, n \text{ any positive integers.} \quad (\text{E4})$$


We shall often make use of the following elementary theorem (proof is trivial):

*The number of ways in which  $r$  indistinguishable objects can be distributed into  $n$  bins is given by  $\binom{n+r-1}{r}$ . The number of ways of doing this so that no bin is empty is given by  $\binom{r-1}{n-1}$ .*

Finally some definitions:

$$K \equiv |N| + |M| \quad , \quad d_0 \equiv \binom{K}{|N|} = \binom{K}{|M|} . \quad (\text{E5})$$

In the following we shall take  $N > 0$  and  $M > 0$  to save the writing of absolute value signs.

a.) The diagram :

This is the simplest diagram of Table 3.II. It corresponds to the number of ways in which a lattice walker can go from  $(0,0)$  to  $(N,M)$  in  $K+2$  steps. Consider first two extra vertical steps. From Fig. E.1 there are  $M+1$  up arrows and 1 down arrow to be distributed over  $N+1$  bins so that the down arrow is in a bin by itself. There are  $N+1$  ways to choose a bin for the down arrow. The number of ways in which the  $M+1$  up arrows can be

distributed over the remaining  $N$  bins is given by  $\binom{K}{M+1}$ . The number of ways of going from  $(0,0)$  to  $(N,M)$  with two extra horizontal steps is given from symmetry by exchanging  $N$  and  $M$ . Thus, we have

$$\begin{array}{|} \hline \bullet \\ \hline \bullet \\ \hline \end{array} = (N+1)\binom{K}{M+1} + (M+1)\binom{K}{N+1} = \binom{K}{M} \left[ \frac{N(N+1)}{M+1} + \frac{M(M+1)}{N+1} \right]. \quad (\text{E6})$$

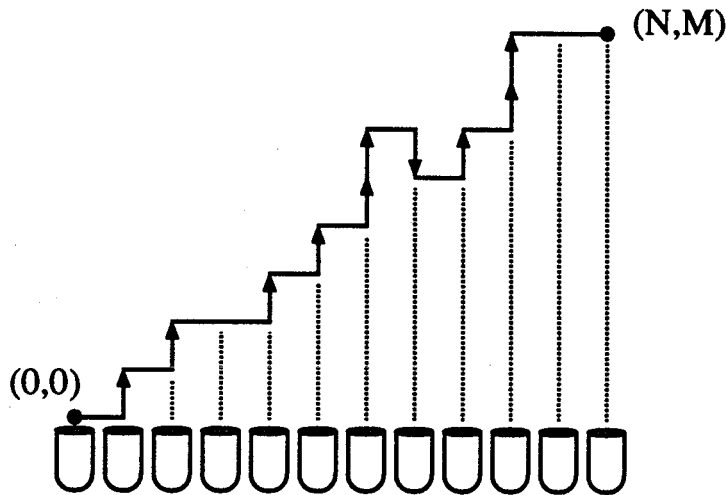


FIG. E.1. The vertical bonds of a step from  $(0,0)$  to  $(N,M)$  may be considered to be distributed over  $N+1$  bins.

b.) General SOS configurations:


A general SOS configuration corresponds to going from  $(0,0)$  to  $(N,M)$  with  $N+M+2M_e$  steps, i.e.,  $M_e$  extra up arrows and  $M_e$  down arrows. The number of ways in which this can be done may be counted as follows:

- Choose 1 out of the  $N+1$  available bins. There are  $\binom{N+1}{1} = N+1$  ways of doing this. Put all down arrows into that bin. There are  $\binom{M_e-1}{1-1} = 1$  ways of doing that. Distribute the  $M+M_e$  up arrows over the  $(N+1)-1$  remaining bins. There are  $\binom{(N+1)-1+M+M_e-1}{M+M_e}$  ways of doing that.
- Choose 2 of the  $N+1$  bins. There are  $\binom{N+1}{2}$  ways of doing this. Put all down arrows into the 2 bins so that there is at least one down arrow in each of the 2 bins (the case where one of the 2 bins is empty has been counted already). There are  $\binom{M_e-2}{2-1}$  ways of doing that. Distribute the  $M+M_e$  up arrows over the  $(N+1)-2$  remaining bins. There are  $\binom{(N+1)-2+M+M_e-1}{M+M_e}$  ways of doing that.
- Keep doing this until all possibilities of distributing down arrows into bins are exhausted: If  $M_e \geq N$ , the process of the previous steps must stop after  $N$  bins have been chosen for down arrows. (One bin must be left for up arrows.) If  $M_e < N$ , the process stops after  $M_e$  bins have been chosen for the down arrows.

Summing over the possibilities of distributing down arrows we get that the number of distinct SOS configurations is given by

$$\sum_{i=1}^{\min(M_e, N)} \binom{N+1}{i} \binom{M_e-1}{i-1} \binom{K+M_e-i}{M+M_e} \quad (E7)$$

At first sight one might worry about the  $\min(\cdot)$  function in the upper limit of the summation. However, the property (E2) of the binomial coefficients ensures that the summation is cut off correctly, whether we take the upper limit to be  $N$  or  $M_e$ .

c.) The diagram :

The number of SOS configurations corresponding to 4 extra vertical bonds can simply be read off from (E7) with  $M_e=2$  as

$$\text{4 vertical:} \quad (N+1) \binom{K+1}{M+2} + \binom{N+1}{2} \binom{K}{M+2} ; \quad (\text{E8})$$

the number for 4 extra horizontal bonds is obtained simply by exchanging  $N$  and  $M$  in (E8).

The remaining configurations correspond to 2 extra horizontal and 2 extra vertical bonds. We use the symbols  $A$ ,  $B$ ,  $C$ , and  $D$  to denote right, left, up, and down arrows, respectively:

$$A \approx \longrightarrow, \quad B \approx \longleftarrow, \quad C \approx \uparrow, \quad D \approx \downarrow \quad . \quad (\text{E9})$$

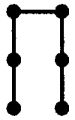
A path from  $(0,0)$  to  $(N,M)$  with 2 extra horizontal and 2 extra vertical steps thus forms a sequence of  $(N+1)$   $A$ 's,  $(M+1)$   $C$ 's, one  $B$ , and one  $D$ . To denote the beginning or end of the sequence we use the symbol  $\square$ . The "backtracking" local configurations  $AB$ ,  $BA$ ,  $CD$ , and  $DC$  are clearly illegal. The possible legal configurations can be counted by enumerating the allowed local environments of the bonds  $B$  and  $D$  as follows:

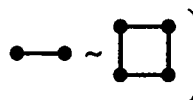
Table E.I

The possible configurations of a path from (0,0) to (N,M) with two extra vertical bonds and two extra horizontal bonds without immediate backtracking

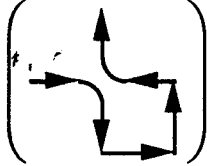
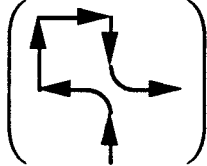
	local configuration(s)	# of A's left over	# of B's left over	# of compatible configurations
[1]	CBC ADA	N-1	M-1	$\frac{(N+M)!}{(N-1)! (M-1)!} = d_0 NM$
[2]	2× ADBC	N	M	$2 \frac{(N+M+1)!}{N! M!} = 2d_0 (K+1)$
[3]	2× □DA CBC	N	M-1	$2 \frac{(N+M)!}{N! (M-1)!} = 2d_0 M$
[4]	2× □BC ADA	N-1	M	$2 \frac{(N+M)!}{(N-1)! M!} = 2d_0 N$
[5]	2× □BDA	N	M+1	$2 \frac{(N+M+1)!}{N! (M+1)!} = 2d_0 \frac{K+1}{M+1}$
[6]	2× □DBC	N+1	M	$2 \frac{(N+M+1)!}{(N+1)! M!} = 2d_0 \frac{K+1}{N+1}$
[7]	2× □BC AD□	N	M	$2 \frac{(N+M)!}{N! M!} = 2d_0$

In this Table, "2×" indicates that for every sequence (configuration) containing the given local configuration(s), another configuration can be obtained by ordering the sequence in reverse.

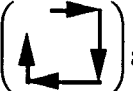

Not all configurations counted in Table E.I belong to the diagram , however.

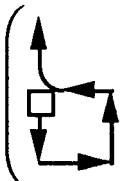
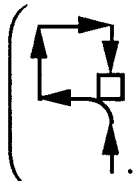
Some configurations belong to the diagram ; others correspond to self-

intersections. For each of the rows of Table E.I, these additional illegal configurations are:

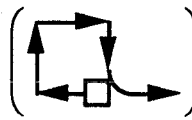
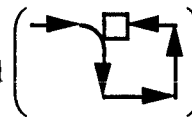
[1] ADACBC,  and CBCADA,  occur in  $\frac{(N+M-1)!}{(N-1)! (M-1)!}$

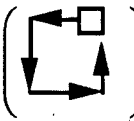
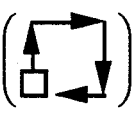
paths of length  $(K+4)$  form  $(0,0)$  to  $(N,M)$ .

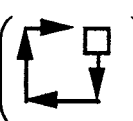
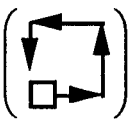
[2]  $2 \times$  ADBC,  and , occur in  $2d_0(K+1)$  paths of length  $(K+4)$  form  $(0,0)$  to  $(N,M)$ .

[3]  $2 \times \square$  DACBC,  and , occur in  $2d_0 \frac{M}{K}$  paths of length  $(K+4)$

form  $(0,0)$  to  $(N,M)$ .

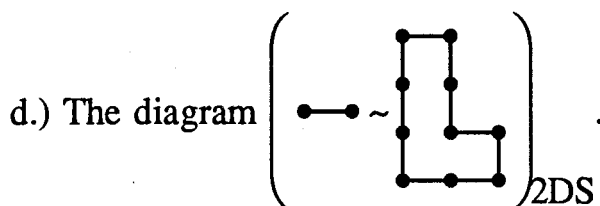
[4]  $2 \times \square$  BCADA,  and , occur in  $2d_0 \frac{N}{K}$  paths of length  $(K+4)$  form  $(0,0)$  to  $(N,M)$ .

[5]  $2 \times \square$  BDAC,  and , occur in  $2d_0$  paths of length  $(K+4)$  form  $(0,0)$  to  $(N,M)$ .

[6]  $2 \times \square$  DBCA,  and , occur in  $2d_0$  paths of length  $(K+4)$  form  $(0,0)$  to  $(N,M)$ .

[7] No illegal terms.

Adding the horizontal and vertical SOS configurations [cf. Eq. (E8)] to the number of configurations listed in Table E.I and subtracting the illegal configurations of the cases [1]-[6], one obtains the result quoted in Table 3.II for diagram # III.



The L-shaped disconnected part can have 8 possible orientations (see Fig. E.2a). The number of straddling configurations is easy to count for orientations 1, 2, 5, and 6. From Fig. E.2b it is obvious that orientations 1 and 2 can each straddle a given realization of the step,  $\bullet \text{---} \bullet$ , at  $2N+M$  places. From symmetry, the corresponding number for orientations 5 and 6 is given by interchanging  $N$  and  $M$ . Thus, orientations 1, 2, 5, and 6 have a total of  $6d_0K$  straddling configurations.

The situation is more complicated for the remaining 4 orientations. Consider orientation 3 (see Fig. E.2c). Each horizontal bond of  $(\bullet \text{---} \bullet)$  can be straddled in 2 ways, each vertical bond, in one way. However, straddling the horizontal bond between bin  $i$  and bin  $(i-1)$  (see Fig. E.2d) automatically straddles the two lowest vertical bonds in bin  $i$ . Denote by  $L_{2v}$  the sum over all the possible configurations of  $(\bullet \text{---} \bullet)$  of the number of vertical bonds of  $(\bullet \text{---} \bullet)$  which, when stacked as in Fig. E.2d, are not the lowest or second lowest bond in their bin (i.e., the number of bonds that “stick out over the line marked by 2” in the figure). In terms of  $L_{2v}$ , the L-shape of orientation 3 has  $2d_0N+L_{2v}$  straddling configurations. We now count  $L_{2v}$  as follows:

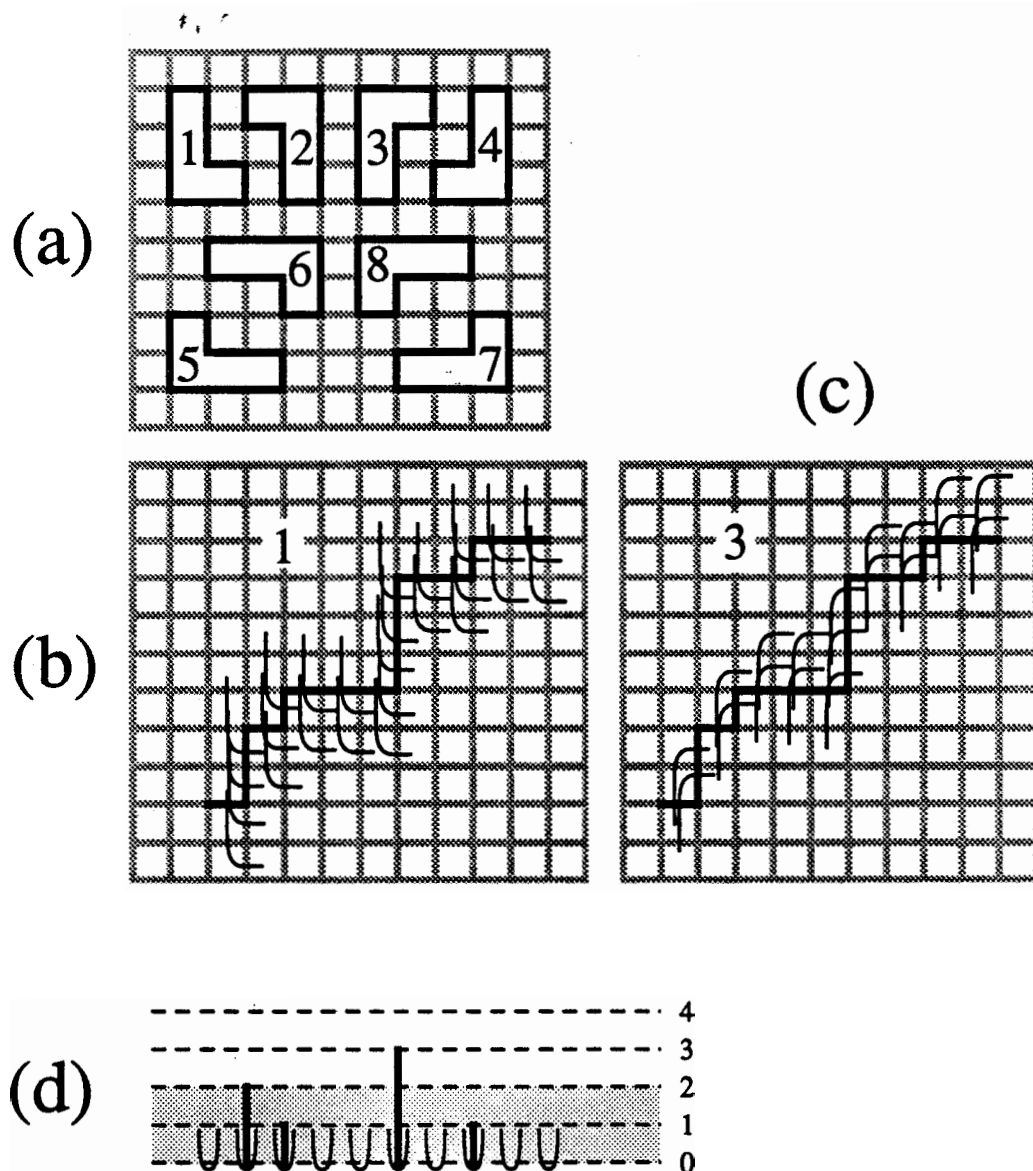


FIG. E.2 (a) The eight orientations of the L shape of diagram #16 (10 extra plaquettets). (b) The possible straddling configurations of the L shape of orientation 1 for a fixed realization of the step. (c) The possible straddling configurations of the L shape of orientation 3 for a fixed realization of the step. (d) The vertical bonds of the realization of the step shown stacked in their bins. To calculate the straddling configurations of orientation 3, the bonds that “stick out” above the line labeled by 2 must be counted for all possible realizations of the step.



- Choose  $i$  of the  $N+1$  bins. There are  $\binom{N+1}{i}$  ways of doing that.
- Put one vertical bond into each of the  $i$  bins.
  - Choose  $j$  of the  $i$  bins just selected. There are  $\binom{i}{j}$  ways of doing that.
  - Fill these  $j$  bins with the  $M-i$  remaining vertical bonds so that none of the  $j$  bins has less than (a total of) 2 vertical bonds. There are  $\binom{M-i-1}{j-1}$  ways of doing that.
  - There are now  $M-i-j$  vertical bonds sticking out above the line at height 2.
  - Sum over  $j$  until all  $i$  bins are exhausted.<sup>†</sup>
- Sum over  $i$  until all  $(N+1)$  bins are used.<sup>†</sup>

Thus, we get

$$L_{2v} = \sum_{i=1}^{N+1} \binom{N+1}{i} \sum_{j=1}^i \binom{i}{j} \binom{M-i-1}{j-1} (M-i-j) + (\text{end effect}) \equiv \Omega(N,M) + (\text{end effect}), \quad (\text{E10})$$

where (end effect) refers to the number of ways in which vertical bonds on the first bin can be straddled that are not included in  $L_{2v}$ . Since the first bin is not preceded by a vertical bond, the two lowest vertical bonds in the first bin (if there are any) can never be automatically straddled by an  $L$  straddling the nonexistent preceding horizontal bond. The end effect is, therefore, given by

---

<sup>†</sup> Again, we need not worry about running out of bonds before running out of bins because of property (D2).

(end effect) = (number of configurations with exactly one bond in the first bin)  
 $+ 2 \times$  (number of configurations with *at least* 2 vertical bonds in the first bin) .

If there is exactly 1 bond in bin 1, then the following horizontal bond always ends at position (1,1). Thus, the number of configurations with exactly one bond in the first bin is simply given by the number of ways in which one can get from (1,1) to (N,M) with  $N+M-2$  steps. Likewise, if we are guaranteed that there are at least 2 bonds in bin 1, the remaining part of (●—●) is tethered at (0,2) and (N,M). The number of configurations with *at least* 2 vertical bonds in the first bin is, therefore, given by the number of ways in which one can go from (0,2) to (N,M) in  $N+M-2$  steps. We obtain

$$(\text{end effect}) = \binom{K-2}{N-1} + 2 \binom{K-2}{N} = d_0 \frac{NM+2[M(M-1)]}{K(K-1)} . \quad (\text{E11})$$

The double sum  $\Omega(N,M)$  is evaluated straightforwardly via repeated application of identity (E4). The only new kind of sum that occurs is of the form

$$S = \sum_{j=1}^i j \binom{i}{j} \binom{M-i-1}{j-1} . \quad (\text{E12})$$

This sum is easily evaluated by writing

$$j \binom{i}{j} = \frac{j i!}{j! (i-j)!} = \frac{i (i-1)!}{(j-1)! (i-j)!} = i \binom{i-1}{j-1} . \quad (\text{E13})$$

Substituting (E13) into (E12) we get

$$S = i \sum_{j=1}^i \binom{M-i-1}{j-1} \binom{i-1}{j-1} = i \sum_{k=0}^{i-1} \binom{M-i-1}{k} \binom{i-1}{i-1-k} = \binom{M-2}{i-1} , \quad (\text{E14})$$

where the last equality follows immediately from identity (E4). After a little algebra of this sort one gets

$$\begin{aligned} \Omega(N,M) &= \\ &= M \binom{K}{N} - (N+1) \left[ \binom{K-1}{N} + \binom{K-2}{N} \right] = \binom{K}{N} \left\{ M - (N+1) \left[ \frac{M}{K} + \frac{M(M-1)}{K(K-1)} \right] \right\}. \end{aligned} \quad (E15)$$

From symmetry it follows that the number of straddling configurations for orientation 4 is the same as that for orientation 3. The number of straddling configurations for orientations 7 and 8 is obtained from the number for 3 and 4 by interchanging  $N$  and  $M$ . Adding up the contributions from all orientations, one obtains the result quoted in Table 3.II for diagram #16.

e) The diagram  $\Delta \left[ \bullet \bullet \sim \left( \begin{array}{c} \square \\ \square \\ \square \\ \square \end{array} \right) \right]$ :

We will evaluate the diagram as a 3D diagram and as a 2D diagram and take the difference (3D)–(2D). First the 2D version.

• The 2D interpretation,  $\left[ \bullet \bullet \sim \left( \begin{array}{c} \square \\ \square \\ \square \\ \square \end{array} \right) \right]_{2D}$ :

We take the 2D system to be rectangular with periodically connected boundaries (a torus) and  $\mathbb{N}^2$  dual sites (squares). In the absence of the interface,  $(\bullet \bullet)$ , the two disconnected diagrams,  $\left( \begin{array}{c} \square \\ \square \end{array} \quad \begin{array}{c} \square \\ \square \end{array} \right)$ , can be placed on the torus in  $\mathbb{N}^2(\mathbb{N}^2 - 5)/2$

ways. The presence of the interface makes some of these configurations impossible. We count these illegal configurations as follows:

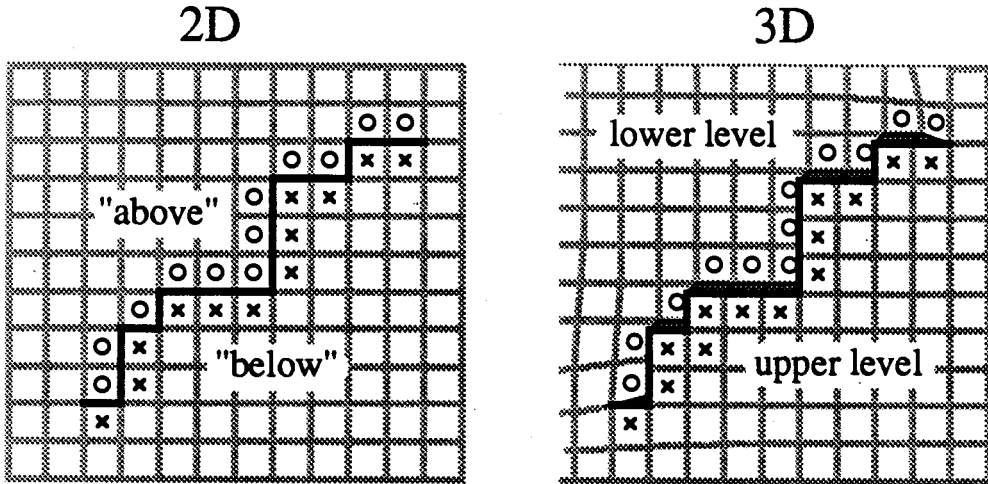




FIG. E.3. Fixed realizations of the diagram (●—●) in the 2D and 3D interpretations. The o's and x's label potential abutting positions. (The elastic energy associated with the lattice distortion due the screw dislocations is not taken into account in the calculations of Section 3. The screw dislocations serve only as a device for enforcing a step.)


Consider a given, fixed realization of (●—●), such as the one shown in Fig. E.3. We perform the counting for a fixed realization and in the end sum over realizations. Denote the number of “abutting-from-below” sites (the x's in Fig. E.3) by  $N_x$  and the number of “abutting-from-above” sites (the o's in Fig. E.3) by  $N_o$ . Note that

$$N_x + N_o = \left( \boxed{\bullet\text{---}\bullet} \sim \begin{array}{c} \bullet \\ \square \\ \bullet \end{array} \right)_A, \tag{E16}$$

where the box around  $\boxed{\bullet\text{---}\bullet}$  indicates that a *fixed* realization of  $\bullet\text{---}\bullet$  is meant (“the box is a snap shot”). We can then enumerate the following possibilities:

[1] One  abuts the step, the other  does not. There are

$$\left( \left( \text{---} \sim \text{square} \right)_A \right) \left[ N^2 - \left( \left( \text{---} \sim \text{square} \right)_A \right) \right] - (\text{dimers})_1 \quad (\text{E17})$$

such illegal configurations, where  $(\text{dimers})_1$  denotes the number of dimer configurations formed under these conditions. (By dimer we mean .)

These dimer configurations must be subtracted since they have already been counted in the disconnected term,  $N^2(N^2 - 5)/2$ .

[2] Both  's abut the step.

[a] Both abut from below. There are

$$\frac{1}{2} N_x(N_x - 1) - (\text{dimers})_{2a} \quad (\text{E18})$$

such illegal configurations not already counted in the disconnected term.

[b] Both abut from above. There are

$$\frac{1}{2} N_o(N_o - 1) - (\text{dimers})_{2b} \quad (\text{E19})$$

such illegal configurations not already counted in the disconnected term.

[c] One abuts from below, the other from above. There are

$$N_o N_x - (\text{dimers})_{2c} \quad (\text{E20})$$

such illegal configurations not already counted in the disconnected term.

In [2][a]-[c] we again needed to subtract dimer configurations which were already included in the disconnected term. We can make the identifications,

$$(\text{dimers})_1 + (\text{dimers})_{2a} + (\text{dimers})_{2b} = \left( \boxed{\bullet\text{---}\bullet} \sim \begin{array}{|c|} \hline \bullet \\ \hline \bullet \\ \hline \bullet \\ \hline \end{array} \right)_A \quad (\text{E21})$$

and

$$(\text{dimers})_{2c} = \left( \boxed{\bullet\text{---}\bullet} \sim \begin{array}{|c|} \hline \bullet \\ \hline \bullet \\ \hline \bullet \\ \hline \end{array} \right)_{2DS} \quad (\text{E22})$$


Subtracting from the disconnected part the illegal contributions from [1] and [2], we finally obtain

$$\left[ \boxed{\bullet\text{---}\bullet} \sim \begin{array}{|c|} \hline \bullet \\ \hline \bullet \\ \hline \bullet \\ \hline \end{array} \right]_{2D} = \mathbb{N}^2(\mathbb{N}^2 - 5)/2 - \left( \mathbb{N}^2 - \frac{1}{2} \right) \left( \boxed{\bullet\text{---}\bullet} \sim \begin{array}{|c|} \hline \bullet \\ \hline \bullet \\ \hline \bullet \\ \hline \end{array} \right)_A + \frac{1}{2} \left( \boxed{\bullet\text{---}\bullet} \sim \begin{array}{|c|} \hline \bullet \\ \hline \bullet \\ \hline \bullet \\ \hline \end{array} \right)_A^2 + \left( \boxed{\bullet\text{---}\bullet} \sim \begin{array}{|c|} \hline \bullet \\ \hline \bullet \\ \hline \bullet \\ \hline \end{array} \right)_A + \left( \boxed{\bullet\text{---}\bullet} \sim \begin{array}{|c|} \hline \bullet \\ \hline \bullet \\ \hline \bullet \\ \hline \end{array} \right)_{2DS} \quad (\text{E23})$$

- The 3D interpretation,  $\left[ \boxed{\bullet\text{---}\bullet} \sim \begin{array}{|c|} \hline \bullet \\ \hline \bullet \\ \hline \bullet \\ \hline \end{array} \right]_{3D}$  :

We assume the 2D interface to be toroidally connected and to have  $\mathbb{N}^2$  plaquettes (see also the discussion in Section 3.3). In the absence of a step there are  $\mathbb{N}^2(\mathbb{N}^2 - 5)/2$  ways of having two desorptions  $\left( \begin{array}{|c|} \hline \bullet \\ \hline \bullet \\ \hline \bullet \\ \hline \end{array} \right)$ , as many ways to have two adsorptions  $\left( \begin{array}{|c|} \hline \bullet \\ \hline \bullet \\ \hline \bullet \\ \hline \end{array} \right)$ , and  $\mathbb{N}^2(\mathbb{N}^2 - 1)$  ways of having both an adsorption and a desorption giving a net disconnected contribution of  $2\mathbb{N}^2(\mathbb{N}^2 - 3)$ . We must now count which of these configurations are not possible in the presence of a step,  $\bullet\text{---}\bullet$ . Again, we consider a fixed realization of the step. Recall that desorptions are allowed to abut the step on the

lower level and adsorptions are allowed to abut the step on the upper level (see Fig. E.3). [“Abutting on the lower (upper) level” in the 3D interpretation corresponds to “abutting form above” (“abutting form below”) in the 2D interpretation.] We can enumerate the following cases:

[1] Two desorptions: .

[a] One desorption abuts on the upper level; the other does not. There are

$$N_x(N^2 - N_x) - \left( \left[ \text{---} \right] \sim \left[ \begin{array}{c} \bullet \\ \bullet \\ \bullet \\ \bullet \end{array} \right] \right)_{2DS} - (\text{dimers})_{1a} \quad (\text{E24})$$

such illegal configurations not already counted in the disconnected term.

[b] Both desorptions abut on the upper level. There are

$$\frac{1}{2} N_x(N_x - 1) - (\text{dimers})_{1b} \quad (\text{E25})$$

such illegal configurations not already counted in the disconnected term.

[2] Two adsorptions: .

[a] One abuts on the lower level; the other does not. There are

$$N_o(N^2 - N_o) - \left( \left[ \text{---} \right] \sim \left[ \begin{array}{c} \bullet \\ \bullet \\ \bullet \\ \bullet \end{array} \right] \right)_{2DS} - (\text{dimers})_{2a} \quad (\text{E26})$$

such illegal configurations not already counted in the disconnected term.

[b] Both abut on the lower level. There are

$$\frac{1}{2} N_o(N_o - 1) - (\text{dimers})_{2b} \quad (\text{E27})$$

such illegal configurations not already counted in the disconnected term.



[3] An adsorption  and a desorption . (Dimer formations are not possible.)

[a]  abuts on the lower level;  does *not* abut on the upper level.

There are

$$N_o(N^2 - N_x - 1) \quad (\text{E28})$$

such illegal configurations not already counted in the disconnected term.

[b]  abuts on the upper level;  does *not* abut on the lower level.

There are

$$N_x(N^2 - N_o - 1) \quad (\text{E29})$$

such illegal configurations not already counted in the disconnected term.

[c] Both abut in illegal positions. There are

$$N_x N_o \quad (\text{E30})$$

such illegal configurations not already counted in the disconnected term.

The overcounted dimer configurations may be identified as

$$(\text{dimers})_{1a} + (\text{dimers})_{1b} + (\text{dimers})_{2a} + (\text{dimers})_{2b} = \left( \left[ \text{---} \sim \begin{array}{|c|} \hline \bullet \\ \hline \bullet \\ \hline \bullet \\ \hline \bullet \\ \hline \end{array} \right]_A \right) \quad (\text{E31})$$

Subtracting from the disconnected part the illegal contributions from [1], [2], and [3], we finally obtain



$$\begin{aligned}
 \left[ \text{---} \sim \left( \begin{array}{c} \square \\ \square \\ \square \end{array} \right) \right]_{3D} &= 2N^2(N^2 - 3) - \left( 2N^2 - \frac{3}{2} \right) \left( \text{---} \sim \square \right)_A + \\
 &\frac{1}{2} \left( \text{---} \sim \square \right)_A^2 + \left( \text{---} \sim \begin{array}{c} \square \\ \square \end{array} \right)_A + 2 \left( \text{---} \sim \begin{array}{c} \square \\ \square \\ \square \end{array} \right)_{2DS} \quad (E32)
 \end{aligned}$$

Neglecting the  $N^2$  dependent parts [they can be checked to cancel in the expansion of the logarithms (see Section 3.3)], the difference between the 3D and 2D interpretations of the diagram is given by

$$\Delta \left[ \text{---} \sim \left( \begin{array}{c} \square \\ \square \\ \square \end{array} \right) \right] = \left( \text{---} \sim \square \right)_A + \left( \text{---} \sim \begin{array}{c} \square \\ \square \end{array} \right)_{2DS} \quad (E33)$$





The sum over the realizations of  $\text{---}$  is trivial *in this case* and simply amounts to dropping the box on  $\square$ .

### Comments:

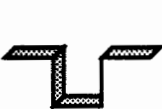

- 1.) All diagrams were checked by explicitly enumerating all possible configurations (at a given order) for various small values of  $N$  and  $M$  [ $(N, M)$  on the order of  $\sim(4, 4)$ ].
- 2.) The results of the combinatorics for diagrams interpreted as 2D diagrams were checked to give the correct low- $T$  expansion of the exactly known facet shape and interfacial free energy of the rectangular Ising model.
- 3.) Had we chosen to enforce an interface containing a single step by appropriately fixing the signs of the spins on the boundary (instead of introducing screw dislocations),

the combinatorics would have been considerably more difficult. For example, the bins used in the combinatorics of (2D) SOS configurations could not have been filled with an arbitrary number of bonds since these bonds would eventually run into the boundary. Because the cutoff for filling a given bin so that bonds do not run into the boundary, depends on the actual spatial position of the bonds, the concept of bins is no longer very useful and the combinatorics of SOS configurations cannot be reduced to an occupancy problem.

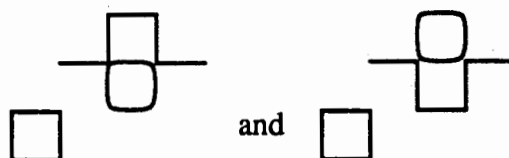
4.) The diagrams containing multiply disconnected parts are the most difficult diagrams to evaluate. The difficulties stem from a.) the interference between diagrams at the same order (i.e., from having to make sure that the same configuration is not counted in the evaluation of different diagrams) and from b.) the fact that summing over realizations of the “bare” step does, generally, also lead to overcounting. Consider, for example, the diagram

$\Delta \left[ \text{diagram} \sim \left( \text{diagram} \right) \right]$ . This diagram interferes with the diagram  $\text{diagram} \sim \text{diagram}$ : An allowed configuration at this order is  +  +  = .

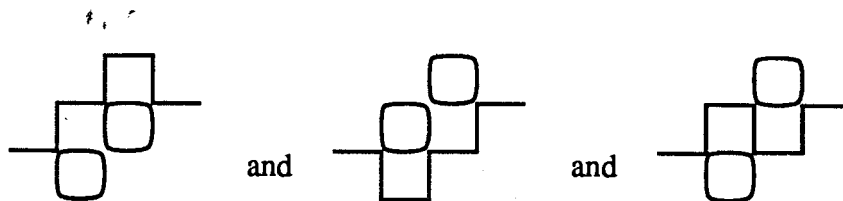
However, at the same order, this is clearly also an allowed configuration of the diagram

$\text{diagram} \sim \text{diagram}$ , i.e.,  + . -- The overcounting from the sum over

configurations arises from the equivalence of local configurations such as



and also



The latter type of overcounting occurs both in the 2D and 3D interpretations, but the number of overcounted configurations is not always the same in the two cases. Careful analysis, to the order of the expansion in Section 3, shows that the various overcountings cancel when one takes the difference (3D)–(2D). Whether or not this is a general principle has yet to be established.

# References

- Abraham, D. B. (1986). In "Phase Transitions and Critical Phenomena", Vol. 10 (C. Domb and J. L. Lebowitz, eds.), pp. 2-69. Academic, New York.
- Adler, J. (1987). *Phys. Rev. B* **36**, 2473.
- Akutsu, N. and Akutsu, Y. (1987a). *J. Phys. Soc. Jpn.* **56**, 1443.
- Akutsu, N. and Akutsu, Y. (1987b). *J. Phys. Soc. Jpn.* **56**, 2248.
- Andreev, A. F. (1981). *Zh. Eksp. Teor. Fiz.* **80**, 2042 [*Sov. Phys. JETP* **53**, 1063 (1982)].
- Avron, J. E. and Zia, R. K. P. (1988). *Phys. Rev. B* **37**, 6611.
- Avron, J. E., Taylor, J. E. and Zia, R. K. P. (1983). *J. Stat. Phys.* **33**, 493.
- Avron, J. E., van Beijeren, H., Schulman, L. S. and Zia, R. K. P. (1982). *J. Phys. A* **15**, L81.
- Balibar, S., and Castaing, J. (1980). *Phys. Lett.* **41**, L329.
- Burgoyne, P. N. (1963). *J. Math. Phys.* **4**, 1320.
- Burton, W. K., Cabrera, N. and Frank, F. C. (1951). *Philos. Trans. Roy. Soc. London, Ser. A* **243**, 299.
- Cabrera, N. (1964). *Surf. Sci.* **2**, 320.
- Caginalp, G. and Fisher, M. E. (1979). *Commun. Math. Phys.* **65**, 247.
- Calheiros, F., Johannesen, S. and Merlini, D. (1987). *J. Phys. A* **20**, 5991.
- Callen, H. B. (1960). "Thermodynamics". John Wiley & Sons, New York.
- Cheng H. and Wu, T. T. (1967). *Phys. Rev.* **164**, 719.
- Chui, S. T. and Weeks, J. D. (1976). *Phys. Rev. B* **14**, 4978.
- Curie, P. (1885). *Bull. Soc. Mineralog. de France* **8**, 145.
- Dinghas, A. (1944). *Zeits. f. Kristallog.* **105**, 304
- Dobrushin, R. L., Kotecký, R. and Shlosman, S. B. (1989). In "Stochastic Methods in Mathematics and Physics: Proceedings of the Twenty-Fourth Karpacz Winter School, Karpacz, Poland, Jan. 13-27, 1988", (R. Gielerak and W. Karwowski, eds.), pp 221-229. World Scientific, Singapore.
- Fan, C. and Wu, F. Y. (1969). *Phys. Rev.* **179**, 560.

- Fan, C. and Wu, F. Y. (1970). *Phys. Rev. B* **2**, 723.
- Federer, H. (1969). "Geometric Measure Theory". Springer Verlag, New York.
- Feller, W. (1957). "An Introduction to Probability Theory and Its Applications", Vol. 1. John Wiley, New York.
- Feynman, R. P. (1972). "Statistical Mechanics", pp 136-150. Benjamin/Cummings, Reading, Mass.
- Fisher, D. S. and Weeks, J. D. (1983). *Phys. Rev. Lett.* **50**, 1077.
- Fisher, M. E. (1969). *J. Phys. Soc. Japan (Suppl.)* **26**, 87.
- Fisher, M. E. and Caginalp, G. (1977). *Commun. Math. Phys.* **56**, 11.
- Fisher, M. E. and Ferdinand, A. E. (1967). *Phys. Rev. Lett.* **19**, 169.
- Fradkin, E. (1983). *Phys. Rev. B* **28**, 5338.
- Fradkin, E., Huberman, B. A. and Shenker, S. H. (1978). *Phys. Rev. B* **18**, 4789.
- Gallet, F., Nozières, P., Balibar, S. and Rolley, E. (1986). *Europhys. Lett.* **2**, 701.
- Gaunt, D. S. and Guttman, A. J. (1974). In "Phase Transitions and Critical Phenomena", Vol. 3 (C. Domb and M. S. Green, eds.), pp. 181-243. Academic, New York.
- Griffiths, R. B. (1980). In "Phase Transitions in Surface Films", (J. G. Dash and J. Ruvalds, eds.), pp. 1-27. Plenum, New York.
- Herring, C. (1951). *Phys. Rev.* **82**, 87.
- Herring, C. (1953). In "Structure and Properties of Solid Surfaces", (R. Gomer and G. Smith, eds.), pp 5-81. Chicago Univ. Press, Chicago.
- Heyraud, J. C. and Métois, J. J. (1983). *Surf. Sci.* **128**, 334.
- Hilton, H. (1903). "Mathematical Crystallography". Oxford.
- Holzer, M. (1990a). *Phys. Rev. Lett.* **64**, 653.
- Holzer, M. (1990b). "Exact Equilibrium Crystal Shapes in Two Dimensions for Free-Fermion Models", Simon Fraser University preprint.
- Holzer, M. and Wortis, M. (1989). *Phys. Rev. B* **40**, 11044.
- Hurst, C. A. (1966). *J. Math. Phys.* **7**, 305.
- Hurst, C. A. and Green, H. S. (1960). *J. Chem. Phys.* **33**, 1059.
- Huse, D. A., van Saarloos, W. and Weeks, J. D. (1985). *Phys. Rev. B* **32**, 233.

- Jayaprakash, C. and Saam, W. F. (1984a). *Phys. Rev. B* **30**, 3916.
- Jayaprakash, C., Rottman, C. and Saam, W. F. (1984b). *Phys. Rev. B* **30**, 6549.
- Jayaprakash, C., Saam, W. F. and Teitel, S. (1983). *Phys. Rev. Lett.* **50**, 2017.
- Kac, M. and Ward, J. C. (1952). *Phys Rev.* **88**, 1332.
- Kano, K. and Naya, S. (1953). *Prog. Theor. Phys.* **10**, 158.
- Kasteleyn, P. W. (1961). *Physica* **27**, 1209.
- Kasteleyn, P. W. (1963). *J. Math. Phys.* **4**, 287.
- Keshishev, K.O., Parshin, A. Ya., and Babkin, A.V. (1981). *Sov. Phys. JETP* **53**, 362.
- Kosterlitz, J. M. and Thouless, D. J. (1973). *J. Phys. C* **6**, 1181.
- Kotecký, R. (1988). In "Proceedings of the Ninth International congress of mathematical physics", (B. Simon, I.M. Davies, and A. Truman, eds.). Hilger, Bristol, England.
- Kramers, H. A. and Wannier, G. K. (1941). *Phys. Rev.* **60**, 252.
- Landau, J, Lipson, S.G., Maattanen, L.M., Balfour, L.S., and Edwards, D.O. (1980). *Phys Rev. Lett.* **45**, 31.
- Landau, L. D. and Lifshitz, E. M. (1968). "Statistical Physics", 2nd edn., pp 447-454. Pergamon, Oxford.
- Leamy, H. J., Gilmer, G. H. and Jackson, K. A. (1975). In "Surface Physics of Crystalline Materials", p. 169. Academic, New York.
- Lieb, E. H. (1967). *Phys. Rev. Lett.* **19**, 108.
- Lieb, E. H. and Wu, F.Y. (1972). In "Phase Transitions and Critical Phenomena", Vol. 1. (C. Domb and M. S. Green, eds.). Academic, New York.
- Liebmann, H. (1914). *Zeits. f. Kristallog.* **53**, 171.
- McCoy, B. and Wu, T. T. (1973). "The Two Dimensional Ising Model", pp. 299-305. Harvard, Cambridge, Mass.
- Minkowski, H (1903). *Math. Ann.* **57**, 447.
- Minkowski, H (1911). "Gesammelte Abhandlungen". B.G. Teubner, Leipzig und Berlin.
- Mon, K. K., Wansleben, S., Landau, D. P. and Binder, K. (1988). *Phys. Rev. Lett.* **60**, 708.
- Mon, K. K., Wansleben, S., Landau, D. P. and Binder, K. (1989). *Phys. Rev. B* **39**, 7089.
- Morita, T. (1986). *J. Phys. A* **19**, 1197 (1986).

- Onsager, L. (1944). *Phys. Rev.* **65**, 117.
- Pawley, G. S., Swendsen, R. H. D., Wallace, J. and Wilson, K. G. (1984). *Phys. Rev. B* **29**, 4030.
- Pokrovsky, V. L. and Talapov, A.L. (1979). *Phys. Rev. Lett.* **42**, 65.
- Rottman, C. and Wortis, M. (1981). *Phys. Rev. B* **24**, 6274.
- Rottman, C. and Wortis, M. (1984a). *Phys. Rep.* **103**, 59 .
- Rottman, C. and Wortis, M. (1984b). *Phys. Rev. B* **29**, 328.
- Ryazanov, G. V. (1970). *Zh. Eksp. Teor. Fiz.* **59**, 1000 [*Sov. Phys. JETP* **32**, 544 (1971)].
- Shaw, L. J. and Fisher, M. E. (1989). *Phys. Rev. A* **39**, 2189.
- Sherman, S. (1960). *J. Math. Phys.* **1**, 202.
- Sherman, S. (1963). *J. Math. Phys.* **4**, 1213.
- Shi, A.-C. and Wortis, M. (1988). *Phys. Rev. B* **37**, 7793.
- Slater, J. (1941). *Chem Phys.* **9**, 16.
- Sutherland, B. (1967). *Phys. Rev. Lett.* **19**, 103.
- Sutherland, B. (1970). *J. Math. Phys.* **11**, 3183.
- Swendsen, R. H. (1978). *Phys. Rev. B* **17**, 3710 .
- Syozi, I. (1972). In "Phase Transitions and Critical Phenomena", Vol. 1 (C. Domb and M. S. Green, eds.), pp. 269-329. Academic, New York.
- Taylor, J. E. (1974). *Symposia Mathematica* **14**, 499.
- Taylor, J. E. (1978). *Bull. Amer. Math. Soc.* **84**, 568.
- Temperley, H. N. V. and Fisher, M. E. (1961). *Phil. Mag.* **6**, 1061.
- Vaidya, H. G. (1976). *Phys. Lett.* **57A**, 1.
- Vaks, V. G., Larkin, A. L. and Ovchinnikov, Yu N. (1965). *Zh. eksp. theo. Fiz.* **49**, 1180 (*Soviet Phys. JETP* **22**, 820 (1966)).
- van Beijeren, H. (1977). *Phys. Rev. Lett.* **38**, 993.
- van Beijeren, H. and Nolden, I. (1987). In "Topics in Current Physics", Vol. 43 (W. Schommers and P. von Blanckenhagen, eds.), pp. 259-300. Springer Verlag, Berlin.
- van der Eerden, J. P. and Knops, H. J. F. (1978). *Phys. Lett.* **66A**, 334.

- Vdovichenko, N. V. (1964). *Zh. Eksp. Teor. Fiz.* **47**, 715 [*Sov. Phys. JETP* **20**, 477 (1965)].
- von Laue, M. (1943). *Zeits. f. Kristallog.* **105**, 124.
- Watson, P. G. (1968). *J. Phys. C* **1**, 575.
- Weeks, J. D. (1980). In "Ordering in Strongly Fluctuating Condensed Matter Systems", (T. Riste, ed.). Plenum, New York.
- Weeks, J. D., Gilmer, G. H. and Leamy, H. J. (1973). *Phys. Rev. Lett.* **31**, 549.
- Whitney, H. (1937). *Composito Mathematica* **4**, 276.
- Widom, B. (1965). *J. Chem. Phys.* **43**, 3892.
- Wolf, P.E., Balibar, S. and Gallet, F. (1983). *Phys. Rev. Lett.* **51**, 1366.
- Wortis, M. (1988). In "Chemistry and Physics of Solid Surfaces", Vol. VII (R. Vanselow, ed.), pp. 367-405. Springer Verlag, Berlin.
- Wu, F. Y. (1967). *Phys. Rev. Lett.* **18**, 605.
- Wu, F. Y. (1968). *Phys. Rev.* **168**, 539.
- Wulff, G. (1901). *Zeits. f. Kristallog.* **34**, 449.
- Zia, R. K. P. (1978). *Phys. Lett.* **64A**, 345.
- Zia, R. K. P. (1984). In "Proceedings of the Twenty-Sixth Scottish Universities Summer School in Physics on Statistical and Particle Physics: Common Problems and Techniques, Edinburgh, 1983", (K. C. Bowler and A. J. McKane, eds.), pp. 247-301. Scottish Universities Summer School in Physics, Edinburgh.
- Zia, R. K. P. (1986). *J. Stat. Phys.* **45**, 801.
- Zia, R. K. P. (1988). In "Proceedings of the 1988 Workshop on Statistical Mechanics, Academia Sinica, Taiwan", (C. K. Hu, ed.). World Scientific, Singapore.
- Zia, R. K. P. and Avron, J. E. (1982). *Phys. Rev. B* **25**, 2042.
- Zia, R. K. P. and Gittis, A. (1987). *Phys. Rev. B* **35**, 5907.